NORTHWESTERN UNIVERSITY

VISCOELASTIC BEHAVIOR OF POLYMER MATRIX COMPOSITES WITH INTERPHASE EFFECTS: THEORETICAL MODELS AND FINITE ELEMENT ANALYSIS

A THESIS

SUBMITTED TO THE GRADUATE SCHOOL
IN PARTIAL FULFILLMENT OF THE REQUIREMENTS

for the degree
MASTER OF SCIENCE
FIELD OF MECHANICAL ENGINEERING

by
Frank Fisher

EVANSTON, ILLINOIS
December 1998

ABSTRACT

This thesis will investigate the accuracy of mechanical property predictions for a three phase viscoelastic (VE) matrix-based composite using two different micromechanical models: the Mori-Tanaka method and a solution based on the stress fields in an analogous elasticity problem derived by Benveniste. The former was chosen because it is a standard micromechanical tool which has had success modeling a wide range of problems. The latter was chosen because it keeps the physicality of an annular interphase surrounding the fiber intact. The solutions given by these two methods were compared to those obtained using finite element analysis (FEA), where the mesh was continually refined until an appropriate convergence criterion was satisfied. Since both the FEA and micromechanical solutions model a composite with transversely isotropic properties, the FEA results will be assumed to provide the exact numerical solution.

For all work completed in this thesis the composite will consist of an elastic fiber surrounded by an annular viscoelastic interphase, which in turn is embedded in a binding, viscoelastic matrix. Given the viscoelastic nature of the constituent materials one should expect that the composite behavior as a whole will also be viscoelastic. In order to utilize elasticity solutions which exist in the literature it is necessary to invoke the dynamic correspondence principle. This allows a viscoelasticity problem in the time domain to be solved using a suitable elasticity solution in the frequency domain. Such solutions will enable the determination of the overall effective properties of the composite as a function of constituent volume fractions and phase properties. For simplicity the solutions discussed in this thesis will involve isotropic phase properties, although these solutions can be extended for more complex constituent behavior.

Several case studies will be presented which show the effective composite properties predicted using each of the micromechanical models and compare these results with those obtained using FEA. Whereas the MT method better approximates the viscoelastic behavior of the composite, the Benveniste solution may be more useful from a design perspective because it always provides conservative estimates of the composite moduli. In either case, while the micromechanical methods may provide “orders of magnitude” approximations for the composite properties, they fail to accurately predict the composite behavior when compared to the FEA results. The results presented in this thesis indicate that this is due to

the phase-averaging process which is necessary for these micromechanical solutions. This process fails to model the complex stress state which exists in the composite.

In addition, the finite element analysis was used to investigate the physical aging of the viscoelastic composite. Specifically, we used the methods of this thesis to investigate whether the existence of an interphase with viscoelastic properties different from that of the bulk matrix could be responsible for the difference in shift rates β_{22} and β_{66} which is seen experimentally. Preliminary FEA results indicate that, while a relatively small volume fraction of interphase can play a significant role in determining the aging characteristics of the composite, the interphase does not cause a difference in the shift rates describing the physical aging of E_T and β_T.

ACKNOWLEDGMENTS

If only I had the time and patience to list all of the people who have helped make this thesis a reality. Nonetheless, to start I would like to thank my advisor, Dr. Cate Brinson, who served as an patient guide and a source of ideas and impetus during this endeavor. I would like to thank the other professors who were so kind as to serve on my thesis committee: Dr. Isaac Daniel and Dr. Kenneth Shull. I would also like to recognize the other members of Dr. Brinson's research group who have in some way contributed to the successful completion of this work: Dr. Roger Bradshaw, Dr. Miinshiou Huang, Dr. Alex Bekkar, Wen-Sheng Lin, Xiujie Gao, Tao Bai, and Nagendra Akshantala.

I would also like to thank my various roommates who have provided insight in their fields of research and at times much needed emotional support - both inside and outside of the research lab. John Dolbow has put in three hard years living with me – enough said. Brad Kinsey was on occasion successful in getting me out of the classroom and onto the basketball court. Roger ("El Gato") Chen and Andrew ("The Macho Man") Savage have accounted for endless stories. "Stone Cold" Jay Terry served as vice president of the Adam Schiff fan club. I may have completed my research without these roommates, but I probably would not have enjoyed it.

I would also like to take a moment to thank friends from home and the University of Pittsburgh, each of which is unique and has a special place in my heart . I wouldn't mention all of them by name for fear of even leaving one friend off of the list, but I would be remiss not to at least mention a special few with whom I feel especially close: Chris (a.k.a the "Baron"), Chuck, Hammer, Murph, Colleen, Aaron, Shannon, Greg, and Sophie.

Finally, I'd like to thank my parents for providing me the opportunity to follow my dreams. Had I known when I was younger how lucky I was to have you as parents maybe I would have been a little more appreciative then. You didn't write the book on parenting - if you had the world would be a much better place.

This page left intentionally blank.

TABLE OF CONTENTS

1. INTRODUCTION

Polymer matrix composites (PMCs), particularly those consisting of fiber reinforcement, have become an increasingly popular material for use in structural applications. The primary benefit of such systems are impressive strength-to-weight ratios. Other additional benefits, such as improved corrosion resistance and material property tailorability, can be of significance for specialized applications. Due to the unique properties of PMCs, they are being considered for such diverse applications as civil structure reinforcement, aircraft and spacecraft skins, and biological implants.

One area of concern with the use of PMCs is the difficulty in modeling their overall mechanical behavior. Due to the time-dependent nature of the mechanical properties, and in particular the polymeric matrix, the overall effective behavior of the composite will be viscoelastic. Solution of the viscoelasticity problem in the time domain can be computationally prohibitive due to the convolution integral form of the constitutive equations. However, a simpler approach can be implemented which allows solutions of suitable elasticity problems in the time domain to be exploited. This approach renders viscoelasticity solutions in the frequency domain where the complex material moduli consists of real and imaginary components.

A further area of complication in the analysis of PMCs is the existence of an interphase region of significant dimensions. For PMCs interphase volume fractions on the order of 25% have been reported experimentally using a method, similar to scanning electron microscopy, called secondary ion mass spectroscopy (Thomason 1995). In such cases one may expect the interphase region to play a significant role in determining the overall strength of the composite. The goal of this work is to extend elasticity solutions for multi-phase materials so that an in-depth study on the role of a viscoelastic interphase on the mechanical behavior of polymeric composites can be undertaken. Such analytical models may prove useful in efforts to

1.) develop more accurate models for predicting overall composite behavior
2.) assess the mechanical properties of the interphase region

3.) provide a better model with which to develop "engineered interphases", where an intentional coating is applied to the included phases to optimize properties
4.) experimentally measure the extent of the interphase through mechanical tests
5.) extend knowledge of the role of the interphase for more complex composite behavior, such as damage tolerance, physical aging, and moisture absorption

A review of the literature leads to a large source of models developed for the prediction of the overall effective elastic properties for composite materials. Excellent review articles are provided by Hashin (1983) and Christensen (1990). The latter, in particular, focuses on micromechanical models developed for elastic composites, although his discussion focuses mainly on those with spherical inclusions. He generalizes these models into five distinct categories: the differential method views the overall composite as a sequence of dilute suspensions, and looks at the convergence of the composite moduli as the number of inclusions fills the entire composite volume. The self-consistent and the generalized self-consistent models (Christensen and Lo 1979) both involve embedding the inclusion phase within an infinite medium, the distinction being that in the generalized version the infinite medium assumes the unknown mechanical properties of the composite material. The Mori-Tanaka (MT) method, originally derived to yield the energy for materials with misfitted inclusions, has been extended by several researchers to predict the mechanical behavior of composite materials (Mori and Tanaka 1973; Benveniste 1987). The final model is the composite spheres (cylinders) model, also referred to as the replacement method, which was developed by Hashin (1962). Christensen notes that although many of these models predict similar results for low volume fractions of inclusions, large discrepancies (by orders of magnitude) can arise when analyzing composites with either large volume fractions of inclusions or where there exists a large variance in constituent mechanical properties.

In addition to the above review articles, several recent works have used micromechanical methods. Norris (1990) adapts the differential method to study the effective moduli of two-phase platelet reinforced elastic composites. Qui and Weng (1991) used the composite cylinder assembly to study elastic composites with thick interphases. Mahiou and Beakou (1998) implemented Aboudi's method of cells to model imperfect

phase bonding in fiber-reinforced composites. Weng (1984) has used the Mori-Tanaka method for elastic composites with spherical inclusions. Other researchers have also used the MT method to study composite behavior (Zhao and Weng 1990; Qui and Weng 1991a; Chen 1992). Many other additional micromechanical analyzes of effective composite behavior can be found in the literature, see, for example, Avery and Herakovich (1986) and Mikata (1994).

Analysis of viscoelastic composites using micromechanical techniques is much less developed. Early work in this area was pioneered by Hashin (1965; 1966; 1970a; 1970b) and Schapery (1967; 1969). Several researchers have recently looked at the effect of inclusion shape on mechanical properties for two phase VE composites (Wang and Weng 1992; Li and Weng 1994). Brinson and Lin (1996; 1998) have compared the results of the MT method for two-phase VE composites with those acquired via a finite element analysis. Li and Weng (1996) studied a viscoelastic interphase with the composite cylinder model and found that in composites where the interphase is softer than the matrix, a pronounced decrease in effective composite strength is realized.

Another manner with which to analyze interphase effects on composite materials is the use of various techniques which bound the effective material moduli. The most straightforward of these is the Reuss-Voigt bounds, commonly referred to as the rule of mixtures. Since these bounds do not take into account phase geometry, they are often too far separated and of limited practical use. A more rigorous set of bounds for the effective elastic moduli of multiphase composites were developed by Hashin and Shtrikman (1962) using a variational approach. These bounds were rederived and extended by Walpole (1969), who analyzed the problem using the Green's function. These bounds, typically referred to as the Hashin-Shtrikman-Walpole (HSW) bounds, are often quite useful in the study of elastic materials. Weng noted that there is a relation between the MT method and the Hashin-Strikman-Walpole bounds for elastic multiphase composites (Weng 1990).

These bounds are also valid for viscoelastic materials in the Laplace domain, where the equations and boundary conditions of the elasticity formulation have been transformed into Laplace space via the correspondence principle. However, it has been shown that they

are not rigorous in the Fourier domain, where the complex moduli are written in terms of storage and loss components. Gibiansky and coworkers (1993a; 1993b) have recently developed a complex derivation, based on the HSW bounds, to bound the effective composite moduli in the Fourier plane. Although useful for certain applications, these bounds will not be examined in detail in this thesis.

In this thesis two elasticity solutions for multiphase composites will be extended into the viscoelastic regime to examine interphase effects: a version of the popular Mori-Tanaka method (Mori and Tanaka 1973; Weng 1984; Benveniste 1987), and a micromechanical method developed by Benveniste (1989). In addition to these two solutions, a finite element analysis (FEA) using a unit cell approach with a hexagonal array will be implemented to provide a criterion with which to judge the accuracy of the analytical solutions. Although the micromechanical methods assume a random distribution of inclusions and the FEA assumes that the inclusions are aligned in an hexagonal array, each method will yield transversely isotropic composite behavior. Thus we believe that such a comparison is justified. The FEA represents an extension of previous work which sought to determine the overall composite behavior of a two-phase viscoelastic composite (Brinson and Knauss 1992).

The first analytical method used to determine the viscoelastic behavior of a three-phase composite is based on the Mori-Tanaka method. Key to their analysis is Eshelby's (1957) solution for the stress field within an ellipsoidal inclusion. The Mori-Tanaka method has been extended by various authors in a wide range of problems and has become a very popular tool for analysis of multiphase materials (Benveniste 1987; Zhao and Weng 1990; Wang and Weng 1992). The current work will extend the model proposed by Weng (1984) to study a three phase fibrous composite consisting of viscoelastic phase materials.

As used in this thesis, the Mori-Tanaka method will treat the fiber and the interphase regions as separate, distinct regions of a given volume fraction within the binding matrix (see Figure 3.1). It will *not* make the distinction of an annular interphase region surrounding the fiber inclusion. Recent work completed by Luo and Weng (1987; 1989) sought to extend Eshelby's solutions for a three-phase concentric alignment of inclusions.

Here they derive slightly different forms of the Eshelby S-tensor describing the perturbed strains which exist due to the fiber/interphase and interphase/matrix interactions. The altered S-tensors, which can then be substituted into the original MT method, allow for the physicality of the annular interphase to remain intact. This particular extension of the MT method will be considered at a later date.

The second analytical model utilizes a model originally proposed by Benveniste (1989) to study the stress fields for materials with coated inclusions (see Figure 2.4). Based on a generalized self-consistent model proposed by Christensen and Lo for a two-phase composite (Christensen and Lo 1979), the displacements of each phase for a related *auxiliary* problem are written explicitly in terms of unknown constants. These constants are determined by satisfying relevant boundary conditions, allowing the local fields in the fiber and interphase regions to be determined. Thus the relationship between an appropriate far-field applied stress and the average stresses in the included phases for a single coated-particle embedded in an infinite matrix can be found. This solution is then used to determine the unknown average matrix stresses for the composite, which accounts for particle interaction.

Although the Benveniste solution is based in part on the "average stress in the matrix" concept of the Mori-Tanaka method, it is a different method of solution due to a) the consideration of the boundary conditions at the interfaces, and b) the lack of evaluation of the Eshelby tensor. Although the Benveniste solution can be carried out for all five of the transversely isotropic properties of a fibrous composite, this thesis will concentrate on the transverse properties of the composite, which are typically considered to be matrix-dominated properties. Other effective composite properties can be determined by analyzing the composite response given a different applied far-field stress (Benveniste, Dvorak et al. 1989).

In order to compare the results of these two micromechanical solutions, a finite element analysis of the problem will be completed. This FEA model is based on the work of Brinson and Knauss (1992), which used the dynamic correspondence principle to solve the boundary value problem on a unit cell to obtain the effective complex moduli of the

composite. Other researchers have also used FEA to study the influence of the inclusion on composite properties with elastic phase materials (Broutman and Agarwal 1974; Haoran, Feng et al. 1995; Jacobs and Verpoest 1998; Wacker, Bledzki et al. 1998). Viscoelastic interphase/interface studies using FEA have also been completed (Gosz, Moran et al. 1991; Yi, Pollack et al. 1995). For this thesis the concentric fiber-interphase region will be assumed to exist in a hexagonal array such that the overall behavior of the composite is transversely isotropic, in order to allow direct comparison to the results to the Mori-Tanaka and Benveniste solutions.

The purpose of this thesis is to determine the accuracy of two micromechanical models in predicting the effect of a viscoelastic interphase on the mechanical properties of a three-phase composite. Chapter 2 presents background information on viscoelasticity and the role of the interphase in polymeric composites. Chapter 3 introduces the Mori-Tanaka method by presenting the derivation for an elastic composite. It then briefly discusses simplifications which arise for cylindrical inclusions, and finally extends the MT method for viscoelastic materials. Chapter 4 introduces the Benveniste solution from the standpoint of an elastic composite. After discussing the auxiliary problems which must be analyzed for its solution, the solution is extended for VE composites. Chapter 5 explains the finite element analysis completed for this work. Chapter 6 uses the methods developed in the preceding chapters to perform comparison studies using each of the micromechanical models. Results in this chapter will show the accuracy with which the micromechanical models predict the complex composite moduli determined by the FEA over a wide range of frequencies. Finally, the models developed in this thesis will be used to investigate the impact of the interphase on the shift rates describing the physical aging of the polymer matrix composites.

2. BACKGROUND

2.1 VISCOELASTICITY AND THE DYNAMIC CORRESPONDENCE PRINCIPLE

The constitutive equation for a viscoelastic material can be written in terms of a Stieltjes integral equation of the form

$$\sigma_{ij}(t) = \int_{0}^{t} C_{ijkl}(t-\tau) \frac{d\varepsilon_{kl}(\tau)}{d\tau} d\tau \tag{2.1}$$

where C_{ijkl} is the time-dependent modulus of the material, and σ_{ij} and ε_{kl} are the stress and strain tensors, respectively. Analogous to the situation for an elastic analysis, the time-dependent stress and strain tensors can be written in terms of deviatoric (s_{ij}, e_{ij}) and dilitational ($\sigma_{kk}, \varepsilon_{kk}$) components,

$$s_{ij}(t) = \sigma_{ij}(t) - \frac{1}{3}\sigma_{kk}(t)\delta_{ij}\ , \quad e_{ij}(t) = \varepsilon_{ij}(t) - \frac{1}{3}\varepsilon_{kk}(t)\delta_{ij} \tag{2.2}$$

With substitution of (2.2) into (2.1), the constitutive law for a linear, isotropic viscoelastic material can be written in terms of the time-dependent shear modulus G(t) and bulk modulus K(t) as follows

$$s_{ij}(t) = \int_{0}^{t} 2G(t-\tau) \frac{de_{ij}(\tau)}{d\tau} d\tau \tag{2.3}$$

$$\sigma_{kk}(t) = \int_{0}^{t} 3K(t-\tau) \frac{d\varepsilon_{ij}(\tau)}{d\tau} d\tau \tag{2.4}$$

In general solution of constitutive equations involving convolution integrals of this type are computationally prohibitive. Taylor and co-workers (1970) have developed a procedure which simplifies the analysis of such a constitutive equation, yet even this analysis requires a finite time discretization process which limits the realistic time scales which can be studied.

However, it is possible to completely avoid time domain analysis of the problem by utilizing the *dynamic correspondence principle*. This tool allows the mechanical characterization of viscoelastic materials to be accomplished by studying complex mechanical properties in the transformed domain. The definition of the appropriate complex phase moduli will be derived below for the case of isotropic phase materials.

To present the derivation, consider a separable form for the displacements *u* of the form

$$u_i(\mathbf{x},t) = \bar{u}_i(\mathbf{x},\omega)\, e^{i\omega t} \tag{2.5}$$

where ω is frequency. Given these displacements, strain fields can be determined using the strain-displacement relationship

$$\varepsilon_{ij} = \frac{1}{2}(u_{i,j} + u_{j,i}) = \bar{\varepsilon}_{ij}(\omega)\, e^{i\omega t} \tag{2.6}$$

Substitution of (2.6) into (2.3) and (2.4), respectively, yields

$$\bar{s}_{ij} = 2\bar{G}^*(\omega)\bar{\varepsilon}_{ij}\ ,\ \bar{\sigma}_{kk} = 3\bar{K}^*(\omega)\bar{\varepsilon}_{kk} \tag{2.7}$$

where

$$\bar{K}^*(\omega) \equiv i\omega\bar{K}(\omega) = i\omega\int_0^\infty K(t)\, e^{-i\omega t}\, dt \tag{2.8}$$

$$\bar{G}^*(\omega) \equiv i\omega\bar{G}(\omega) = i\omega\int_0^\infty G(t)\, e^{-i\omega t}\, dt \tag{2.9}$$

are the complex bulk moduli $\bar{K}^*(\omega)$ and the complex shear moduli, $\bar{G}^*(\omega)$, respectively. The complex moduli are often written in terms of the storage and loss moduli, i.e.,

$$\bar{K}^*(\omega) = K'(\omega) + iK''(\omega), \quad \bar{G}^*(\omega) = G'(\omega) + iG''(\omega) \tag{2.10}$$

where single and double primes denote the storage and loss moduli, respectively. The storage modulus is a measure of the energy stored and recovered by a viscoelastic material per cycle of sinusoidal deformation, whereas the loss moduli is a measure of the energy dissipated as heat for a similar cycle (Tschogel 1989). Note that as written in (2.10) both storage and loss moduli are real quantities.

The constitutive equations given in (2.7) are identical to that of a standard elasticity formulation, where now all field quantities are complex. Thus there is a direct analogy between elasticity problems in the time domain and viscoelasticity problems in the frequency domain. This relationship can be exploited through the dynamic correspondence principle by taking the Laplace or Fourier transform of elasticity solutions and replacing the elastic moduli by corresponding complex viscoelastic moduli using (2.8) and (2.9). The benefit of such a scheme is obvious: the large supply of tools which have been developed for the analysis of elastic problems can readily be applied to problems involving viscoelastic materials.

2.2 THE INTERPHASE REGION IN POLYMERIC COMPOSITES

This thesis analyzes two micromechanical approaches with which the effect of a viscoelastic interphase on the overall effective moduli of fibrous composites may be studied. These models will be compared to the results of a detailed FEA. Before discussing the theoretical aspects of this investigation, it is worthwhile to discuss the interphase region in polymeric composites.

The interphase (called a "mesophase" by certain authors) is an annular region surrounding the inclusions in a multiphase material. It is an inhomogeneous region with non-constant properties typically intermediate to those of the main bulk constituent materials of the composite. The origin of the interphase may be due to voids, mechanical imperfections, unreacted polymer components, physiochemical interactions, limited

macromolecular mobility due to the absorption on the fiber surface, and other inconsistencies (Theocaris 1985; Papanicolaou, Messinis et al. 1989; Gardner, Pittman et al. 1993). For glass-fiber epoxy composites, the interphase region can be further complicated by coupling agents and processing aids used to treat the fibers prior to introduction into the epoxy resin (Bank and Gentry 1995; Thomason 1995). Regardless of its cause, the interphase region, although often a relatively small amount of the total volume fraction of a composite, can play a crucial role in determining its overall mechanical properties.

In addition to these "unintentional" interphase regions, some researchers have sought to take advantage of the unique role of the interphase by developing "engineered interphases". This refers to the deliberate treatment of the fiber phase, or the introduction of a novel third phase, with properties and dimensions controlled by the manufacturer in order to optimize composite performance. Such interphases, with mechanical properties typically on the order of magnitude of those of the matrix, show promise for increasing the strength and fracture toughness of composite materials, particularly by reducing the stress-concentrations in the matrix due to the presence of the fibers (Termonia 1990; Gardner, Pittman et al. 1993). Nellipappan and coworkers (1997) sought to determine the optimal characteristics of an engineered interphase for a polymeric particulate composite. It is anticipated that the results of this thesis will be useful for studying the effects of either type of interphase discussed here.

To better analyze the results of the current work, the interphase will be assumed to have constant material properties distinct from those of the bulk phases, although other researchers have used more complex models. One such model assumes that interphase properties vary continuously as a function of position, with consistency enforced at the fiber and matrix interfaces (Papanicolaou, Messinis et al. 1989; Mikata 1994). The models developed in this thesis could be extended in such a manner, although the introduction of a finite number of annular interphase regions to model non-constant interphase properties would be required.

Another difficulty associated with modeling the interphase region is the characterization of its location and extent. Unfortunately, little work has been done to

characterize the thickness of this region. In the past, the thickness of the interphase in fibrous composites has been estimated between 30 to 240 nm by various researchers, as reported by Termonia (1990). Papanicolaou (1989), basing his estimates on thermal capacity measurements, found the interphase thickness to be on the order of hundreds of nanometers for a fiber diameter of 12 μm. This corresponds to a fiber volume fraction over 12 times greater than that of the interphase for a fiber volume fraction of 0.65. This fiber diameter is typical of a commercial glass fiber for use in polymer composites, where diameters are on the order of 15 μm; see Thomason (1995) for a representative listing of glass fiber diameters.

Other researchers have *estimated* interphase thicknesses for polymeric composite studies. Termonia (1990), performing an FEA study on elastic interphase effects, set the thickness of the interphase equal to 9% of the fiber diameter, suggesting a fiber volume fraction approximately 5 times that of the interphase. Ho and Drzal (1996) used a finite element approach to study the effectiveness of a microindentation technique to measure interphase properties. They assumed that the fiber volume fraction was about 12 times that of the interphase volume fraction. Gardner (1993) used an adaptation of Aboudi's method of cells to determine the residual stresses in polymer matrix composites. They chose to use a fiber volume fraction of 36% and an interphase volume fraction of 24%, a rather large value in comparison with the other works referenced in this section. However, the rationale behind the selection of the interphase volume fractions was not presented in any of these studies, and the choices of these authors seem to be rather arbitrary.

Theocaris (1985) estimated values of the interphase thickness by comparing experimental data for the longitudinal elastic modulus of an epoxy-glass fiber composite with a micromechanical model; these values can be found in Table 2.1. He suggests that the volume fraction of the interphase, v_i, can be related to the volume fraction of the fiber, v_f, by the following relationship

$$v_i = 0.123\, v_f^2 \tag{2.11}$$

Although at low fiber volume fractions this model may significantly underestimate the

extent of the interphase, at fiber volume fractions typical those of PMC materials (roughly 60%), this equation predicts fiber volume fractions approximately 10~15 times larger than that of the interphase. At high volume fractions those values certainly agree with the work of other researchers presented in this section.

v_f (%)	v_i (%)	v_m (%)
0	0	100.00
10	0.123	89.877
20	0.492	79.508
40	1.960	58.040
50	3.075	46.925
60	4.428	35.572
65	5.200	29.800
70	6.030	23.970

Table 2.1. Values of characteristic interphase volume fractions for an E-Glass fiber-epoxy resin unidirectional composite. (Theocaris 1985)

Work done on block copolymers, which could directly relate to polymer fiber – polymer matrix composites, suggests interphase volume fractions for polymer-polymer interactions can range between zero (total phase separation) and 100% (completely miscible). The interphase region will typically be rich in one of the constituent materials (Henderson and Williams 1985; Spontak, Williams et al. 1988). Such composites could have extensive interphase regions, and the ability to accurately predict the influence of the interphase on composite behavior would seem critical for these materials.

Clearly, researchers to date have used a wide range of interphase volume fractions for the modeling of interphase effects, with fiber volume fractions typically ranging from approximately 5 to 20 times that of the interphase region. More work, especially of an experimental nature, needs to be done to accurately assess the dimensions and composition

of the interphase in polymeric composites. One such study, by Thomason (1995), used secondary ion mass spectroscopy (s.i.m.s) to measure the thickness of an epoxy-glass fiber interphase as approximately 1 m, corresponding to a fiber volume fraction 7~7.5 times greater than the interphase. He acknowledged that this value is higher than the value of 30 to 240 nm typically quoted in the literature. Alternative methods to characterize the interphase region of polymer composites are being developed, including atomic force microscopy (ATM) (Mai, Mader et al. 1998) and scanning force microscopy (SFM) (Munz, Sturm et al. 1998).

A more accurate understanding of the factors which affect the thickness of the interphase region will be crucial as models which use the interphase dimension to predict overall composite behavior are developed and refined. At the current time, there is little consensus as to a standard value for the interphase thickness of a PMC. In addition, one may expect that the volume fraction of the interphase will be dependent on the combination of the fiber and matrix materials used within a particular composite. Thus for a majority of the work in this thesis, the interphase volume fraction was set equal to 10% of the total volume fraction of the composite. Although this value may be high, particularly for low fiber volume fractions, it was chosen to emphasize the influence of the interphase on the effective properties of the composite and thus improve our ability to compare the results of the micromechanical models.

2.3 THE PHYSICAL MODEL

This thesis seeks to determine the overall mechanical properties of a three phase viscoelastic composite consisting of cylindrical fibers surrounded by an annular interphase and embedded in a binding, continuous matrix. Here it will be assumed that both the matrix and interphase are isotropic, linear viscoelastic materials, and that the fiber is isotropic and elastic. It is assumed that there is perfect bonding between the phases.

Although the viscoelastic components of these composites will typically feature temperature-dependent properties, the current work does not investigate such effects, and

thus isothermal conditions should be assumed. Glass transition temperature (T_g) effects will be neglected, although it should be noted that the glass transition temperature of the interphase region may vary significantly from those of the fiber and matrix phases. The T_g of the interphase can play an important role in the processing of the polymer composite, as processing temperatures greater than that of the interphase will allow greater molecular mobility within the interphase region, improving the ability of the interphase to properly bond with the fiber and matrix materials (Thomason 1995).

A fibrous composite will in general be transversely isotropic, and its mechanical behavior quantified by five independent properties (for example, the axial modulus E_A, transverse Young's modulus E_T, axial shear modulus $\square_A$, transverse shear modulus $\square_T$, and the plane strain bulk modulus k). It is typically understood that the axial modulus E_A is primarily a fiber-dominated property, while the other four properties can vary significantly depending on interphase and matrix volume fractions and properties (Li and Weng 1996). In order to better focus the efforts of this research, the transverse Young's modulus E_T of the composite will be studied unless otherwise noted.

For this investigation two hypothetical isotropic, linear viscoelastic (VE) materials, a "stiff" polymer and a "soft" polymer, were implemented as either the matrix or interphase materials in a three-phase composite. The designation of "stiff" or "soft" material as the interphase and matrix material was varied throughout the analysis. This allowed analysis of the composite behavior when the interphase was either the softest phase in the composite or when the interphase had properties intermediate those of the fiber and matrix materials. At all times the fiber was the stiffest of the three phases within the composite. The values of the elastic moduli for the fiber are given in Table 2.2.

For all viscoelastic materials the time-dependent bulk and shear moduli were represented using the standard Prony series representation of the form

Elastic Properties
G = 40,000
K = 100,000

Table 2.2. Mechanical properties of hypothetical isotropic, elastic fibers.

Stiff Material

G_∞ = 100	
K_∞ = 8000	
τ_j^G	G_j
3	3.162
10	17.783
32	100.000
100	316.228
316	1000.000
1000	5623.413
3162	10000.000
10000	562.341
31623	141.254
100000	56.234
316228	17.783
1000000	5.623
3162278	3.162
10000000	1.778
τ_j^K	K_j
10000	40000

Soft Material

G_∞ = 3.162	
K_∞ = 200	
τ_j^G	G_j
0.032	2.512
0.100	10.000
0.316	56.234
1.000	316.228
3.162	1000.000
10.000	199.526
31.623	50.119
100.000	19.953
316.228	12.589
1000.000	2.512
3162.278	1.698
10000.000	1.202
31622.777	1.148
100000.000	1.096
τ_j^K	K_j
100	3000
316.228	100

Table 2.3. Prony series terms for the viscoelastic moduli of the "stiff" and "soft" hypothetical materials. (Brinson and Lin 1998)

$$A(t) = A_{\infty} + \sum_{j=1}^{N} A_j \, e^{-t/\tau_j} \qquad (2.12)$$

where A_j and τ_j are the relaxation spectra and relaxation times, respectively, and A_{∞} is the rubbery asymptotic modulus of either the shear or bulk modulus. The parameters used to represent the viscoelastic behavior of the hypothetical "stiff" and "soft" materials are given in Table 2.3. A plot showing the mechanical behavior of the time-dependent constituent phase materials is shown in Figure 2.1. The corresponding complex moduli of the viscoelastic constituent materials, obtained via the correspondence principle, are presented in Figures 2.2 and 2.3 for the storage and the loss moduli, respectively.

Figure 2.4 shows a schematic of the applied loading in the transverse plane to determine E_T of the composite. The unit cell models used for the FEA analysis, assuming the fiber-interphase inclusions are aligned in an hexagonal array, are shown in Figures 2.5 and 2.6. Due to natural symmetry a hexagonal array represents the transversely isotropic behavior of fibrous composites (Lin 1996). Because voids within the composite are neglected, the sum of the volume fractions of the phases, denoted c_f, c_g, and c_m (fiber, interphase, and matrix phase, respectively) must equal unity. The displacement on the right hand side of the unit cell in Figure 2.5 is specified to ensure the side remains straight and parallel. The complex boundary conditions imposed on the unit cell for the case of transverse normal loading are:

$$\begin{array}{lll} \bar{u}_x = 0 & \bar{T}_y = 0 & \text{on } x = 0 \\ \bar{u}_y = 0 & \bar{T}_x = 0 & \text{on } y = 0 \\ \bar{u}_x = -\bar{b} & \bar{T}_y = 0 & \text{on } x = W \\ \bar{u}_y = \bar{u}_o + 0\,i & \bar{T}_x = 0 & \text{on } y = L \end{array} \qquad (2.13)$$

$$W = \sqrt{3}\,L$$

An example of a mesh generated for the finite element analysis can be found in Appendix A.1.

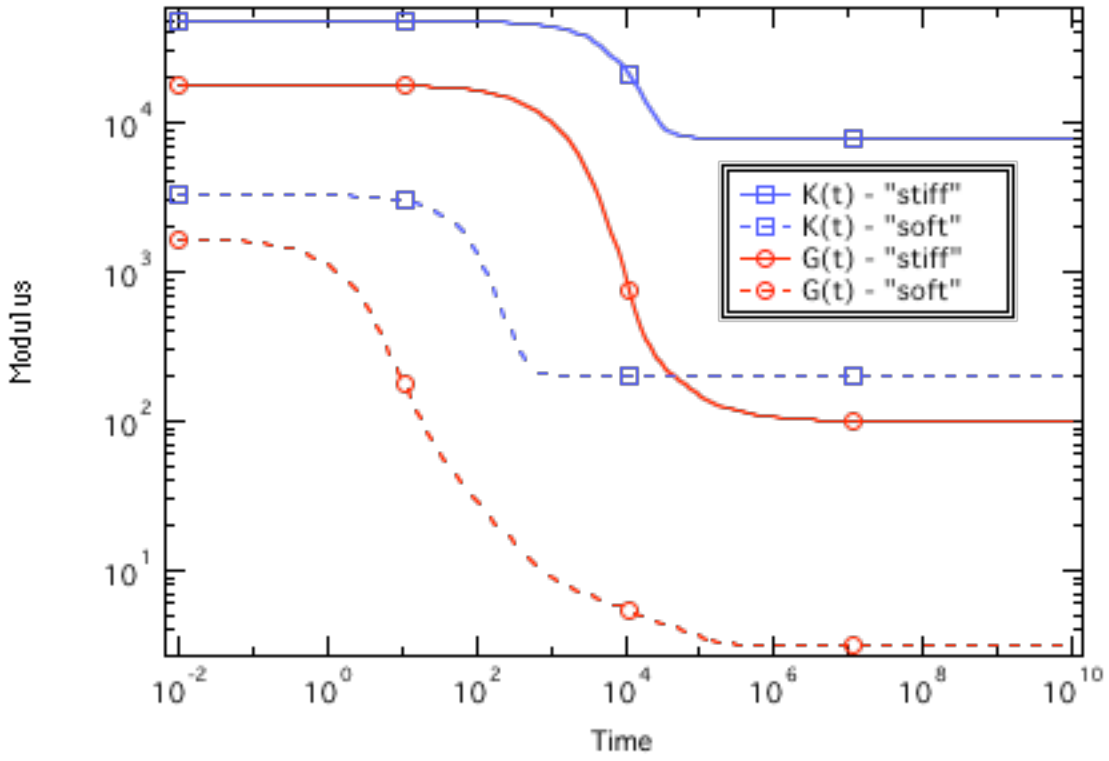

Figure 2.1. Viscoelastic phase properties in the time domain.

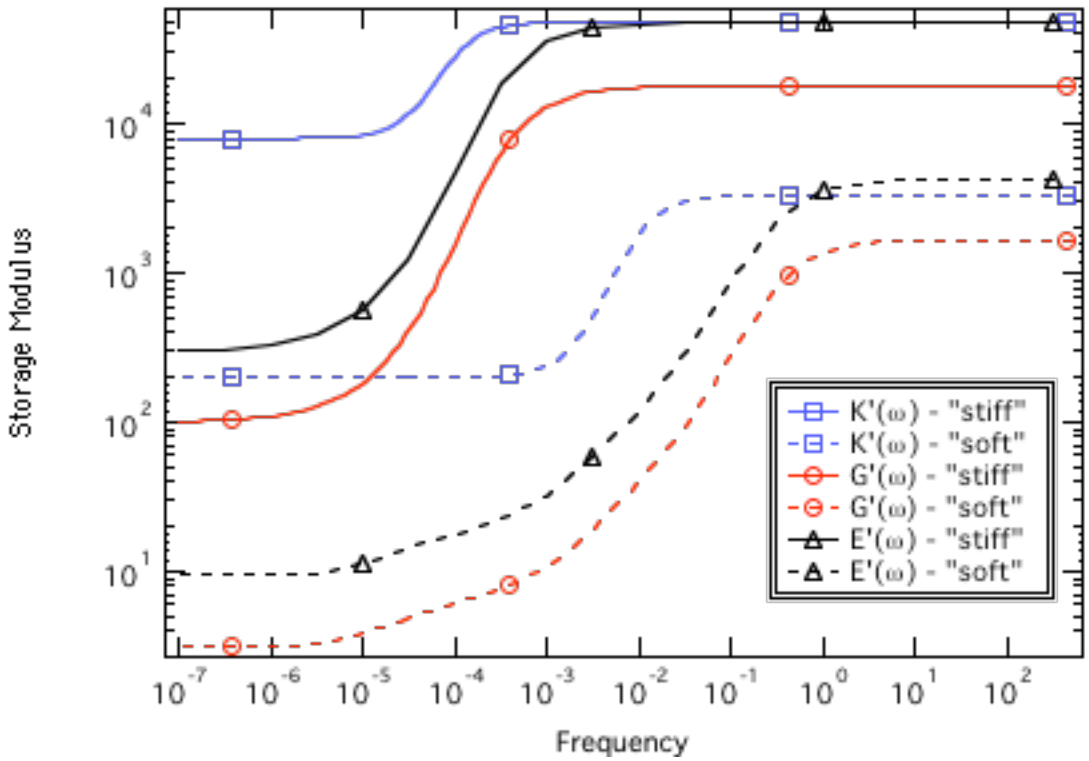

Figure 2.2. Complex storage moduli for viscoelastic phase materials.

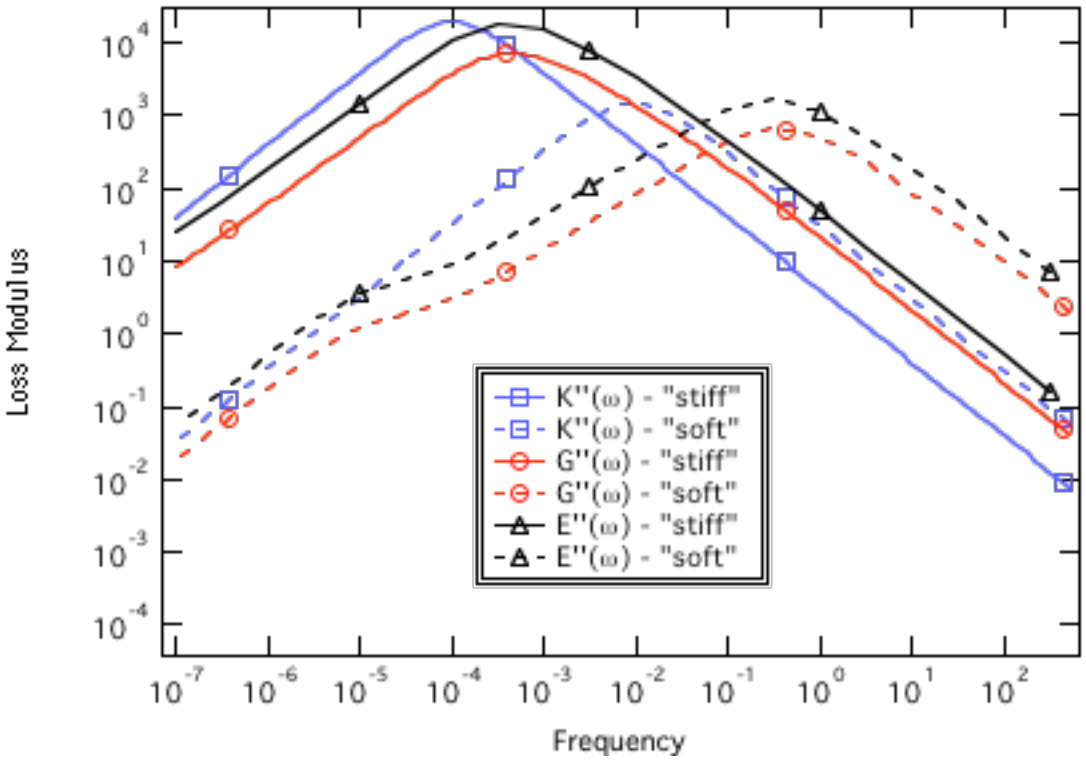

Figure 2.3. Complex loss moduli for viscoelastic phase materials.

The finite element method was also used to investigate the behavior of the overall transverse shear modulus as a function of phase properties and geometry. Following previous work in this area (Brinson 1990), the unit cell necessary to model such behavior is shown in Figure 2.6. The boundary conditions which must be enforced on the unit cell to determine the transverse shear modulus are given below,

$$
\begin{aligned}
&\bar{u}_y = 0 \qquad \bar{T}_x = 0 \qquad \text{on } x = 0 \\
&\bar{u}_x = 0 \qquad \bar{T}_y = 0 \qquad \text{on } y = 0 \\
&\bar{u}_y = 0 \qquad \bar{T}_x = 0 \qquad \text{on } x = W \\
&\bar{u}_x = \bar{u}_o + 0\,i \qquad \bar{T}_y = 0 \qquad \text{on } y = L \\
&W = \sqrt{3}\,L
\end{aligned}
\tag{2.14}
$$

Further discussion of the finite element implementation for this thesis will be postponed until Chapter 5. Meshes for a given geometry can be used independent of the type of boundary conditions applied to the unit cell.

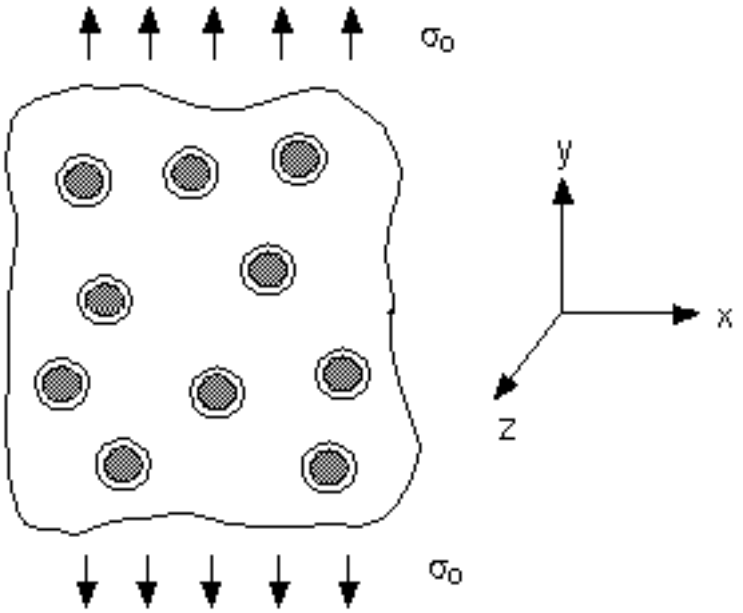

Figure 2.4. Three phase composite model – transverse normal loading.

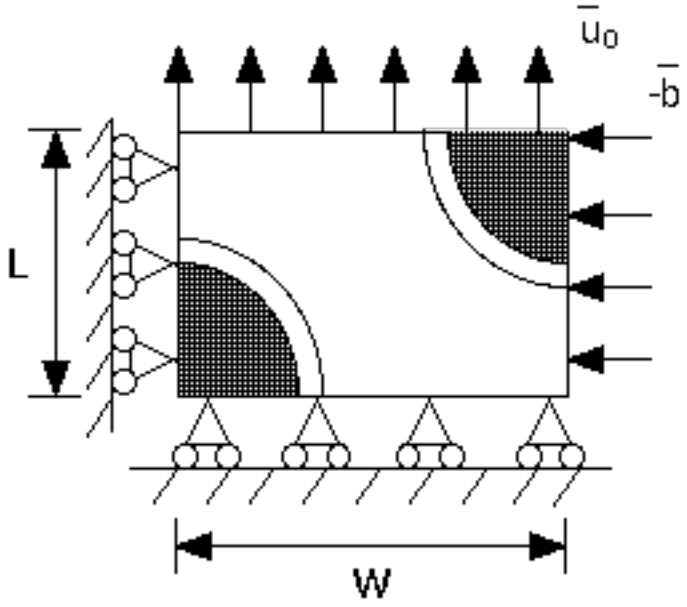

Figure 2.5. Unit cell finite element analysis for a three phase composite – transverse Young's modulus (hexagonal array)

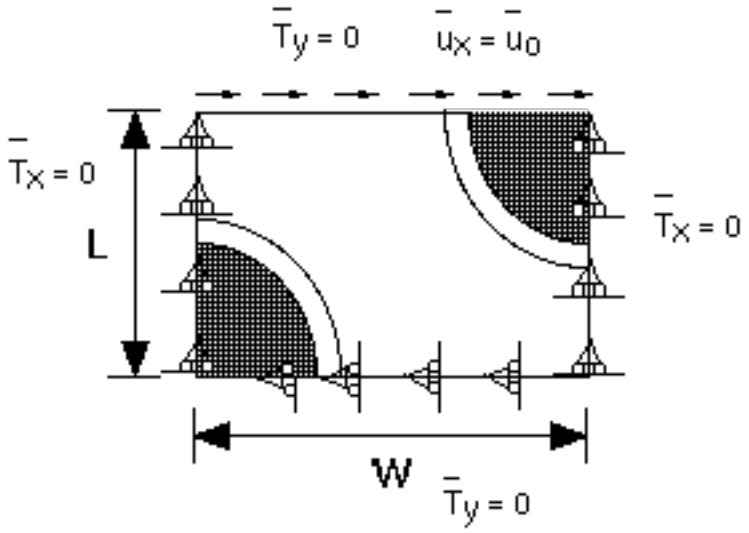

Figure 2.6. Unit cell finite element analysis for a three phase composite – transverse shear modulus (hexagonal array)

2.4 PHYSICAL AGING OF VISCOELASTIC MATERIALS

Much effort to date has focused on the physical aging of polymers. Physical aging has been the subject of numerous investigations, and only a very brief description of its background is warranted here. For a more in-depth review of the subject, several books discuss physical aging and its effect on the mechanical behavior of polymeric materials (Struik 1978; Ferry 1980).

Physical aging is due to the fact that a polymeric material, below its glass transition temperature T_g, is in a non-equilibrated thermodynamic state. As the time below T_g continues to increase, the polymer slowly approaches its equilibrium state; this is realized by a gradual decrease in volume, among other phenomena. The time below T_g is referred to as the aging time t_e. As the process of physical aging continues, the mechanical behavior of the material changes; as the volume decreases, the material becomes stiffer and less ductile. In most instances of physical aging of polymeric materials, the material property curves at different initial aging times can be superposed through a horizontal shift. The amount of shifting necessary to superpose the material curves is referred to as the aging time shift factor a_{t_e}. An example of the use of a_{t_e} to shift moduli curves is given in Figures 6.42 and

6.45. For a wide variety of materials, including PMCs, experiments have shown that the shift factors are linearly related to the initial aging time in log-log space via the shift rate μ,

$$\mu = -\frac{d \log a_{t_e}}{d \log t_e} \tag{2.15}$$

Thus the shift rate μ is a material parameter which may be used to determine the modulus for a given amount of initial aging time given the master reference curve. Physical aging therefore has the effect of altering the relaxation times of the polymeric material, corresponding to the horizontal shifting of the curves. Along these lines, the relaxation times of the aged material are related to the relaxation times of the reference material via

$$\xi(t_e) = \frac{\xi(t_{e,ref})}{a_{t_e}} \tag{2.16}$$

where $t_{e,ref}$ is the reference aging time. For our purposes the reference aging time can be set equal to one without loss of generality. More complicated versions of physical aging, and in particular effective time theory (Brinson and Gates 1995), were not investigated in this thesis.

For an isotropic material one value of μ is sufficient to characterize the physical aging of all mechanical properties (Struik 1978). However, experimental work (Gates and Feldman 1993; Hastie and Morris 1993) suggests that different shift rates, μ_{22} and μ_{66}, are necessary to characterize the physical aging of polymeric composites subjected to transverse normal and transverse shear loadings, respectively. This is despite the fact that the transverse shear and Young's moduli are both matrix-dominated properties. The fact that the shift rates measured for these variables is different may suggest that there are fundamental differences in the way in which composite materials respond to such loadings. We will use the methods developed in this thesis to investigate whether the existence of an interlayer with distinct viscoelastic and aging properties could be responsible for the different shift rates measured experimentally.

3. MORI-TANAKA METHOD

3.1 INTRODUCTION

In this section the derivation of the Mori-Tanaka method for the determination of the effective properties of an elastic composite is briefly presented. More detailed derivations can be found in the literature (Mori and Tanaka 1973; Weng 1984; Benveniste 1987). The extension of this method for viscoelastic materials will be postponed until Section 3 of this chapter.

As will be seen below, the Mori-Tanaka method entails use of the Eshelby tensor to account for cylindrical included phases. Thus the standard MT method cannot capture the exact geometry of the interphase problem, where the interphase is an annular region surrounding each cylindrical fiber inclusion. Consequently, for the MT analysis here, we will approximate the fiber-interphase problem using a composite with distinct cylindrical inclusions of the interphase material in addition to the cylindrical fiber inclusions (see Figure 3.1). Since the Mori-Tanaka method is such a standard and popular micromechanical tool, it will be useful to determine the accuracy of the approximate solution the Mori-Tanaka method provides in this context. On completion of this work it was discovered an extension of the Mori-Tanaka method for annular regions has been developed (Luo and Weng 1989), but this has not yet been examined for the VE problem considered here. Such as analysis may provide further insight as to the role of the interphase in the determination of composite behavior. A more sophisticated micromechanical solution which keeps intact the physicality of the annular interphase will be presented in Chapter 4.

Consider the three phase composite material shown in Figure 3.1. Again, this is a simplification of the actual geometry of the problem shown in Figure 2.4. Here we assume that the individual phases which comprise the composite are elastic in nature and are denoted *f*, *g*, and *m* for the fiber, interphase, and matrix, respectively. In addition,

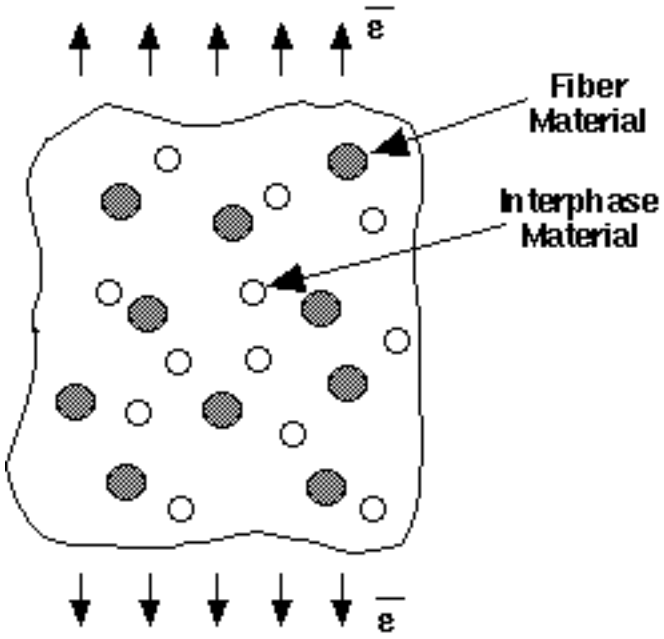

Figure 3.1. Interphase modeled as a distinct inclusion region for the Mori-Tanaka method.

we will consider an identically shaped comparison material, assumed to have the mechanical properties of the matrix.

Further assume that both the composite material and the comparison material are subjected to a prescribed boundary displacement condition causing a uniform strain $\bar{\varepsilon}$ in each material, where an overbar $(\bar{\bullet})$ here and throughout this section denotes an uniform value. (Note that an equivalent derivation can proceed using a prescribed traction condition, see Weng (1984).) The stresses required within the composite and the comparison material, respectively, to cause this uniform strain $\bar{\varepsilon}$ are given by

$$\bar{\sigma} = \mathbf{L}\bar{\varepsilon}\,, \quad \bar{\sigma}_o = \mathbf{L}_m\bar{\varepsilon} \tag{3.1}$$

where $\mathbf{L}$ is the effective modulus of the composite and $\mathbf{L}_m$ is the modulus of the matrix.

However, the actual average stress of the matrix material within the composite will differ from the stress of the comparison material, $\bar{\sigma}_o$, due to the stress-concentrations caused by the fiber and interphase regions. Denoting this average difference as $\tilde{\sigma}$, it follows from (3.1) that the stress in the matrix material within the composite, $\bar{\sigma}_m$ is

$$\bar{\sigma}_m = \bar{\sigma}_o + \tilde{\sigma} = \mathbf{L}_m(\bar{\varepsilon} + \tilde{\varepsilon}) \tag{3.2}$$

The average stresses of the included phases (i.e. the fiber and the interphase), on the other hand, will differ from that of the matrix phase within the composite. Writing this additional stress perturbance of phase *k* as σ_k^{pt}, the stress state in each phase can now be represented (where σ_m^{pt} is zero by definition)

$$\sigma_k = \sigma_o + \tilde{\sigma} + \sigma_k^{pt} = \mathbf{L}_k\left(\bar{\varepsilon} + \tilde{\varepsilon} + \varepsilon_k^{pt}\right) \qquad k=\{f,g,m\} \tag{3.3}$$

where $\mathbf{L}_k$ represents the modulus of the *k*th phase. Likewise, the strain in each phase can be written in terms of the material compliances, $\mathbf{M}_k$ where k={f,g,m}, given that the standard inverse relationship between modulus and compliance exists. By definition the perturbed stress within the matrix, σ_m^{pt}, is identically zero, and one can write

$$\varepsilon_k = \bar{\varepsilon} + \tilde{\varepsilon} + \varepsilon_k^{pt} = \mathbf{M}_k\sigma_k = \mathbf{M}_k\left(\bar{\sigma}_o + \tilde{\sigma} + \sigma_k^{pt}\right) \qquad k=\{f,g,m\} \tag{3.4}$$

Equation (3.3) can be recast in terms of the matrix modulus using the idea of an equivalent transformation strain ε_k^*, the strain which would be necessary to restore the transformed inclusion back to its original, pre-deformed shape (Weng 1984). Using this idea,

$$\sigma_k = \bar{\sigma}_o + \tilde{\sigma} + \sigma_k^{pt} = \mathbf{L}_m\left(\bar{\varepsilon} + \tilde{\varepsilon} + \varepsilon_k^{pt} - \varepsilon_k^*\right) \qquad k=\{f,g\} \tag{3.5}$$

where

$$\varepsilon_k^{pt} = \mathbf{S}_k\varepsilon_k^* \tag{3.6}$$

and $\mathbf{S}_k$ is the Eshelby tensor (Eshelby 1957), the components of which are given in Appendix A.2 for circular, cylindrical inclusions. The Eshelby tensor is a function of the shape of the inclusion and the material properties of the matrix.

Using (3.6), equation (3.5) provides the average stress for each included (i.e. non-matrix) phase of the composite, namely,

$$\sigma_k = \sigma_o + \tilde{\sigma} + \sigma_k^{pt} = \mathbf{L}_m \left\{ \varepsilon + \tilde{\varepsilon} + \varepsilon_k^* (\mathbf{S}_k - \mathbf{I}) \right\} \qquad k=\{f,g\} \quad (3.7)$$

From consistency considerations, we must enforce that the sum of the volume average strains within the composite is equal the total resultant strain of the composite material, ε. Using (3.4), this condition yields

$$\varepsilon = \sum_k c_k \varepsilon_k = \sum_k c_k \left\{ \varepsilon + \tilde{\varepsilon} + \mathbf{S}_k \varepsilon_k^* \right\} = \varepsilon + \tilde{\varepsilon} + \sum_k c_k \mathbf{S}_k \varepsilon_k^* \qquad k=\{f,g,m\} \quad (3.8)$$

where ε and $\tilde{\varepsilon}$ are identical for all phases, the sum of all volume fractions is equal to unity (assuming zero void content), and the summation index *k* is over all phases within the composite. Note that by definition the transformation strain of the matrix ε_m^* is identically zero. Equating the first and last terms of (3.8), one can show that

$$\tilde{\varepsilon} = -\sum_k c_k \mathbf{S}_k \varepsilon_k^* \qquad k=\{f,g\} \quad (3.9)$$

Finally, it is necessary to evaluate the average phase strain, ε_k, of the included phases within the composite. Consider the slightly altered form of (3.7) using (3.4),

$$\sigma_k = \mathbf{L}_k \varepsilon_k = \mathbf{L}_m \left(\varepsilon + \tilde{\varepsilon} + \varepsilon_k^{pt} - \varepsilon_k^* \right) = \mathbf{L}_m \left(\varepsilon_k - \varepsilon_k^* \right) \qquad k=\{f,g\} \quad (3.10)$$

Solving this expression for ε_k,

$$\varepsilon_k = -\left(\mathbf{L}_k - \mathbf{L}_m \right)^{-1} \varepsilon_k^* \qquad k=\{f,g\} \quad (3.11)$$

Rewriting (3.4), and substituting appropriate expressions,

$$\varepsilon_k = \bar{\varepsilon} + \tilde{\varepsilon} + \varepsilon_k^{pt} = \bar{\varepsilon} + \tilde{\varepsilon} + \mathbf{S}_k \varepsilon_k^* \qquad k=\{f,g\} \quad (3.12)$$

$$\left(\frac{\mathbf{L}_m}{\mathbf{L}_k - \mathbf{L}_m}\right) \varepsilon_k^* = -\tilde{\varepsilon} - \sum_n c_n \mathbf{S}_n \varepsilon_n^* + \mathbf{S}_k \varepsilon_k^* \qquad k,n=\{f,g\} \quad (3.13)$$

$$\mathbf{S}_k \varepsilon_k^* + \left(\frac{\mathbf{L}_m}{\mathbf{L}_k - \mathbf{L}_m}\right) \varepsilon_k^* + \sum_n c_n \mathbf{S}_n \varepsilon_n^* = -\tilde{\varepsilon} \qquad k,n=\{f,g\} \quad (3.14)$$

Now define the strain-concentration tensor $\mathbf{A}_k$ such that it relates the uniform strain $\bar{\varepsilon}$ to the transformation strain of the *k*-th included (non-matrix) phase, ε_k^*,

$$\varepsilon_k^* = \mathbf{A}_k \bar{\varepsilon} \qquad k=\{f,g\} \quad (3.15)$$

Substitution into (3.14) yields

$$\left[\mathbf{S}_k + \left(\frac{\mathbf{L}_m}{\mathbf{L}_k - \mathbf{L}_m}\right)\mathbf{A}_k + \sum_n c_n \mathbf{S}_n \mathbf{A}_n\right] = -\mathbf{I} \qquad k,n=\{f,g\} \quad (3.16)$$

where *n* is a dummy variable summed over all included phases, and ***I*** is the fourth-order identity tensor. Solution of (3.16) provides the strain-concentration tensors $\mathbf{A}_f$ and $\mathbf{A}_g$ describing the strain state in the fiber and interphase regions, respectively.

Going back to (3.12), the strain in each of the included phases can be now be written as

$$\varepsilon_k = \left[\mathbf{I} - \sum_n c_n \mathbf{S}_n \mathbf{A}_n + \mathbf{S}_k \mathbf{A}_k\right] \qquad k,n=\{f,g\} \quad (3.17)$$

Averaging the stresses over all phases, starting with (3.5) and using (3.2) and (3.7),

$$\begin{aligned}\bar{\sigma} &= \sum_k c_k \sigma_k = \sum_k c_k \left(\sigma_o + \bar{\sigma} + \sigma_k^{pt}\right) \\ &= \sigma_o + \bar{\sigma} + \sum_k c_k \sigma_k^{pt} \qquad k=\{f,g,m\} \qquad (3.18) \\ &= \sigma_o - \mathbf{L}_m \sum_k c_k \mathbf{S}_k \varepsilon_k^* + \mathbf{L}_m \sum_k c_k \varepsilon_k^* (\mathbf{S}_k - \mathbf{I})\end{aligned}$$

where σ_o and $\bar{\sigma}$ are constant for all phases. Further simplifying (3.18), and using the constitutive law for the comparison material given in (3.1),

$$\begin{aligned}\bar{\sigma} = \mathbf{L}\bar{\varepsilon} &= \mathbf{L}_m \bar{\varepsilon} - \mathbf{L}_m \sum_k c_k \varepsilon_k^* \\ &= \mathbf{L}_m \bar{\varepsilon} - \mathbf{L}_m \sum_k c_k \mathbf{A}_k \bar{\varepsilon}\end{aligned} \qquad k=\{f,g\} \quad (3.19)$$

at which point the effective modulus of the composite, **L**, is found to be

$$\mathbf{L} = \mathbf{L}_m \left[\mathbf{I} - \sum_k c_k \mathbf{A}_k\right] \qquad k=\{f,g\} \quad (3.20)$$

In application, the determination of the strain concentration tensors in (3.16) is used with (3.20) to determine the effective modulus of a multiphase composite. This completes the derivation of the Mori-Tanaka for the determination of the effective modulus for a multiphase composite.

Once the effective modulus of the composite has been determined, one can determine the five transversely isotropic material properties. Assuming that the modulus is written in the standard contracted notation such that

$$\begin{aligned}\sigma_{11} &= \sigma_1, \sigma_{22} = \sigma_2, \sigma_{33} = \sigma_3 \\ \sigma_{23} &= \sigma_4, \sigma_{13} = \sigma_5, \sigma_{12} = \sigma_6\end{aligned} \qquad (3.21)$$

where the fibers are aligned in the 1-direction, five independent engineering constants can be determined as follows (Aboudi 1991):

$$
\begin{aligned}
E_A &= L_{11} - 2L_{12}^2/(L_{22}+L_{33}) \\
\nu_A &= L_{12}/(L_{22}+L_{23}) \\
\nu_T &= (L_{11}L_{23} - L_{12}^2)/(L_{11}L_{22} - L_{12}^2) \\
\mu_T &= L_{44} \\
\mu_A &= L_{66}
\end{aligned}
\tag{3.22}
$$

where E_A is the axial modulus, ν_A the axial Poisson's ratio, ν_T the transverse Poisson's ratio, μ_T the transverse shear modulus, and μ_A is the axial shear modulus. Assuming that the material is in a state of plane strain, the transverse Young's modulus is given by

$$
E_T = \frac{\sigma_{22}}{\varepsilon_{22}} = L_{22} - \frac{L_{23}^2}{L_{22}} \tag{3.23}
$$

Using the dynamic correspondence principle, the work of this section can readily be extended to viscoelastic materials by replacing elastic stiffness and compliance terms with the corresponding complex moduli terms. This extension will be discussed in Section 3.3.

3.2 Simplifications for Cylindrical Inclusions

The analysis in the preceding section is valid assuming that the inclusions are ellipsoidal regions. Weng (1990) showed that, for an elastic analysis of cylindrical inclusions, the Mori-Tanaka method will coincide with the Hashin-Shtrikman-Walpole upper (lower) bounds should the matrix be the hardest (softest) phase. Otherwise, the Mori-Tanaka method falls somewhere within these bounds.

Such an observation is powerful in that the Hashin-Shtrikman-Walpole bounds are algebraic expressions which can be evaluated directly, sidestepping the machinery of the Mori-Tanaka method described above. This is a particularly attractive feature when considering composites with multiple phases. In his paper Weng (1990) presents the solution for five transversely isotropic parameters of a multiphase cylindrical fibrous composite as follows,

$$k = \left[\sum_k c_k / (k_k + m_m)\right]^{-1} - m_m$$

$$l = \left[\sum_k c_k l_k / (k_k + m_m)\right] \cdot \left[\sum_k c_k / (k_k + m_m)\right]^{-1} \tag{3.24}$$

$$n = \sum_k c_k n_k + \left[\sum_k c_k l_k\right] \left[\sum_s c_s (l_s - l_k) / (k_s + m_m)\right] / (k_k + m_m) \Big/ \left[\sum_k c_k / (k_k + m_m)\right]$$

$$m = \left[\sum_k c_k / [m_k + m_m k_m / (k_m + 2m_m)]\right]^{-1} - m_m k_m / (k_m + 2m_m)$$

$$p = \left[\sum_k c_k / (p_k + p_m)\right]^{-1} - p_m$$

where the subscripts *k* and *s* refer to the corresponding phase property {f,g,m}, and subscript *m* refers to the matrix phase. Here *k* is the plain strain bulk modulus, *l* the transverse cross modulus and *n* the axial modulus under a uniaxial strain, *m* the transverse shear modulus, and *p* is the axial shear modulus. Once five independent transversely isotropic material parameters have been determined, one can derive auxiliary engineering constants (such as the transverse Young's modulus) using appropriate relationships.

Although this simplification is only valid in those instances where the matrix is the softest or the hardest of the composite phases, this situation is often relevant as the interphase typically has properties intermediate to those of the fiber and matrix. Evaluation of (3.24) simply requires the substitution of volume fractions and phase properties into the appropriate algebraic expressions, whereas (3.16) requires more advanced methods to determine the strain-concentration tensors $\mathbf{A}_k$ and the composite modulus $\mathbf{L}$. Thus the expressions of this section can be quite useful for the study of certain classes of composite systems.

3.3 EXTENSION FOR VISCOELASTIC MATERIALS

Using the correspondence principle introduced in Chapter 2 of this thesis, it is straightforward to extend the Mori-Tanaka solution for composites with viscoelastic constituent phases. Only the highlights of the extension will be shown here. It is first necessary to take the Laplace (or Fourier) transform of the tensor equation in (3.16), which is now rewritten as

$$\left[\bar{\mathbf{S}}_k^*(s) + \frac{\bar{\mathbf{L}}_m^*(s)}{\bar{\mathbf{L}}_k^*(s) - \bar{\mathbf{L}}_m^*(s)}\right]\mathbf{A}_k(s) - \sum_n c_n\, \bar{\mathbf{S}}_n^*(s)\mathbf{A}_n(s) = \mathbf{I} \qquad k=\{f,g\} \qquad (3.25)$$

where the standard notation for the transformed moduli is used, *n* is a dummy variable summed over all included phases (i.e. {f,g}), ***I*** is again the fourth-order identity tensor, and $\bar{\mathbf{S}}_k^*(s)$ are the transformed Eshelby tensors, evaluated by replacing the elastic moduli of the Eshelby tensor (given in Appendix A.2 for circular cylinders) with the corresponding transformed moduli. Once the strain-concentration factors $\mathbf{A}_k(s)$ have been determined within the transformed domain via (3.25), they can be used to find the effective transformed modulus of the viscoelastic composite, $\bar{\mathbf{L}}^*(s)$, via the Laplace transform of (3.20), which is given below

$$\bar{\mathbf{L}}^*(s) = \bar{\mathbf{L}}_m^*(s)\left[\mathbf{I} - \sum_k c_k\, \mathbf{A}_k(s)\right] \qquad k=\{f,g\} \quad (3.26)$$

Relations similar to (3.22) and (3.23) in Laplace space can then be used to determine the effective viscoelastic engineering constants for the composite. It should be noted that a procedure identical to that presented in this section can be undertaken using the Fourier transform rather than the Laplace transform. In this instance the effective viscoelastic engineering constants will be given in complex form.

Likewise, the simplification of the Mori-Tanaka method for cylindrical inclusions, which holds when the matrix material is either the hardest or the softest phase material, can also be extended for viscoelastic composites by a similar procedure. Specifically, one must replace the elastic moduli terms in (3.24) with the corresponding transformed moduli. The

expression for the plane-strain bulk modulus for a viscoelastic composite with multiple cylindrical inclusions could thus be written

$$\bar{k}^{*}(s) = \left[\sum_{k} c_k \Big/ \left\{\bar{k}_k^{*}(s) + \bar{m}_m^{*}(s)\right\}\right]^{-1} - \bar{m}_m^{*}(s) \qquad (3.27)$$

The other transversely isotropic effective properties of (3.24) can be rewritten in an analogous manner. Again, the Fourier transform can replace the Laplace transform in the discussion above, such that the effective properties of the composite will be in the complex form covered in Chapter 2.

4. ANALYTICAL INTERPHASE SOLUTION (BENVENISTE METHOD)

4.1 INTRODUCTION

Another micromechanical method has been proposed to evaluate the effective properties of a three phase elastic composite. This model can also be converted to a viscoelastic solution using the correspondence principle discussed earlier. Specifically, the model introduced by Benveniste et al. (1989) is concerned with the evaluation of the local fields of composites with coated inclusions. It is derived for a three phase composite consisting of an annular interphase surrounding a cylindrical fiber within a binding matrix. The solution for the transverse Young's modulus of the composite will be considered as the superposition of the two problems as shown in Figure 4.1; the solution for the axial shear modulus is considered in Section 4.6.

For this method the local stress fields in the fiber and matrix are approximated by those fields found when a *single* fiber-interphase inclusion is embedded in an infinite matrix medium subjected to appropriate far-field stresses. Particle interaction is described by the determination of the unknown average matrix stresses, a procedure similar to that used in the Mori-Tanaka method and described in detail below. Although the Benveniste paper presents this procedure for the determination of five transversely isotropic mechanical properties, we will only concentrate on the effective transverse Young's modulus, transverse shear modulus, and axial shear modulus of the composite. Other moduli for the composite are determined by considering different far-field loadings and will not be considered here. The interested reader is referred to the original work of Benveniste for the derivation of other composite properties.

4.2 AUXILIARY PROBLEMS FOR TRANSVERSE YOUNG'S MODULUS OF THE COMPOSITE

The first step of this procedure is to determine the average phase stresses in the fiber and interphase regions for a single fiber-interphase inclusion in an infinite matrix. This will be accomplished via analysis of appropriate *auxiliary problems*. The auxiliary problems necessary to determine the transverse Young's modulus of the three phase composite are shown in Figure 4.2; that necessary for the axial shear modulus is shown in Figure 4.3. The average stress fields of the included phases for each of these auxiliary problems will be determined. The derivation presented within this section will follow the original work of Benveniste (1989) and be valid for elastic phase materials. Once the field averages of the included phases in the auxiliary problems have been determined, the analysis proceeds to determine the average stresses in the matrix material, accounting for particle interaction as described later in this chapter. The extension of this model for viscoelastic materials, using the correspondence principle, will be given in Section 7 of this chapter.

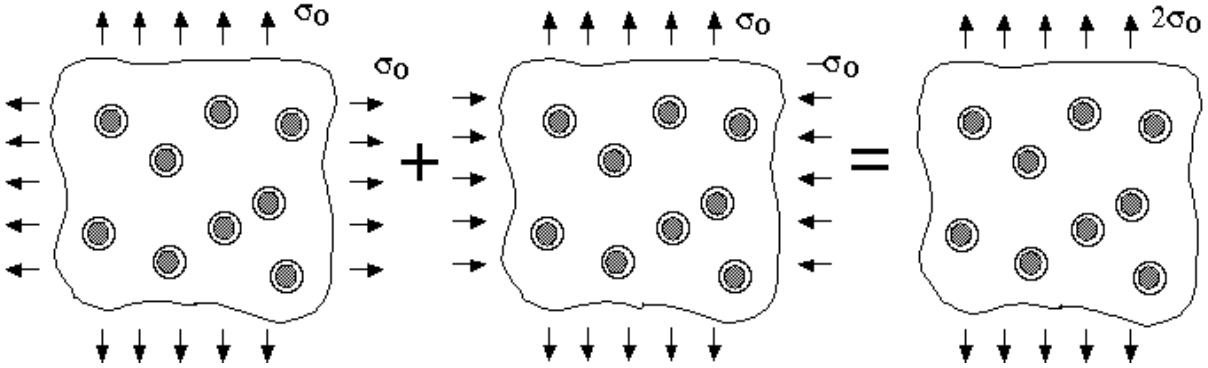

Figure 4.1. Superposition of transverse hydrostatic loading and transverse shear loading for the determination of the transverse Young's modulus.

4.3 TRANSVERSE HYDROSTATIC LOADING AUXILIARY PROBLEM

To solve for the effective transverse Young's modulus of the composite a superposition approach will be used, requiring solution of two separate loading problems as shown in Figure 4.1. The transverse hydrostatic auxiliary problem is shown in Figure 4.2a.

The three phase composite consists of a fiber (*f*) coated by an annular interphase region (*g*) and embedded in an infinite matrix (*m*). The areas of the included phases are given by

$$c_f = \pi a^2, \quad c_g = \pi(b^2 - a^2) \tag{4.1}$$

where *a* is the outer radius of the fiber, *b* is the outer radius of the interphase region, and r is the radius extending from an origin fixed at the center of the fiber.

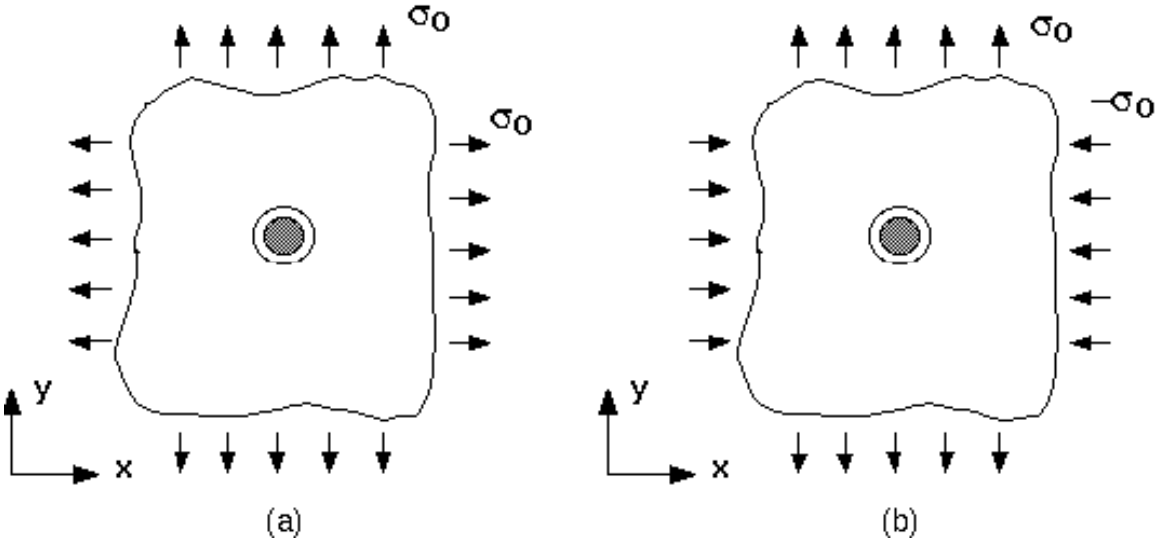

Figure 4.2. Auxiliary problems for the transverse Young's modulus. (a) Transverse hydrostatic loading. (b) Transverse shear loading.

Note that the following far-field boundary conditions exist for the auxiliary problem shown in Figure 4.2a,

$$\sigma_{xx}\big|_{r\to\infty} = \sigma_o \qquad \sigma_{yy}\big|_{r\to\infty} = \sigma_o \tag{4.2}$$

One can verify that this problem is axisymmetric. From standard elasticity theory, the only possible form which the displacements can take is the following (Timoshenko and Goodier 1970)

$$u_r^f = A_f r \ , \ u_r^g = A_g r + \frac{B_g}{r} \ , \ u_r^m = A_m r + \frac{B_m}{r} \tag{4.3}$$

where subscript *r* refers to radial displacements, superscripts refer to the respective phases, and A_k (k={f,g,m}) and B_k (k={g,m}) are unknown quantities which are determined via enforcement of the boundary conditions. All other displacements are identically zero. Throughout this section, arguments of the respective functions will be omitted for clarity unless required to avoid confusion.

The analysis then proceeds along the lines of a standard elasticity solution. The strain fields in each phase can be found from the strain-displacement relations. The only such relations which give non-zero strains for the displacement fields of (4.3) are

$$\varepsilon_{rr} = \frac{\partial u_r}{\partial r} \tag{4.4}$$

$$\varepsilon_{\theta\theta} = \frac{1}{r}\left(\frac{\partial u_\theta}{\partial \theta} + u_r\right)$$

Here we will assume a plane-strain analysis, implying the ε_{zz} strain components are zero. Applying these expressions to the phase displacements given in (4.3), the strain components in each phase can be written as

$$\varepsilon_{rr}^f = A_f \ , \ \varepsilon_{rr}^g = A_g - \frac{B_g}{r^2} \ , \ \varepsilon_{rr}^m = A_m - \frac{B_m}{r^2} \tag{4.5}$$

$$\varepsilon_{\theta\theta}^f = A_f \ , \ \varepsilon_{\theta\theta}^g = A_g + \frac{B_g}{r^2} \ , \ \varepsilon_{\theta\theta}^m = A_m + \frac{B_m}{r^2}$$

Given the strain fields in each phase, one can now use Hooke's Law, given below, to determine the stresses in each phase,

$$\sigma_{ij}^{k} = 2\mu^{k}\varepsilon_{ij}^{k} + \lambda^{k}\varepsilon_{nn}^{k}\delta_{ij} \qquad k=\{f,g,m\} \quad (4.6)$$

where δ_{ij} is the Kronecker function, repeated indices imply summation, and the superscript over the material property again denotes phase. Upon substitution, the stress fields in each phase can be written

$$\begin{aligned}
\sigma_{rr}^{f} &= 2\mu^{f} A_f + \lambda^{f}\left(2A_f\right) = 2A_f\left(\mu^{f} + \lambda^{f}\right) \\
\sigma_{rr}^{g} &= 2\mu^{g}\left[A_g - \frac{B_g}{r^2}\right] + \lambda^{g}\left(2A_g\right) = 2A_g\left(\mu^{g} + \lambda^{g}\right) - 2\mu^{g}\frac{B_g}{r^2} \\
\sigma_{rr}^{m} &= 2\mu^{m}\left[A_m - \frac{B_m}{r^2}\right] + \lambda^{m}\left(2A_m\right) = 2A_m\left(\mu^{m} + \lambda^{m}\right) - 2\mu^{m}\frac{B_m}{r^2}
\end{aligned} \quad (4.7)$$

$$\begin{aligned}
\sigma_{\theta\theta}^{f} &= 2\mu^{f} A_f + \lambda^{f}\left(2A_f\right) = 2A_f\left(\mu^{f} + \lambda^{f}\right) \\
\sigma_{\theta\theta}^{g} &= 2\mu^{g}\left[A_g + \frac{B_g}{r^2}\right] + \lambda^{g}\left(2A_g\right) = 2A_g\left(\mu^{g} + \lambda^{g}\right) + 2\mu^{g}\frac{B_g}{r^2} \\
\sigma_{\theta\theta}^{m} &= 2\mu^{m}\left[A_m + \frac{B_m}{r^2}\right] + \lambda^{m}\left(2A_m\right) = 2A_m\left(\mu^{m} + \lambda^{m}\right) + 2\mu^{m}\frac{B_m}{r^2}
\end{aligned} \quad (4.8)$$

In addition, invoking the assumption of plane strain leads to

$$\sigma_{zz}^{k} = \lambda^{k}\left(\varepsilon_{xx}^{k} + \varepsilon_{yy}^{k}\right) = \lambda^{k}\left(\varepsilon_{rr}^{k} + \varepsilon_{\theta\theta}^{k}\right) \qquad k=\{f,g,m\} \quad (4.9)$$

Now that the displacement and stress fields have been derived for each phase within the *auxiliary* problem, one can enforce suitable boundary conditions. Five boundary conditions will be required to determine the displacement constants. These conditions are given below,

$$
\begin{aligned}
u_r^f = u_r^g \;;\; \sigma_{rr}^f = \sigma_{rr}^g \qquad & \text{at } r = a \\
u_r^g = u_r^m \;;\; \sigma_{rr}^g = \sigma_{rr}^m \qquad & \text{at } r = b \\
\sigma_{rr}^m = \sigma_o \qquad & \text{as } r \to \infty \quad .
\end{aligned}
\tag{4.10}
$$

Inserting the displacement and stress expressions above into the boundary conditions of (4.10), one can solve the following system of equations for the unknown displacement constants in terms of σ_o, material properties, and geometry,

$$
\begin{aligned}
A_f\, a &= A_g\, a + \frac{B_g}{a} \\
A_g\, b + \frac{B_g}{b} &= A_m\, b + \frac{B_m}{b} \\
2\,A_f\left(\kappa^f + \mu^f\right) &= 2\,A_g\left(\kappa^g + \mu^g\right) - 2\mu^g\,\frac{B_g}{a^2} \\
2\,A_g\left(\kappa^g + \mu^g\right) - 2\mu^g\,\frac{B_g}{b^2} &= 2\,A_m\left(\kappa^m + \mu^m\right) - 2\mu^m\,\frac{B_m}{b^2} \\
2\,A_m\left(\kappa^m + \mu^m\right) &= \sigma_o
\end{aligned}
\tag{4.11}
$$

Solving (4.11) completes the determination of the fields associated with the transverse hydrostatic auxiliary problem of a *single* fiber-interphase inclusion embedded within an infinite matrix. Through substitution of these displacement constants , it is possible to solve for the phase-average stresses in the fiber and the interphase, using the expression

$$
\bar{\sigma}_{ij}^k = \frac{\int_0^{2\pi}\int_{r_i}^{r_o} \sigma_{ij}^k \cdot r \; dr\, d\theta}{\pi\left(r_o^2 - r_i^2\right)} \qquad k=\{f,g\} \tag{4.12}
$$

Following Benveniste (1989), one can now define scalar quantity stress-concentration factors W_{TT}^k (transverse direction) and W_{LT}^k (longitudinal direction) which

relate the far-field applied hydrostatic stress of the auxiliary problem to the corresponding phase-average stresses

$$\bar{\sigma}^k_{xx} = W^k_{TT}\,\sigma_o\,,\ \bar{\sigma}^k_{yy} = W^k_{TT}\,\sigma_o$$

$$\bar{\sigma}^k_{zz} = W^k_{LT}\,\sigma_o = 2\nu^k\,W^k_{TT}\,\sigma_o \qquad k=\{f,g\} \qquad (4.13)$$

where the overbars denote phase average stresses, superscript *k* refers to the appropriate phase, and σ_o is the hydrostatic stress applied to the auxiliary geometry of Figure 4.2a. The solution for the stress-concentration factors of the included phases given in (4.13) can be written explicitly as

$$W^f_{TT} = \frac{2A_f}{\sigma_o}\left(\nu^f + \nu^f\right),\ W^f_{LT} = \frac{2A_f\,\nu^f}{\sigma_o} \qquad (4.14)$$

$$W^g_{TT} = \frac{2A_g}{\sigma_o}\left(\nu^g + \nu^g\right),\ W^g_{LT} = \frac{2A_g\,\nu^g}{\sigma_o} \qquad (4.15)$$

These stress-concentration factors, which relate the average phase stresses for the transverse loading *auxiliary* problem, will be used in Section 5 of this chapter to determine the effective transverse Young's modulus of the composite.

4.4 TRANSVERSE SHEAR LOADING AUXILIARY PROBLEM

Now consider the auxiliary problem of Figure 4.2b. Given the geometry considered in the previous section, one can directly write the forms of the phase displacements. These displacements, found via the solutions of equations of equilibrium, are given as (Christensen and Lo 1979; Benveniste, Dvorak et al. 1989)

$$u_r^f = \frac{b\tau_o}{4\mu^f}\left[a_1\left(\kappa^f - 3\right)\left(\frac{r}{b}\right)^3 + d_1\left(\frac{r}{b}\right)\right]\cos 2\theta$$

$$0 \le r \le a \qquad (4.16)$$

$$u_\theta^f = \frac{b\tau_o}{4\mu^f}\left[a_1\left(\kappa^f + 3\right)\left(\frac{r}{b}\right)^3 - d_1\left(\frac{r}{b}\right)\right]\sin 2\theta$$

$$u_r^g = \frac{b\tau_o}{4\mu^g}\left[a_2\left(\kappa^g - 3\right)\left(\frac{r}{b}\right)^3 + d_2\left(\frac{r}{b}\right) + c_2\left(\kappa^g + 1\right)\left(\frac{b}{r}\right) + b_2\left(\frac{b}{r}\right)^3\right]\cos 2\theta$$

$$a \le r \le b \qquad (4.17)$$

$$u_\theta^g = \frac{b\tau_o}{4\mu^g}\left[a_2\left(\kappa^g + 3\right)\left(\frac{r}{b}\right)^3 - d_2\left(\frac{r}{b}\right) - c_2\left(\kappa^g - 1\right)\left(\frac{b}{r}\right) + b_2\left(\frac{b}{r}\right)^3\right]\sin 2\theta$$

$$u_r^m = \frac{b\tau_o}{4\mu^m}\left[2\left(\frac{r}{b}\right) + \left(\kappa^m + 1\right)a_3\left(\frac{b}{r}\right) + c_3\left(\frac{b}{r}\right)^3\right]\cos 2\theta$$

$$r \ge b \qquad (4.18)$$

$$u_\theta^m = \frac{b\tau_o}{4\mu^m}\left[2\left(\frac{r}{b}\right) - \left(\kappa^m - 1\right)a_3\left(\frac{b}{r}\right) + c_3\left(\frac{b}{r}\right)^3\right]\sin 2\theta$$

where all other displacements are equal to zero, and

$$\kappa^k = 3 - 4\mu^k \qquad k=\{f,g,m\} \qquad (4.19)$$

The displacement equations (4.16)-(4.18) contain eight unknown displacement constants, namely, $\{a_1, d_1, a_2, b_2, c_2, d_2, a_3, c_3\}$. To determine these constants the appropriate boundary conditions again must be satisfied. These eight boundary conditions for the case of a transverse shear loading are as follows:

$$u_r^f = u_r^g ; u_\theta^f = u_\theta^g \qquad \text{at r=a}$$
$$u_r^g = u_r^m ; u_\theta^g = u_\theta^m \qquad \text{at r=b} \qquad (4.20)$$

$$\sigma_{rr}^f = \sigma_{rr}^g ; \sigma_{r\theta}^f = \sigma_{r\theta}^g \qquad \text{at r=a}$$
$$\sigma_{rr}^g = \sigma_{rr}^m ; \sigma_{r\theta}^g = \sigma_{r\theta}^m \qquad \text{at r=b}$$

Since the procedure to determine the displacement constants is analogous to that described in the previous section, it will only be briefly highlighted here. The necessary strain-displacement relations are given below,

$$\varepsilon_{rr} = \frac{\partial u_r}{\partial r}$$

$$\varepsilon_{r\theta} = \frac{1}{2}\left[r\frac{\partial}{\partial r}\left(\frac{u_\theta}{r}\right) + \frac{1}{r}\frac{\partial u_r}{\partial \theta} \right] \qquad (4.21)$$

$$\varepsilon_{\theta\theta} = \frac{1}{r}\left[\frac{\partial u_\theta}{\partial \theta} + u_r \right]$$

Once the strains in each phase are determined, Hooke's Law is employed to determine the stresses in each phase. After lengthy manipulations, the stresses in each phase can be written as

$$\sigma_{rr}^f = F^f\left[-2\sigma^f\left(\frac{3a_1(\sigma^f - 3)r^2}{b^3} + \frac{d_1}{b} \right) + \sigma^f\left(\frac{6a_1(\sigma^f - 1)r^2}{b^3} \right)\cos 2\theta \right]$$
$$\sigma_{\theta\theta}^f = F^f\left[-2\sigma^f\left(\frac{3a_1(\sigma^f + 1)r^2}{b^3} - \frac{d_1}{b} \right) + \sigma^f\left(\frac{6a_1(\sigma^f - 1)r^2}{b^3} \right)\cos 2\theta \right] \qquad (4.22)$$
$$\sigma_{r\theta}^f = F^f\left[-2\sigma^f\left(\frac{6a_1 r^2}{b^3} - \frac{d_1}{b} \right)\sin 2\theta \right]$$

$$\sigma_{rr}^{g} = F^{g}\cos 2\theta\left[-2\nu^{g}\left(\frac{3a_2\left(\nu^{g}-3\right)r^2}{b^3}+\frac{d_2}{b}-\frac{c_2\left(\nu^{g}+1\right)b}{r^2}-\frac{3b_2 b^3}{r^4}\right)\right.$$
$$\left.+\left(\frac{6a_2\left(\nu^{g}-1\right)r^2}{b^3}-\frac{2c_2\left(\nu^{g}-1\right)b}{r^2}\right)\right]$$

$$\sigma_{\theta\theta}^{g} = F^{g}\cos 2\theta\left[2\nu^{g}\left(\frac{3a_2\left(\nu^{g}+1\right)r^2}{b^3}-\frac{d_2}{b}+\frac{c_2\left(3-\nu^{g}\right)b}{r^2}+\frac{3b_2 b^3}{r^4}\right)\right.$$
$$\left.+\left(\frac{6a_2\left(\nu^{g}-1\right)r^2}{b^3}-\frac{2c_2\left(\nu^{g}-1\right)b}{r^2}\right)\right] \qquad (4.23)$$

$$\sigma_{r\theta}^{g} = F^{g}\sin 2\theta\left[2\nu^{g}\left(\frac{6a_2 r^2}{b^3}-\frac{d_2}{b}-\frac{2c_2 b}{r^2}-\frac{3b_2 b^3}{r^4}\right)\right]$$

$$\sigma_{rr}^{m} = F^{m}\cos 2\theta\left[2\nu^{m}\left(\frac{2}{b}-a_3\frac{\left(\nu^{m}+1\right)b}{r^2}-\frac{3c_3 b^3}{r^4}\right)+\nu^{m}\left(\frac{2a_3\left(1-\nu^{m}\right)b}{r^2}\right)\right]$$

$$\sigma_{\theta\theta}^{m} = F^{m}\cos 2\theta\left[2\nu^{m}\left(\frac{2}{b}+a_3\frac{\left(3-\nu^{m}\right)b}{r^2}+\frac{3c_3 b^3}{r^4}\right)+\nu^{m}\left(\frac{2a_3\left(1-\nu^{m}\right)b}{r^2}\right)\right] \qquad (4.24)$$

$$\sigma_{r\theta}^{m} = F^{m}\sin 2\theta\left[2\nu^{m}\left(\frac{2}{b}-\frac{2a_3 b}{r^2}-\frac{3c_3 b^3}{r^4}\right)\right]$$

where

$$F^{k} = \frac{b\sigma_o}{4\mu^{k}} \qquad k=\{f,g,m\} \qquad (4.25)$$

Plugging the suitable displacement and stress expressions into the boundary conditions of (4.20), one has the system of eight equations given below with which to determine the eight unknown displacement constants (where α=b/a):

$$\alpha^g\left[a_1\left(\alpha^f-3\right)+d_1\alpha^2\right]=\alpha^f\left[a_2\left(\alpha^g-3\right)+d_2\alpha^2+c_2\left(\alpha^g+1\right)\alpha^4+b_2\alpha^6\right]$$

$$\alpha^g\left[a_1\left(\alpha^f+3\right)-d_1\alpha^2\right]=\alpha^f\left[a_2\left(\alpha^g+3\right)-d_2\alpha^2-c_2\left(\alpha^g-1\right)\alpha^4+b_2\alpha^6\right]$$

$$\alpha^m\left[a_2\left(\alpha^g-3\right)+d_2+c_2\left(\alpha^g+1\right)+b_2\right]=\alpha^g\left[2+a_3\left(\alpha^m+1\right)+c_3\right]$$

$$\alpha^m\left[a_2\left(\alpha^g+3\right)-d_2-c_2\left(\alpha^g-1\right)+b_2\right]=\alpha^g\left[-2-a_3\left(\alpha^m-1\right)+c_3\right] \qquad (4.26)$$

$$2\alpha^g\alpha^f\left\{3a_1\left(\alpha^f-3\right)+d_1\alpha^2\right\}+\alpha^g\alpha^f\left\{6a_1\left(\alpha^f-1\right)\right\}=2\alpha^g\alpha^f$$

$$\alpha\left\{3a_2\left(\alpha^g-3\right)+d_2\alpha^2-c_2\left(\alpha^g+1\right)\alpha^4-3b_2\alpha^6\right\}+$$
$$\alpha^f\alpha^g\left\{6a_2\left(\alpha^g-1\right)-2c_2\left(\alpha^g-1\right)\alpha^4\right\}$$

$$6a_1-d_1\alpha^2=6a_2-d_2\alpha^2-2c_2\alpha^4-3b_2\alpha^6$$

$$2\alpha^m\alpha^g\left\{3a_2\left(\alpha^g-3\right)+d_2-c_2\left(\alpha^g+1\right)-3b_2\right\}+\alpha^m\alpha^g\left\{6a_2\left(\alpha^g-1\right)-2c_2\left(\alpha^g-1\right)\right\}=$$
$$2\alpha^m\alpha^g\left\{-2-a_3\left(\alpha^m+1\right)-3c_3\right\}+\alpha^g\alpha^m\left\{2a_3\left(1-\alpha^m\right)\right\}$$

$$6a_2-d_2-2c_2-3b_2=-2-2a_3-3c_3$$

These stress fields can be converted to Cartesian coordinates via

$$\sigma^k_{xx}=\sigma^k_{rr}\cos^2\theta+\sigma^k_{\theta\theta}\sin^2\theta-2\sigma^k_{r\theta}\sin\theta\cos\theta$$
$$\sigma^k_{yy}=\sigma^k_{rr}\sin^2\theta+\sigma^k_{\theta\theta}\cos^2\theta+2\sigma^k_{r\theta}\sin\theta\cos\theta \qquad k=\{f,g,m\} \quad (4.27)$$
$$\sigma^k_{xy}=(\sigma^k_{rr}-\sigma^k_{\theta\theta})\sin\theta\cos\theta+\sigma^k_{r\theta}(\cos^2\theta-\sin^2\theta)$$

As an additional check, one can verify algebraically that the following condition is satisfied,

$$\sigma^m_{xx}\,l_{r\theta}=-\sigma_o, \qquad \sigma^m_{yy}\,l_{r\theta}=\sigma_o \qquad (4.28)$$

Similar to the procedure of the preceding section, one is now in a position to define stress-concentration scalars, W_{TS}^{k}, which relate the phase-average stresses in the included phases to the far-field applied stress, σ_o,

$$\bar{\sigma}_{xx}^{k} = \nu W_{TS}^{k} \sigma_o, \quad \bar{\sigma}_{yy}^{k} = W_{TS}^{k} \sigma_o \qquad k=\{f,g\} \qquad (4.29)$$

Explicit expressions for these factors are given below,

$$W_{TS}^{f} = \nu \frac{3a_1 a^2}{2b^2} + \frac{d_1}{2} \qquad (4.30)$$

$$W_{TS}^{g} = \nu \frac{3a_2 (b^2 + a^2)}{2b^2} + \frac{d_2}{2} \qquad (4.31)$$

Now that the stress-concentration factors, relating the applied far-field stress to the average stresses in the included phases, have been determined for the transverse shear loading auxiliary problem, we are ready to consider the superposition of the two auxiliary problems. This will be the topic of the next section.

4.5 THE EFFECTIVE TRANSVERSE YOUNG'S MODULUS OF THE COMPOSITE

We have analyzed the auxiliary problems of Figure 4.2 in the previous two sections and are now prepared to superpose the solutions. Using the definitions of the stress-concentration factors given in (4.14)-(4.15) and (4.30)-(4.31), and further assuming that the far-field stress which the fiber-interphase inclusion will experience will be the average stress in the matrix phase, $\bar{\sigma}_{yy}^{m}$, the average stress components in the fiber and interphase region of the *composite* can be written as

$$\bar{\sigma}_{yy}^{k} = \left(W_{TT}^{k} + W_{TS}^{k}\right)\bar{\sigma}_{yy}^{m} \qquad k=\{f,g\} \qquad (4.32)$$

$$\bar{\sigma}_{xx}^{k} = \left(W_{TT}^{k} - W_{TS}^{k}\right)\bar{\sigma}_{yy}^{m} \qquad k=\{f,g\} \qquad (4.33)$$

$$\bar{\sigma}_{zz}^{k} = W_{LT}^{k} \bar{\sigma}_{yy}^{m} \qquad k=\{f,g\} \qquad (4.34)$$

Enforcing that the sum of the average phase stresses in the y-direction must equal the applied far-field stress, $2\Sigma_o$, due to the superposition of the auxiliary problems (see Figure 4.1), yields

$$\begin{aligned} 2\Sigma_o &= \sum_k c_k \bar{\sigma}^k_{yy} = c_m \bar{\sigma}^m_{yy} + c_f \bar{\sigma}^f_{yy} + c_g \bar{\sigma}^g_{yy} \\ &= c_m \bar{\sigma}^m_{yy} + c_f \left(W^f_{TT} + W^f_{TS}\right)\bar{\sigma}^m_{yy} + c_g \left(W^g_{TT} + W^g_{TS}\right)\bar{\sigma}^m_{yy} \end{aligned} \qquad k=\{f,g,m\} \qquad (4.35)$$

where c_f and c_g are the normalized areas of the included phases and $c_m = 1 - c_f - c_g$. Solving for the average y-component of matrix stress in the composite material,

$$\bar{\sigma}^m_{yy} = \frac{2\Sigma_o}{c_m + c_f \left(W^f_{TT} + W^f_{TS}\right) + c_g \left(W^g_{TT} + W^g_{TS}\right)} \qquad (4.36)$$

Likewise, the average x-component of stress in the matrix can be found by enforcing that the overall average stress in this direction equal zero,

$$\bar{\sigma}^m_{xx} = -\frac{c_f \left(W^f_{TT} - W^f_{TS}\right) + c_g \left(W^g_{TT} - W^g_{TS}\right)}{c_m} \bar{\sigma}^m_{yy} \qquad (4.37)$$

Assuming plane strain loading conditions, the average phases stresses in the z-direction are

$$\bar{\sigma}^k_{zz} = \nu^k \left(\bar{\sigma}^k_{xx} + \bar{\sigma}^k_{yy}\right) \qquad k=\{f,g,m\} \qquad (4.38)$$

We are now in a position to evaluate the transverse Young's modulus of the composite. Consider the expression

$$\Sigma_{yy} = \frac{\bar{\Sigma}_{yy}}{E^T} = \sum_k c_k \bar{\varepsilon}^k_{yy} \qquad (4.39)$$

where ε_{yy} is the overall composite strain in the y-direction, $\bar{\sigma}_{yy}$ is the applied far-field stress in the same direction, and E^T is the effective transverse Young's modulus of the composite. For the superposition problem considered here, $\bar{\sigma}_{yy} = 2\sigma_o$ such that (4.39) can be rewritten

$$\frac{2\sigma_o}{E^T} = c_f \bar{\sigma}^f_{yy} + c_g \bar{\sigma}^g_{yy} + c_m \bar{\sigma}^m_{yy} \tag{4.40}$$

Since all phase average stresses have now been determined, the average strain in the phases can be found using Hooke's Law,

$$\bar{\varepsilon}^k_{yy} = \frac{1}{2\mu^k}\left\{\bar{\sigma}^k_{yy} - \nu^k\left(\bar{\sigma}^k_{xx} + \bar{\sigma}^k_{yy} + \bar{\sigma}^k_{zz}\right)\right\} \qquad k=\{f,g,m\} \tag{4.41}$$

where ν^k are the poisson ratios of the isotropic phase materials. Appropriate substitution into the two expressions above, using the average phase stresses, allows for the numerical calculation of the transverse Young's modulus of the composite. This expression is too unwieldy to present in its algebraic form.

As a final note, Benveniste uses the stress-concentration scalars determined previously to calculate the effective transverse shear modulus, μ^T, of the composite. Following a procedure similar to that of this section, the transverse shear modulus of the composite can be written (Benveniste, Dvorak et al. 1989),

$$\frac{1}{2\mu^T} = \frac{c_m \frac{1}{2\mu^m} + c_f \frac{1}{2\mu^f} W^f_{TS} + c_g \frac{1}{2\mu^g} W^g_{TS}}{c_m + c_f W^f_{TS} + c_g W^g_{TS}} \tag{4.42}$$

4.6 THE EFFECTIVE AXIAL SHEAR MODULUS OF THE COMPOSITE

A similar, albeit easier, derivation will yield the axial (or longitudinal) shear modulus of a three phase composite. Because it follows a procedure identical to that of the preceding sections, only an abbreviated presentation will follow.

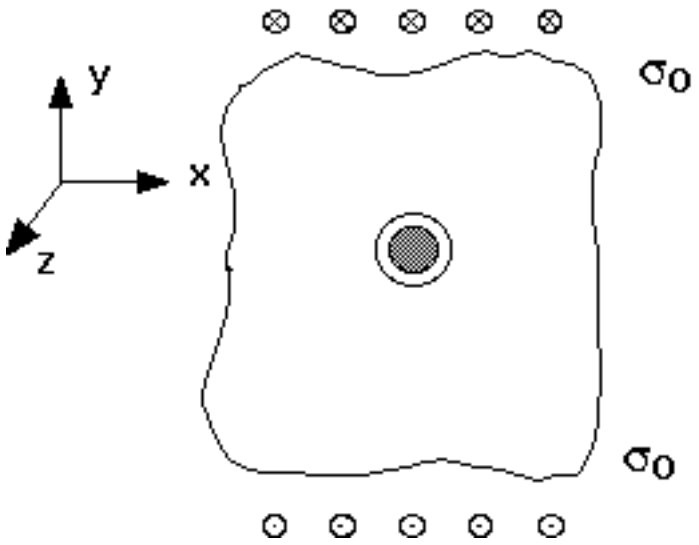

Figure 4.3. Auxiliary geometry for the axial shear modulus.

First, consider the associated auxiliary problem of Figure 4.3. A suitable displacement field for the auxiliary problem can be written as

$$u_z^f = A_f\, r \sin\theta \tag{4.43}$$

$$u_z^g = \left(A_g\, r + \frac{B_g}{r}\right)\sin\theta \tag{4.44}$$

$$u_z^m = \left(A_m\, r + \frac{B_m}{r}\right)\sin\theta \tag{4.45}$$

where all other displacements are equal to zero. The five constants in the above displacement equations can be determined by enforcing continuity of the u_z displacements

and the σ_{rz} stresses at the interfaces r=a and r=b, as well as the far-field condition that $\sigma_{yz}=\sigma_o$ as *r* tends towards infinity. Similar to the preceding sections, we seek to develop a relationship between the far-field applied stress, σ_o, and the phase-average stresses in the auxiliary problem, namely,

$$\bar{\sigma}_{yz}^{k} = W_{LS}^{k}\,\sigma_o \qquad k=\{f,g\} \tag{4.46}$$

The following expression will be necessary to convert from cylindrical to Cartesian stress components,

$$\sigma_{yz} = \sigma_{rz}\sin\theta + \sigma_{\theta z}\cos\theta \tag{4.47}$$

Following the outline of earlier sections, the stress-concentration factors W_{LS}^{k} of (4.46) can be determined explicitly,

$$W_{LS}^{f} = \frac{\bar{\sigma}^{f} A_f}{\sigma_o}\,,\; W_{LS}^{g} = \frac{\bar{\sigma}^{g} A_g}{\sigma_o} \tag{4.48}$$

It can be shown that the unknown average matrix stress can written as

$$\bar{\sigma}_{yz}^{m} = \frac{\sigma_o}{c_m + c_f W_{LS}^{f} + c_g W_{LS}^{g}} \tag{4.49}$$

Using this unknown average matrix stress, along with the stress-concentration factors given in (4.48), it then follows that the effective axial shear modulus of the composite is

$$\mu_A = \frac{c_m + c_f W_{LS}^{f} + c_g W_{LS}^{g}}{\dfrac{c_m}{\mu^{m}} + \dfrac{c_f W_{LS}^{f}}{\mu^{f}} + \dfrac{c_g W_{LS}^{g}}{\mu^{g}}} \tag{4.50}$$

4.7 ADAPTATION FOR VISCOELASTICITY

The formulation of this analytical solution for a three-phase composite with a finite interphase, derived by Benveniste for elastic materials, can be extended to viscoelastic materials using the correspondence principle. Similar to Chapter 3.3, this method will only be highlighted here.

It is first necessary to determine the unknown displacement constants for each of the auxiliary problems, described in Sections 4.3, 4.4, and 4.6 of this thesis, by satisfying the appropriate boundary conditions. To use these equations in the transformed domain it will be necessary to replace all elastic phase moduli by the corresponding complex moduli as discussed in Chapter 2 of this thesis. In the Fourier domain, this will cause the displacement constants to be complex in nature. Standard math packages (such as Matlab) which permit complex algebra should suffice to solve for these unknown parameters.

Once the displacement constants have been determined, one can proceed directly to the definitions of the stress-concentration factors (i.e. W_{TT}^{k}, W_{LT}^{k}, etc.) presented in this chapter. Simply substitute the complex phase moduli for the elastic phase moduli given in these formulas. These stress-concentration factors may also be complex in the Fourier domain. Completing the final steps of Sections 4.5 and 4.6, the effective moduli of the viscoelastic composite will be given in complex form, where the real and imaginary components are the storage and loss moduli as presented in Chapter 2. The results of this formulation will be presented in Chapter 6.

5. FINITE ELEMENT ANALYSIS

5.1 INTRODUCTION

A detailed finite element analysis (FEA) was undertaken on the unit cell models of Figures 5.1 and 5.2. The mesh was continually refined until a convergent solution was found. An hexagonal array of inclusions was used for the FEA to provide the exact numerical solution for a transversely isotropic composite. Although the analytical methods used in this thesis assume a random array of inclusions, the overall composite medium in these models also acts as a transversely isotropic material; thus we believe that comparisons between the micromechanical models and the FEA are warranted. Although stress fields and related localized phenomena (such as plasticity and failure initiation) are very dependent on the inclusion arrangement, it has been shown that the effective properties of composite materials are largely independent of inclusion packing (Ostoja-Starzewski, Alzebdeh et al. 1995). The results of this section will provide a baseline by which the accuracy of the two micromechanical methods presented earlier in this thesis may be judged.

Because it is assumed that the reader is familiar with the finite element method for elastic materials, this chapter will only focus on those changes necessary to modify an elastic finite element code for use with a viscoelastic boundary value problem. Haoran and co-workers (1995) have used the self-consistent method of Benveniste to develop an interphase element for use in an elastic self-consistent finite element analysis. This was done to prevent numerical difficulties which may arise if the interphase is sufficiently stiff. Since such difficulties were not encountered here, these special interphase elements were not used in this thesis. Other interphase elements have been developed to model imperfect bonding between phases (Gosz, Moran et al. 1991).

The Finite Element Analysis Package (FEAP), developed at Berkeley (Taylor 1982) and later modified at Brown University, was used for this work. It was chosen because it is an academic package with an available source code; it is written in a segmented structure which allows for straightforward modification of the program. The FEA work done in this

thesis extends the work of Brinson and co-workers (Brinson 1990; Brinson and Knauss 1992; Brinson and Lin 1998) for two phase viscoelastic materials.

Meshing was done using the FASTQ mesh generation program. The output from this program was input into FEAP for the numerical calculations. The mesh was continuously refined until the convergence of the FEA solution was established. A sample mesh can be found in Appendix A.1.

5.2 Finite Element Formulation for Viscoelastic Analysis

Consider the two-dimensional unit cell analysis of a three phase composite consisting of a circular fiber surrounded by an annular interphase and embedded in a matrix. Perfect bonding is assumed between phases. The unit cells are shown in Figures 5.1 and 5.2 for cases of transverse normal and transverse shear loading, respectively. The boundary conditions placed on these unit cells are given in (5.15) and (5.19). For these models the fiber-interphase inclusions are arranged in a hexagonal array, as is appropriate to represent the transversely isotropic behavior of the composite material (Lin 1996). Whereas the fiber is an isotropic, elastic material, the matrix and interphase materials may be viscoelastic in nature, as outlined in Chapter 2.

Analogous to an elastic FEA, we wish to write the equilibrium equations for the viscoelastic formulation in the form

$$\left[\overline{\mathbf{K}}\right]^{e} \overline{\mathbf{u}} + \overline{\mathbf{f}} = 0 \tag{5.1}$$

where $\left[\overline{\mathbf{K}}\right]^{e}$ represents the transformed element stiffness matrix, $\overline{\mathbf{u}}$ is a vector containing nodal displacements, $\overline{\mathbf{f}}$ is the vector of nodal forces, and $(\overline{\bullet})$ denotes the transformed quantities discussed below.

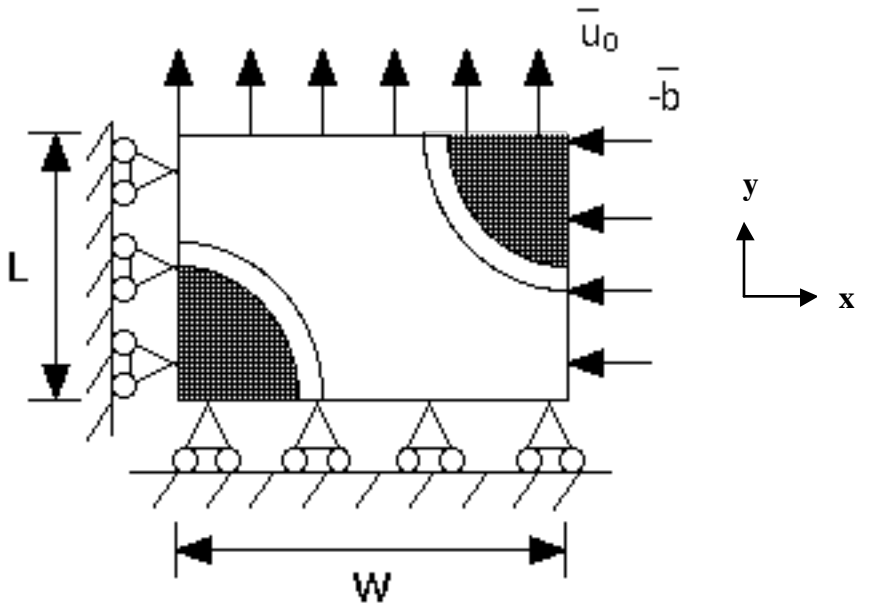

Figure 5.1. Unit cell analysis of a three-phase composite – transverse Young's modulus.

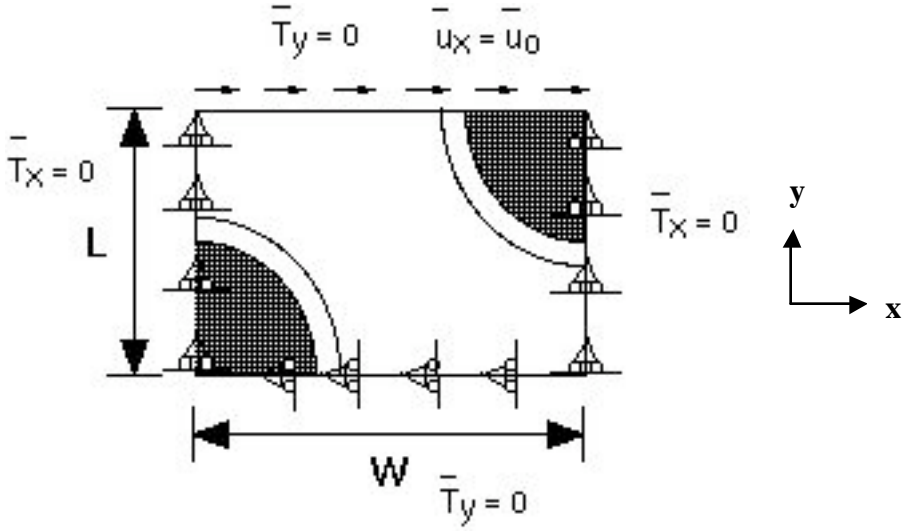

Figure 5.2. Unit cell analysis of a three-phase composite – transverse shear modulus.

We will assume that the time-dependent displacements can be written in separable form as

$$\mathbf{u}_i(\mathbf{x},t) = \hat{\mathbf{u}}_i(\mathbf{x},\omega)e^{i\omega t} \tag{5.2}$$

where **x** is the position vector. Taking the Fourier transform of (5.2) provides the transformed displacements

$$\bar{\mathbf{u}} = \hat{\mathbf{u}}_i(\mathbf{x},\omega) \tag{5.3}$$

The two-dimensional strain vector can be defined as

$$\bar{e} = [\mathbf{B}]\bar{\mathbf{u}} = \begin{Bmatrix} \bar{\varepsilon}_{11} \\ \bar{\varepsilon}_{22} \\ \bar{\varepsilon}_{33} \\ \bar{\varepsilon}_{23} \end{Bmatrix} \tag{5.4}$$

where $[\mathbf{B}]$ is a matrix comprised of the derivatives of the shape functions. As in the elastic formulation, defining the strain in this manner permits the elemental stiffness matrix of (5.1) to be defined as

$$\left[\bar{\mathbf{K}}\right]^e = \int_{V^e} [\mathbf{B}]^T \left[\bar{\mathbf{D}}\right][\mathbf{B}]\, dV^e \tag{5.5}$$

where V^e is the volume of the element. For a linear viscoelastic analysis one may write the governing constitutive equations

$$\bar{\sigma} = \left[\bar{\mathbf{D}}\right]\bar{\varepsilon} \tag{5.6}$$

where $\bar{\sigma}$ is the stress vector corresponding to the strain vector defined earlier.

It is now necessary to determine the form of $\left[\bar{\mathbf{D}}\right]$ above. The deviatoric (s_{ij}, e_{ij}) and dilitational (σ_{kk}, ε_{kk}) components of the stress and strain tensors were written in terms of time-dependent properties for viscoelastic materials in (2.2). Implementing the

correspondence principle, the transform of these equations in the Fourier domain are given below,

$$\bar{s}_{ij} = \bar{\sigma}_{ij} - \frac{1}{3}\bar{\sigma}_{kk}\delta_{ij}$$
$$\bar{e}_{ij} = \bar{\varepsilon}_{ij} - \frac{1}{3}\bar{\varepsilon}_{kk}\delta_{ij} \tag{5.7}$$

Further, given a linear, isotropic viscoelastic material, the constitutive laws of the phase materials can be written as

$$\bar{s}_{ij}(\omega) = 2i\omega\,\bar{G}(\omega)\bar{e}_{ij}$$
$$\bar{\sigma}_{kk}(\omega) = 3i\omega\,\bar{K}(\omega)\bar{\varepsilon}_{kk} \tag{5.8}$$

where $\bar{s}_{ij}$, $\bar{e}_{ij}$, $\bar{\sigma}_{kk}$, and $\bar{\varepsilon}_{kk}$ are the transformed stress and strain fields, and $\bar{G}(\omega)$ and $\bar{K}(\omega)$ are the half-sided Fourier transform of the shear and bulk moduli. For a more explicit derivation, please refer to Chapter 2.

The dilitational and deviatoric components of the stresses in (5.8) can be recombined using (5.7) to yield

$$\bar{\sigma}_{ij} = 2i\omega\,\bar{G}(\omega)\bar{\varepsilon}_{ij} + i\omega\left(\bar{K}(\omega) - \frac{2}{3}\bar{G}(\omega)\right)\bar{\varepsilon}_{kk}\delta_{ij} \tag{5.9}$$

Using (5.9), the constitutive law in (5.6) can now be written in the transformed domain as

$$\begin{bmatrix}\bar{\sigma}_{11}\\ \bar{\sigma}_{22}\\ \bar{\sigma}_{33}\\ \bar{\sigma}_{23}\end{bmatrix} = \begin{bmatrix} i\omega\left(\frac{4}{3}\bar{G}+\bar{K}\right) & i\omega\left(-\frac{2}{3}\bar{G}+\bar{K}\right) & i\omega\left(-\frac{2}{3}\bar{G}+\bar{K}\right) & 0\\ i\omega\left(-\frac{2}{3}\bar{G}+\bar{K}\right) & i\omega\left(\frac{4}{3}\bar{G}+\bar{K}\right) & i\omega\left(-\frac{2}{3}\bar{G}+\bar{K}\right) & 0\\ i\omega\left(-\frac{2}{3}\bar{G}+\bar{K}\right) & i\omega\left(-\frac{2}{3}\bar{G}+\bar{K}\right) & i\omega\left(\frac{4}{3}\bar{G}+\bar{K}\right) & 0\\ 0 & 0 & 0 & 2i\omega\bar{G}\end{bmatrix}\begin{bmatrix}\bar{\varepsilon}_{11}\\ \bar{\varepsilon}_{22}\\ \bar{\varepsilon}_{33}\\ \bar{\varepsilon}_{23}\end{bmatrix} \tag{5.10}$$

where the 4 x 4 matrix in (5.10), referred to as $\left[\bar{\mathbf{D}}\right]$, may be written in terms of real and imaginary components,

$$\left[\overline{\mathbf{D}}\right] = \left[\mathbf{D}\right]_{\mathrm{Re}} + \mathrm{i}\left[\mathbf{D}\right]_{\mathrm{Im}} \tag{5.11}$$

Upon substitution, the element stiffness matrix of (5.5) can now be written in the transformed domain as

$$\begin{aligned}\left[\overline{\mathbf{K}}\right]^{\mathrm{e}} &= \int_{V^{\mathrm{e}}} \left[\mathbf{B}\right]^{\mathrm{T}} \left[\overline{\mathbf{D}}\right]\left[\mathbf{B}\right] \mathrm{d}V^{\mathrm{e}} \\ &= \int_{V^{\mathrm{e}}} \left[\mathbf{B}\right]^{\mathrm{T}} \left\{\left[\mathbf{D}\right]_{\mathrm{Re}} + \mathrm{i}\left[\mathbf{D}\right]_{\mathrm{Im}}\right\}\left[\mathbf{B}\right] \mathrm{d}V^{\mathrm{e}} \\ &= \left[\hat{\mathbf{K}}\right]^{\mathrm{e}}_{\mathrm{Re}} + \mathrm{i}\left[\hat{\mathbf{K}}\right]^{\mathrm{e}}_{\mathrm{Im}}\end{aligned} \tag{5.12}$$

Note that **B** does *not* contain complex quantities. It is necessary, however, to reformat the **B** matrix in a manner different from an elastic analysis in order to account for the extra degrees of freedom required by the real and imaginary components of the other matrices.

Upon substitution of the above results into (5.1), one can now write the equilibrium equations in the transformed domain as

$$\left[\left[\hat{\mathbf{K}}\right]^{\mathrm{e}}_{\mathrm{Re}} + \mathrm{i}\left[\hat{\mathbf{K}}\right]^{\mathrm{e}}_{\mathrm{Im}}\right]\left\{\overline{\mathbf{u}}_{\mathrm{Re}} + \mathrm{i}\,\overline{\mathbf{u}}_{\mathrm{Im}}\right\} + \left\{\overline{\mathbf{f}}_{\mathrm{Re}} + \mathrm{i}\,\overline{\mathbf{f}}_{\mathrm{Im}}\right\} = \mathbf{0} \tag{5.13}$$

or, in matrix form,

$$\begin{bmatrix}\left[\hat{\mathbf{K}}\right]^{\mathrm{e}}_{\mathrm{Re}} & \left[\hat{\mathbf{K}}\right]^{\mathrm{e}}_{\mathrm{Im}} \\ \left[\hat{\mathbf{K}}\right]^{\mathrm{e}}_{\mathrm{Im}} & \left[\hat{\mathbf{K}}\right]^{\mathrm{e}}_{\mathrm{Re}}\end{bmatrix}\begin{Bmatrix}\overline{\mathbf{u}}_{\mathrm{Re}} \\ \overline{\mathbf{u}}_{\mathrm{Im}}\end{Bmatrix} + \begin{Bmatrix}\overline{\mathbf{f}}_{\mathrm{Re}} \\ \overline{\mathbf{f}}_{\mathrm{Im}}\end{Bmatrix} = \begin{Bmatrix}\mathbf{0} \\ \mathbf{0}\end{Bmatrix} \tag{5.14}$$

where the second row of (5.14) has been multiplied by (–1) so that the stiffness matrix is symmetric. Note that (5.14) is analogous to the elastic form of the FEA solution, except that the number of degrees of freedom have been doubled and quantities may be complex.

The FEAP code was modified in such a way to permit the solution of (5.14) for a series of frequencies (in the preceding derivation the dependence of the solution on the frequency ω was not written explicitly). The input procedure of the FEAP code was extended to allow for time-dependent material properties, and the dimensions of certain matrices were altered to account for complex quantities. Implementing the results of this section, a complete profile of various effective storage and loss moduli may now be determined over a wide range of frequencies.

The FEAP code was also modified to enable physical aging of the constituent phases of the composite, following the work of Chapter 2.4. This procedure was straightforward and will not be discussed here. The remaining two sections of this chapter discuss the specifics of modeling the transverse normal and transverse shear problems. Results obtained using these finite element models will be given in Chapter 6.

5.3 TRANSVERSE YOUNG'S MODULUS

The unit cell and boundary conditions necessary to model the transverse Young's modulus of the composite shown in Figure 5.1 are given below,

$$\begin{array}{lll} \bar{u}_x = 0 & \bar{T}_y = 0 & \text{on } x = 0 \\ \bar{u}_y = 0 & \bar{T}_x = 0 & \text{on } y = 0 \\ \bar{u}_x = \Delta\bar{b} & \bar{T}_y = 0 & \text{on } x = W \\ \bar{u}_y = \bar{u}_o + 0\,i & \bar{T}_x = 0 & \text{on } y = L \end{array} \qquad (5.15)$$

$$W = \sqrt{3}\,L$$

To modify the boundary conditions for the viscoelastic domain, replace the time-dependent boundary conditions $u_y = u_o e^{i\Omega t}$ and $u_x = \Delta b e^{i\Omega t}$ with the transformed boundary conditions $\bar{u}_y = \bar{u}_o$, $\bar{u}_x = \Delta\bar{b}$ as in Figure 5.1. Note that the second boundary condition, the prescribed displacement at x=W, will be used to ensure that the right hand side of the unit cell remains straight and parallel. For a hexagonal array, $W = \sqrt{3}\,L$.

The displacement $\bar{b}$ is chosen in an iterative fashion such that a suitable $\bar{b}$ is determined which satisfies the condition

$$\int_0^L \bar{T}_x \, dy = 0 \qquad \text{at } x=W \qquad (5.16)$$

where $\bar{T}_x$ are the resultant nodal tractions on the right hand side of the unit cell. First, an arbitrary displacement $\bar{b}$ is chosen and the resulting average $\bar{T}_x$ calculated. This value of $\bar{T}_x$ is then used to determine the value of $\bar{b}$ necessary such that (5.16) is satisfied. In general $\bar{b}$ will be complex. This provides boundary conditions which are consistent with those shown in Figure 5.1. Other methods which can be employed in order for the FEA to satisfy (5.16) are discussed in the literature (Brinson and Knauss 1992).

To determine the effective transverse Young's modulus of the composite, the average resulting normal stress, $\sigma_{y,ave}$, was obtained by summing the resultant nodal forces

at y=L and dividing by the area of the top face of the unit cell. The applied normal strain prescribed across the top face of the unit cell is given by

$$\varepsilon_y = \frac{\bar{u}_o}{L} \tag{5.17}$$

The effective complex transverse Young's modulus of the composite is then calculated as

$$\bar{E}^{T^*}(\omega) = i\omega \bar{E}(\omega) \equiv \frac{\sigma_{y,ave}}{\varepsilon_y} \tag{5.18}$$

5.4 TRANSVERSE SHEAR MODULUS

The unit cell necessary to model the transverse shear modulus of the composite is shown in Figure 5.2. The boundary conditions specified on this unit cell are given below (Brinson 1990),

$$\begin{aligned}
&\bar{u}_y = 0 && \bar{T}_x = 0 && \text{on } x = 0 \\
&\bar{u}_x = 0 && \bar{T}_y = 0 && \text{on } y = 0 \\
&\bar{u}_y = 0 && \bar{T}_x = 0 && \text{on } x = W \\
&\bar{u}_x = \bar{u}_o + 0\,i && \bar{T}_y = 0 && \text{on } y = L \\
&&& W = \sqrt{3}\,L
\end{aligned} \tag{5.19}$$

Solution of this problem is more straightforward in that it does not entail iteration to provide suitable boundary conditions. Applying a uniform displacement across the top face of the unit cell, the shear modulus is determined via

$$\bar{G}^{T^*}(\omega) = i\omega \bar{G}(\omega) \equiv \frac{\sigma_{xy,ave}}{\varepsilon_{xy}} \tag{5.20}$$

where $\sigma_{xy,ave}(\omega)$ is the sum of the resultant nodal forces along the top face of the unit cell in the x-direction divided by the width of the unit cell, and $\varepsilon_{xy} \equiv \frac{\bar{u}_o}{L}$.

6. RESULTS AND DISCUSSION

6.1 INTRODUCTION

The analytical models discussed in the previous sections were used to predict the effective behavior of composites as a function of the properties and volume fraction of the interphase. The results of the investigation will be presented below, along with a comparison of the results obtained from a finite element analysis following the outline of Chapter 5. Although it would be impractical to present every possible composite configuration in this thesis, these results should provide insight as to the ability of the analytical models to capture the mechanical behavior of the composites as predicted by the more extensive FE analysis.

6.2 APPROPRIATE USE OF BOUNDS FOR SOLUTIONS

The storage and loss components of the transverse Young's modulus of a composite consisting of 30% elastic fiber, 10% stiff interphase, and 60% soft matrix are shown in Figures 6.1 and 6.2. (Here and throughout this chapter, "stiff" (or "soft") refers to a constituent phase with materials properties of the "stiff" (or "soft") idealized polymers of Chapter 2.) Included in the figures are the standard Reuss and Voigt bounds (i.e. the Rule of Mixtures) for the given composite configuration. As one can see from Figure 6.2, the loss moduli solutions appear to violate these bounds at certain frequencies, particularly those intermediate of the high frequency (glassy) and low frequency (rubbery) domains. This behavior was typical of all of the material properties and composite configurations investigated in this thesis.

This apparent discrepancy is caused by the fact that these bounds are not in fact valid in the frequency domain. Schapery (1967) notes that, for composites with isotropic phase materials, the corresponding bounds from elasticity are valid on the "operational moduli" of the composite. These operational moduli are the analog of the complex moduli discussed in this thesis when the Laplace (rather than the Fourier) transform is

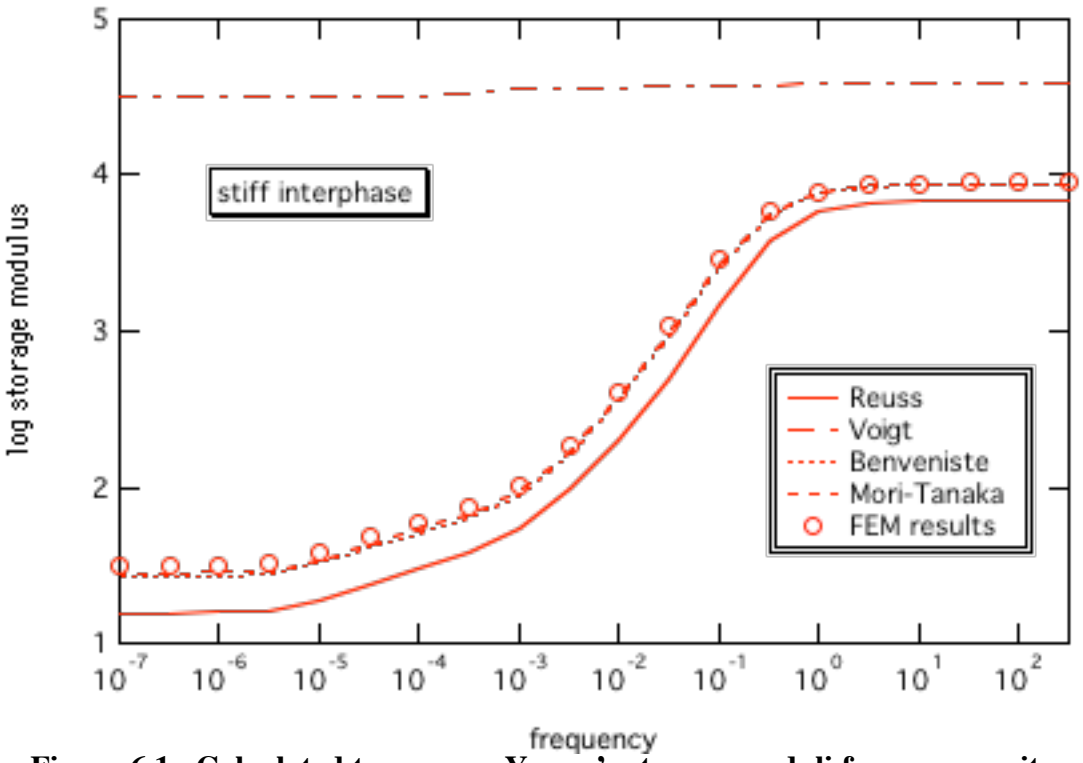

Figure 6.1. Calculated transverse Young's storage moduli for a composite with 30% elastic fiber, 10% stiff interphase, 60% soft matrix.

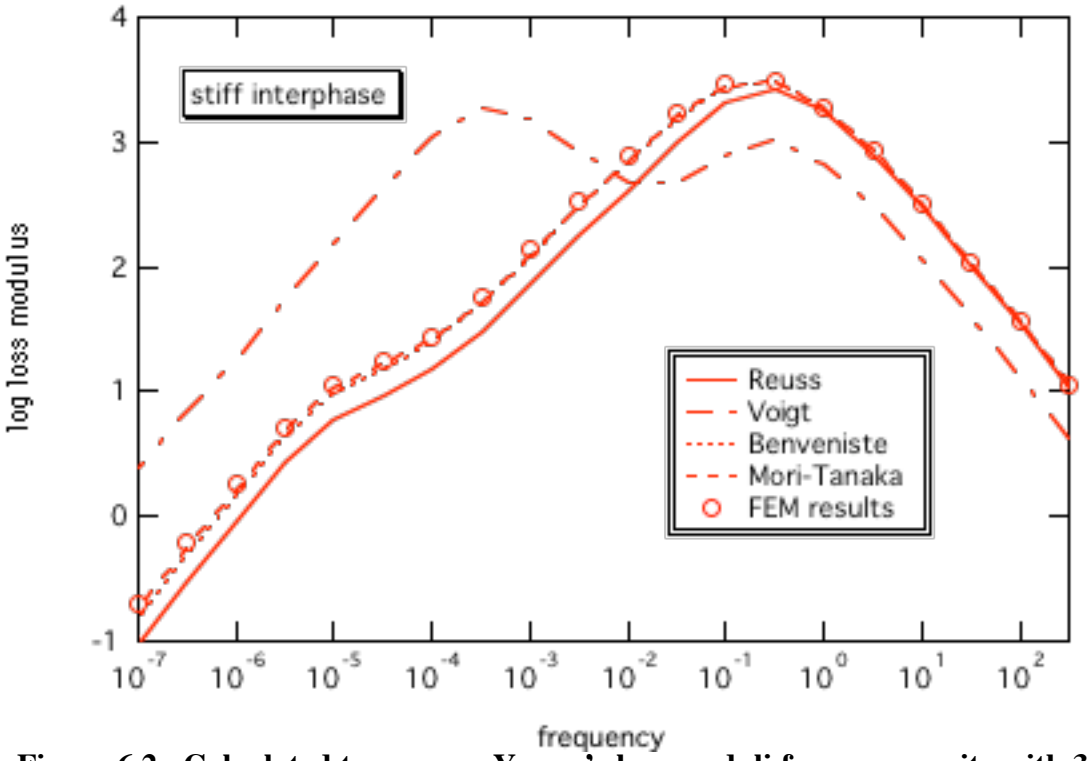

Figure 6.2. Calculated transverse Young's loss moduli for a composite with 30% elastic fiber, 10% stiff interphase, 60% soft matrix.

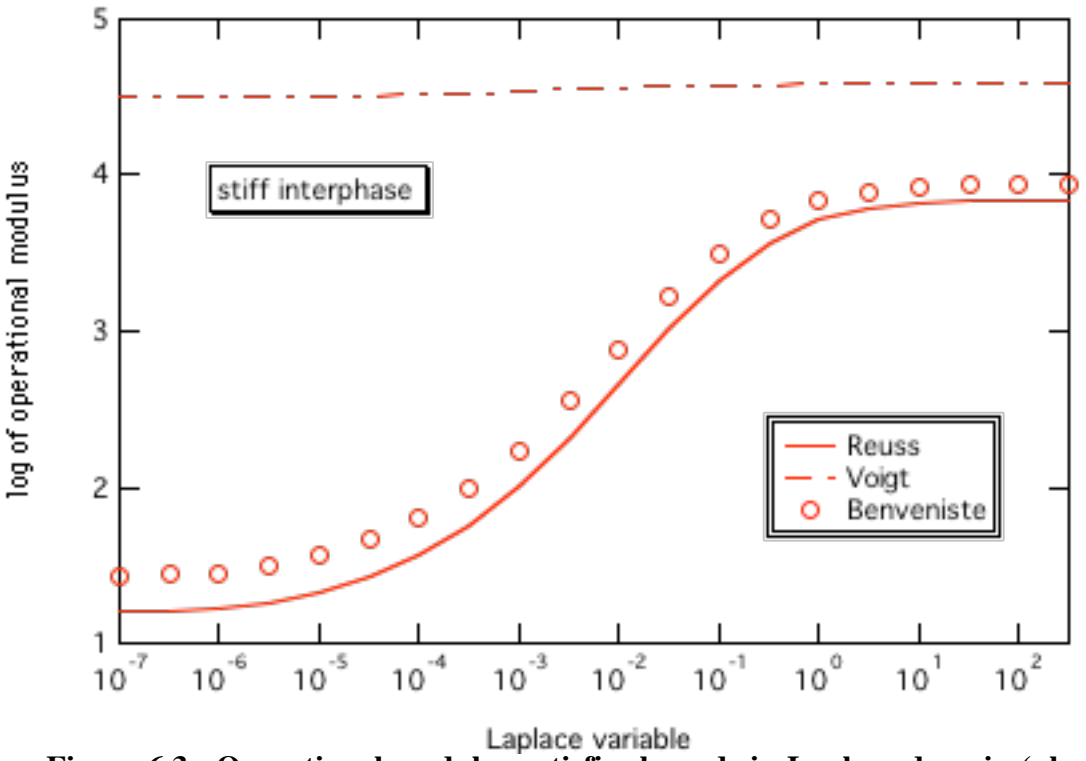

Figure 6.3. Operational modulus satisfies bounds in Laplace domain (phase properties same as those of Figures 6.1 and 6.2.)

used within the context of the dynamic correspondence principle to formulate the viscoelastic solution. Note that when formulated in the Laplace domain, the composite moduli are real numbers only.

Figure 6.3 shows that the predicted Benveniste operational moduli for the same composite configuration shown in Figures 6.1 and 6.2; it does indeed fall within the Reuss/Voigt bounds in the Laplace domain. While the Reuss/Voigt bounds and the tighter HSW bounds (not shown) are valid for multiphase composites with aligned, identically shaped inclusions (as is the case in this thesis), these bounds may not hold for multiphase composites with inclusions of different shapes (Qui and Weng 1990).

The material properties in the frequency domain, namely the storage and loss moduli, provide physical insight into the mechanical behavior of the composite. Thus, the models studied in this thesis will be analyzed almost exclusively in this domain, and the discussion of bounds for these solutions will not be continued. Gibiansky and co-workers

(1993; 1993) have developed methods for developing appropriate bounds for a viscoelastic composite material in the Fourier domain; however, their work to date is limited to two phase materials, and they have obtained solutions for only a limited number of mechanical properties.

6.3 COMPARISON OF MODEL PREDICTIONS

The results of the numerical simulations for the overall composite mechanical behavior as a function of interphase properties and volume fractions are presented. All cases presented in this thesis assume an elastic fiber with the mechanical properties given in Chapter 2; this was done in an effort to isolate the effects of the interphase on the overall composite behavior. Figures 6.1 and 6.2 indicate that the Mori-Tanaka and the Benveniste solutions are in very good agreement for this particular configuration. Additional results are presented for the following cases:

- 30% elastic fiber, 10% soft interphase, 60% stiff matrix (Figures 6.4 and 6.5)
- 60% elastic fiber, 10% stiff interphase, 30% soft matrix (Figures 6.6 and 6.7)
- 60% elastic fiber, 10% soft interphase, 30% stiff matrix (Figures 6.8 and 6.9)

Figures 6.10-6.13 show frequency domain plots (for the storage moduli only) comparing analytical and FEA solutions for the transverse shear modulus. Since the results for the transverse shear modulus are similar to those for the transverse Young's modulus, a detailed discussion of the former will not be included.

Analysis of the transverse Young's modulus results shows that the Benveniste and Mori-Tanaka solutions are practically identical for those composites where the matrix is the softest of the three phase materials. While the results of these two methods agree quite well with the detailed finite element analysis for low volume fraction of inclusions, the solutions drift from the FEA analysis as the inclusion volume fraction is increased. This is consistent with the fact that both micromechanical methods are derived using the analysis of a single inclusion within an infinite medium; as the concentration of

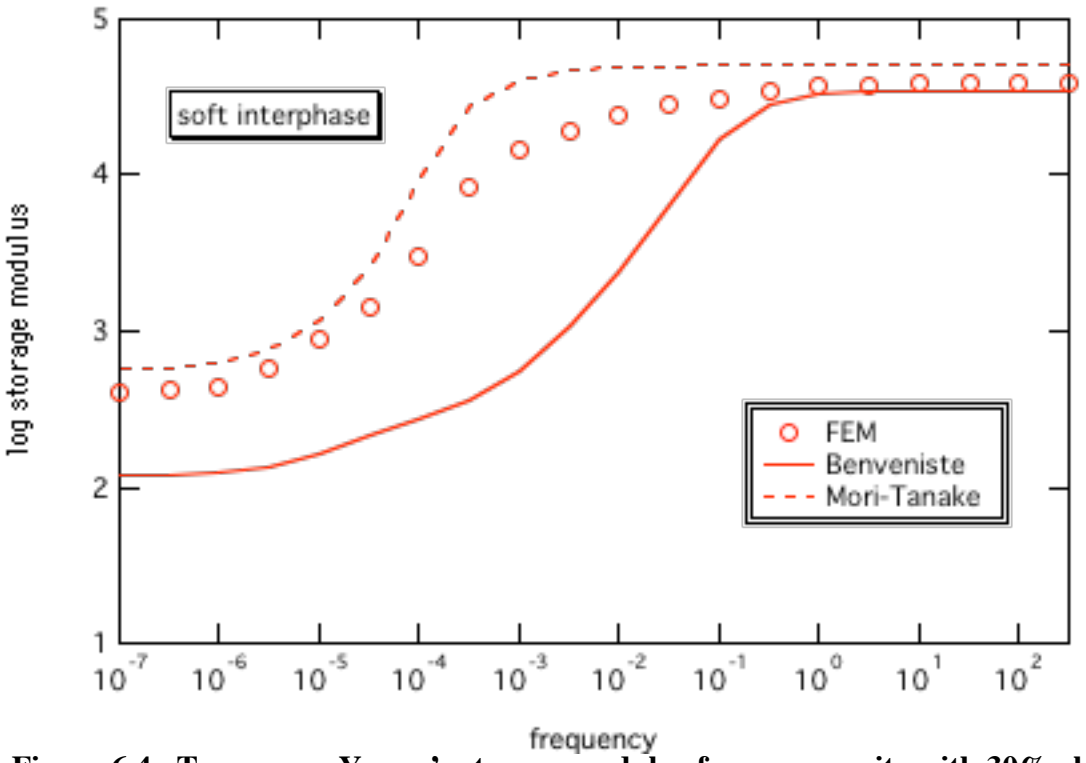

Figure 6.4. Transverse Young's storage modulus for a composite with 30% elastic fiber, 10% soft interphase, 60% stiff matrix.

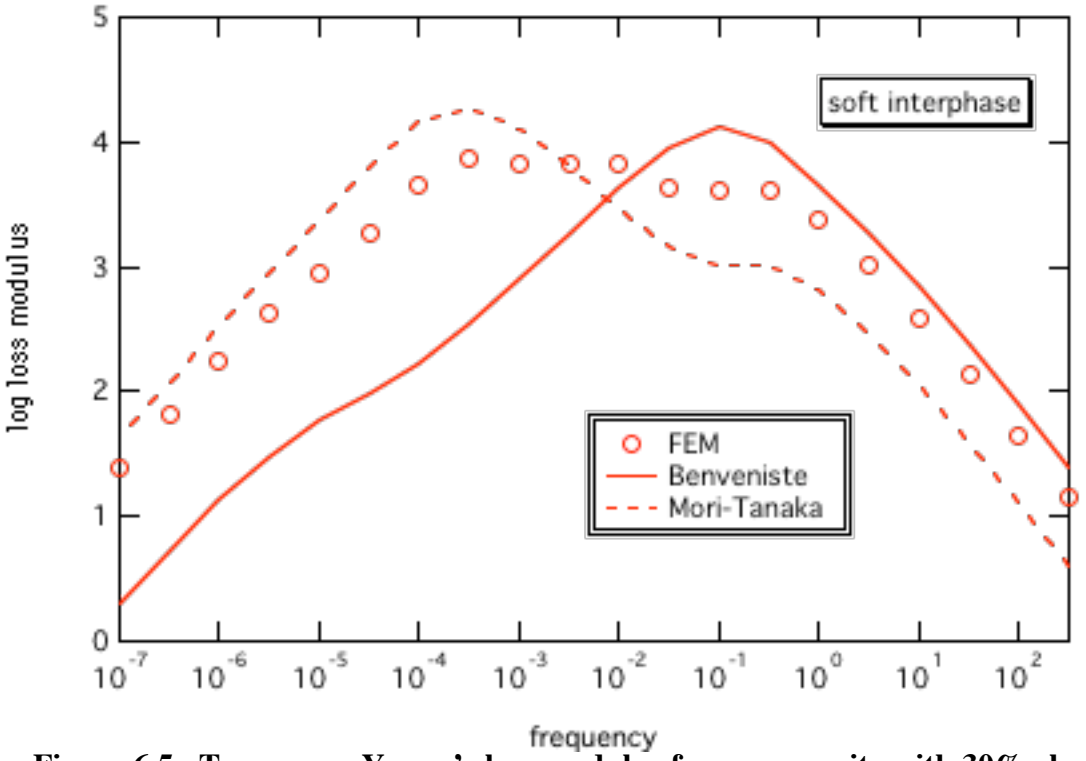

Figure 6.5. Transverse Young's loss modulus for a composite with 30% elastic fiber, 10% soft interphase, 60% stiff matrix.

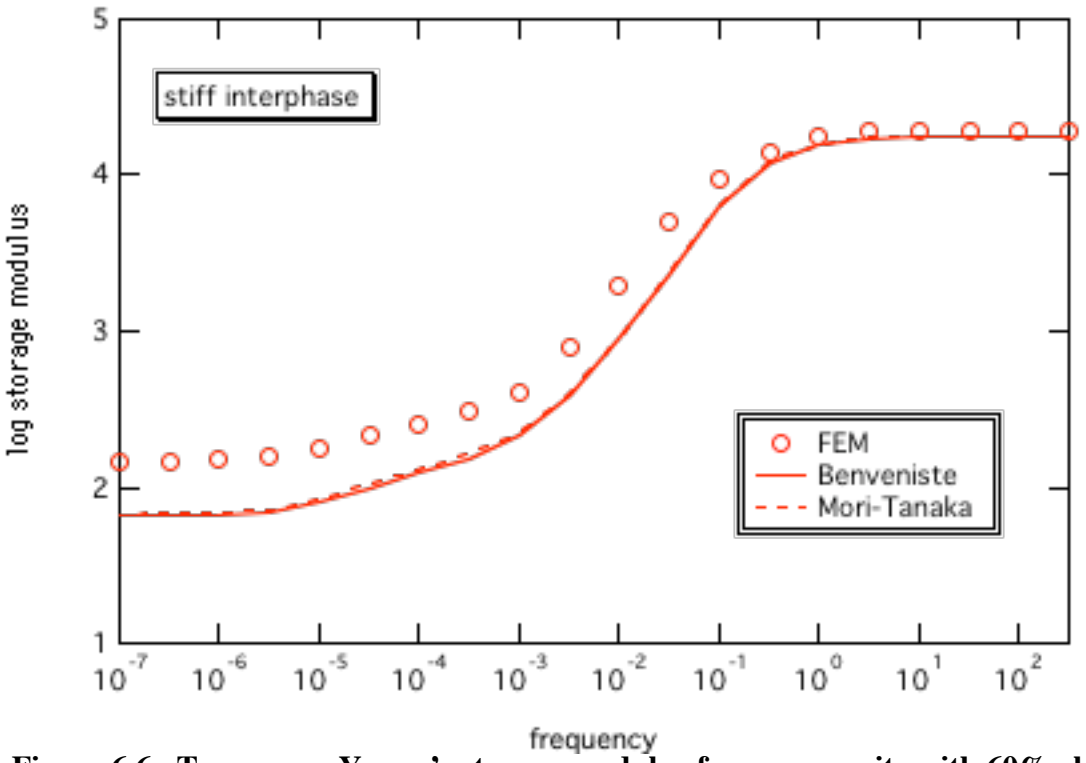

Figure 6.6. Transverse Young's storage modulus for a composite with 60% elastic fiber, 10% stiff interphase, 30% soft matrix.

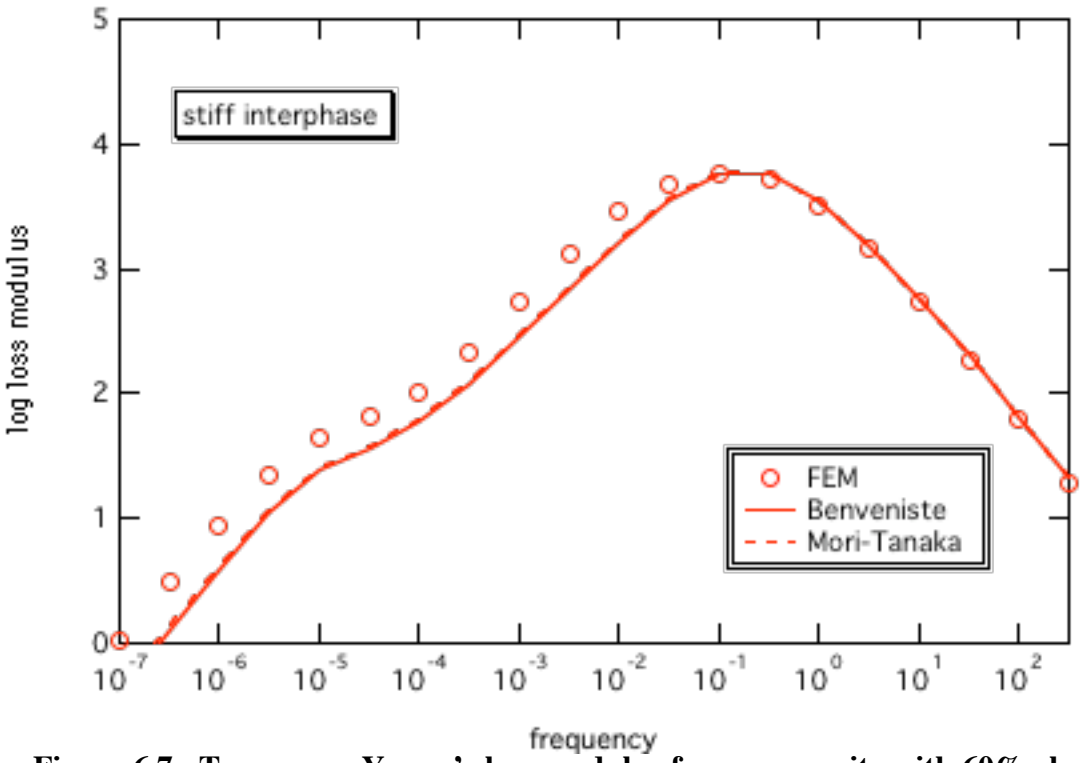

Figure 6.7. Transverse Young's loss modulus for a composite with 60% elastic fiber, 10% stiff interphase, 30% soft matrix.

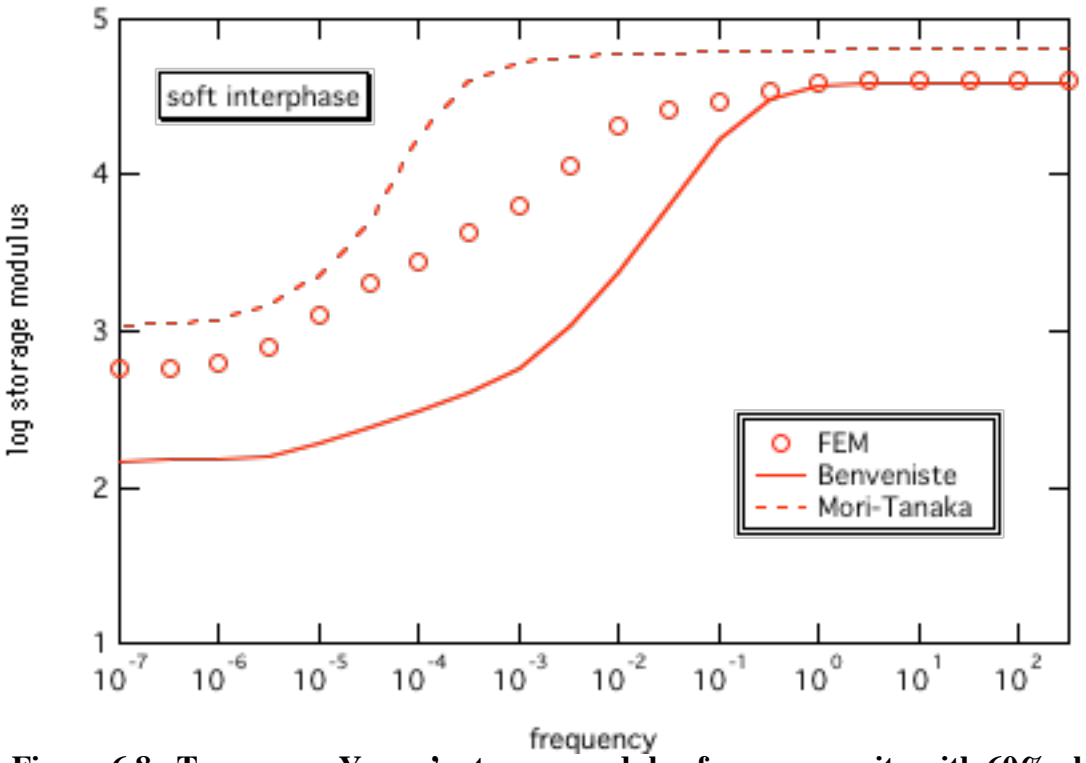

Figure 6.8. Transverse Young's storage modulus for a composite with 60% elastic fiber, 10% soft interphase, 30% stiff matrix.

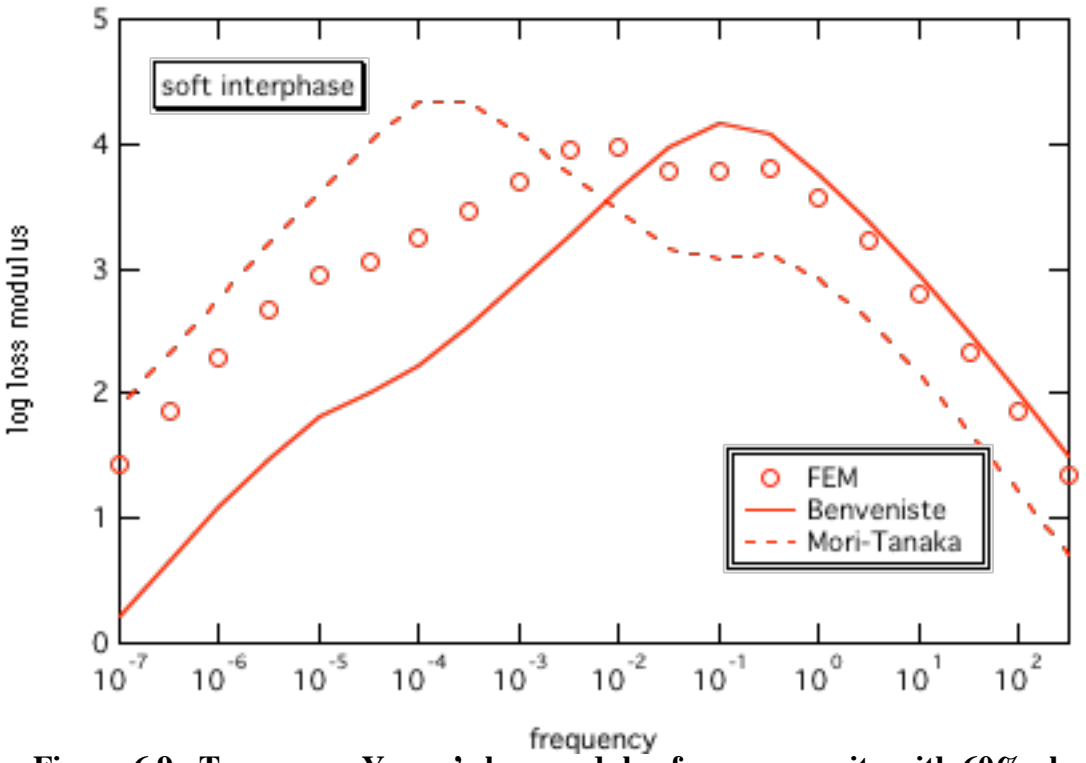

Figure 6.9. Transverse Young's loss modulus for a composite with 60% elastic fiber, 10% soft interphase, 30% stiff matrix.

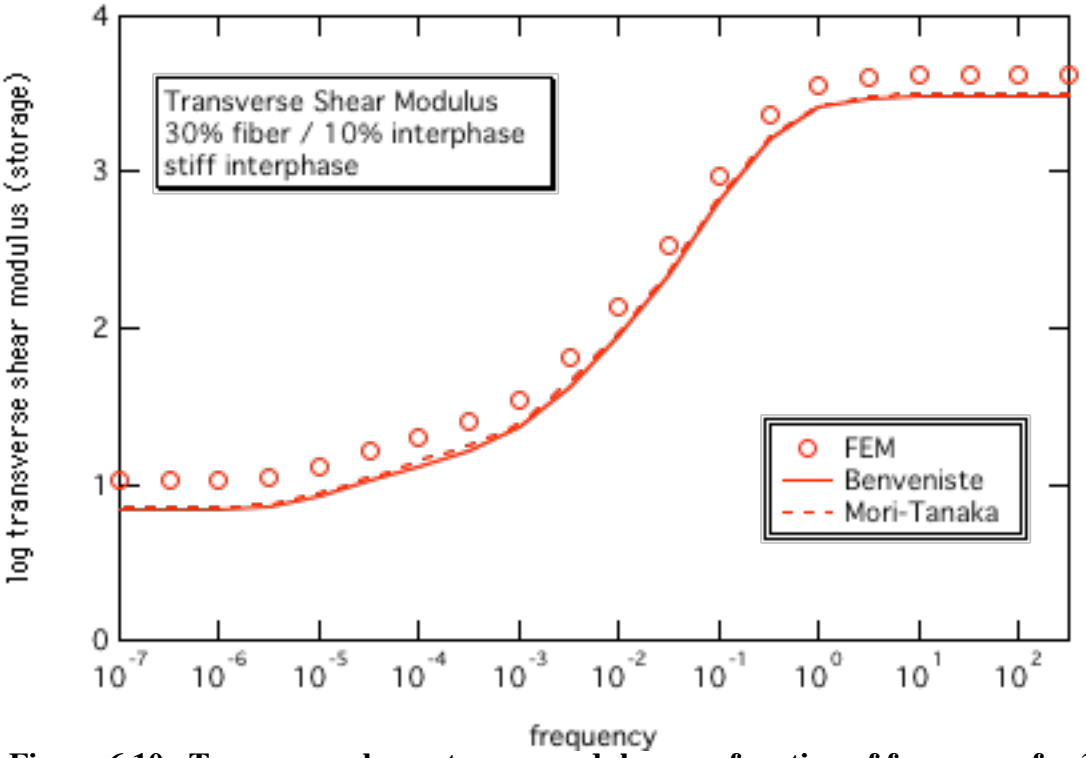

Figure 6.10. Transverse shear storage modulus as a function of frequency for 30% fiber, 10% stiff interphase, 60% soft matrix composite.

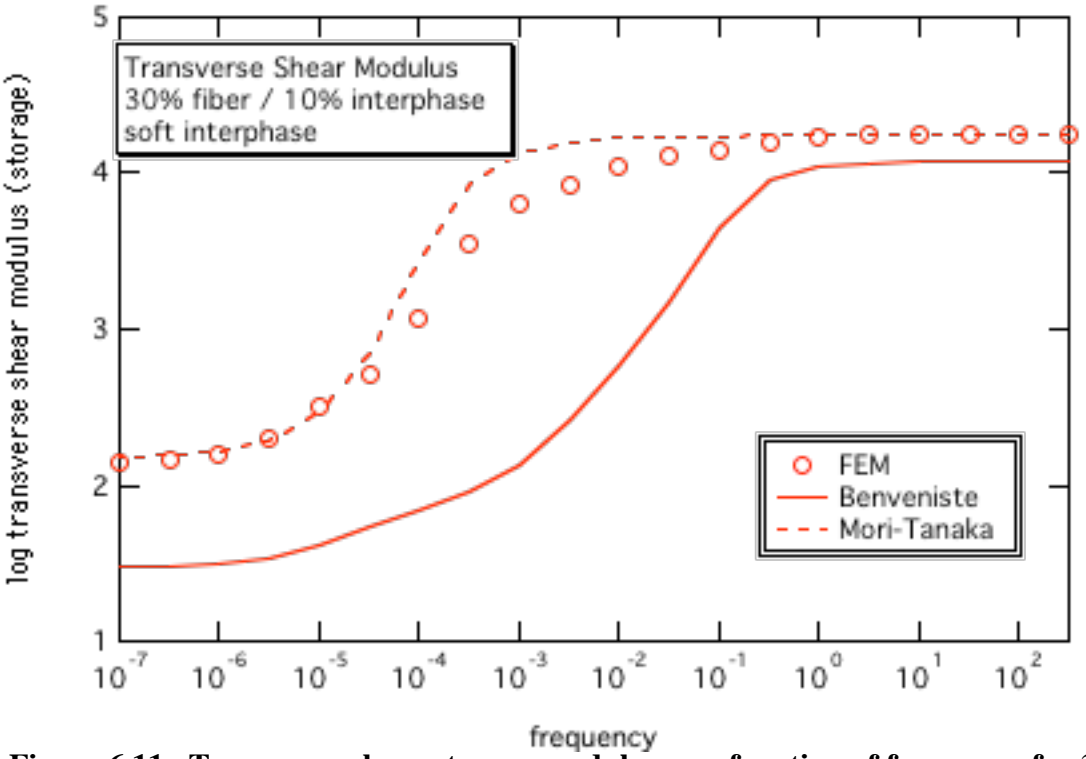

Figure 6.11. Transverse shear storage modulus as a function of frequency for 30% fiber, 10% soft interphase, 60% stiff matrix composite.

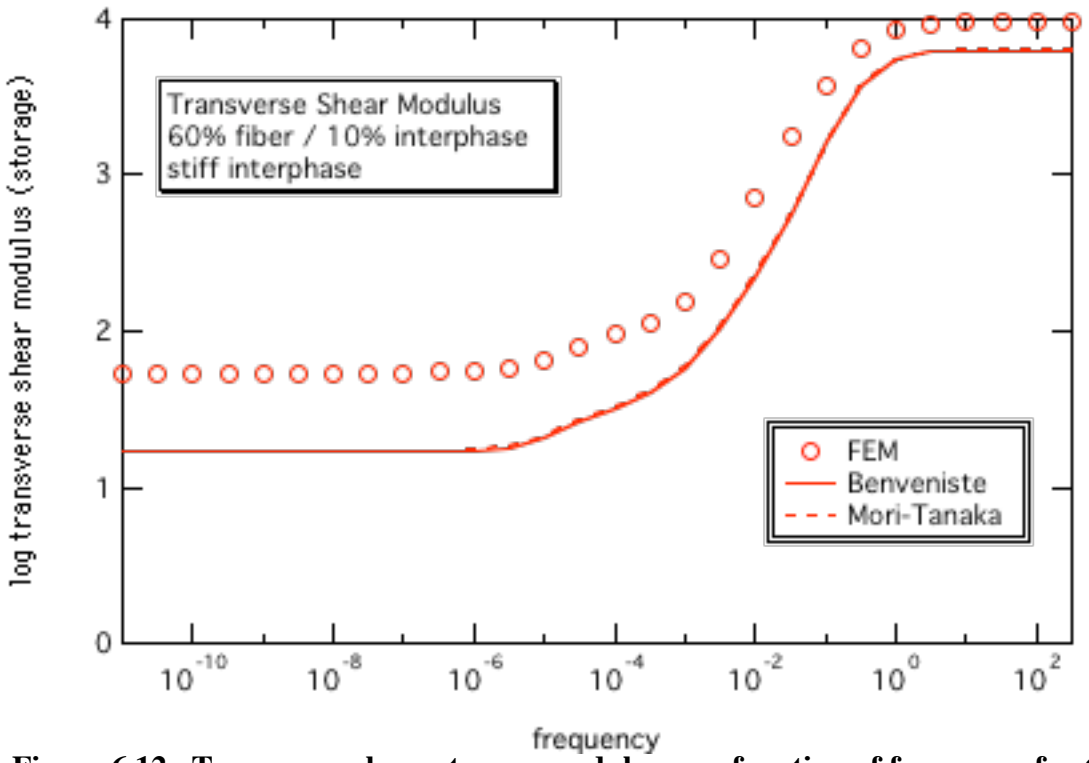

Figure 6.12. Transverse shear storage modulus as a function of frequency for 60% fiber, 10% stiff interphase, 60% soft matrix composite.

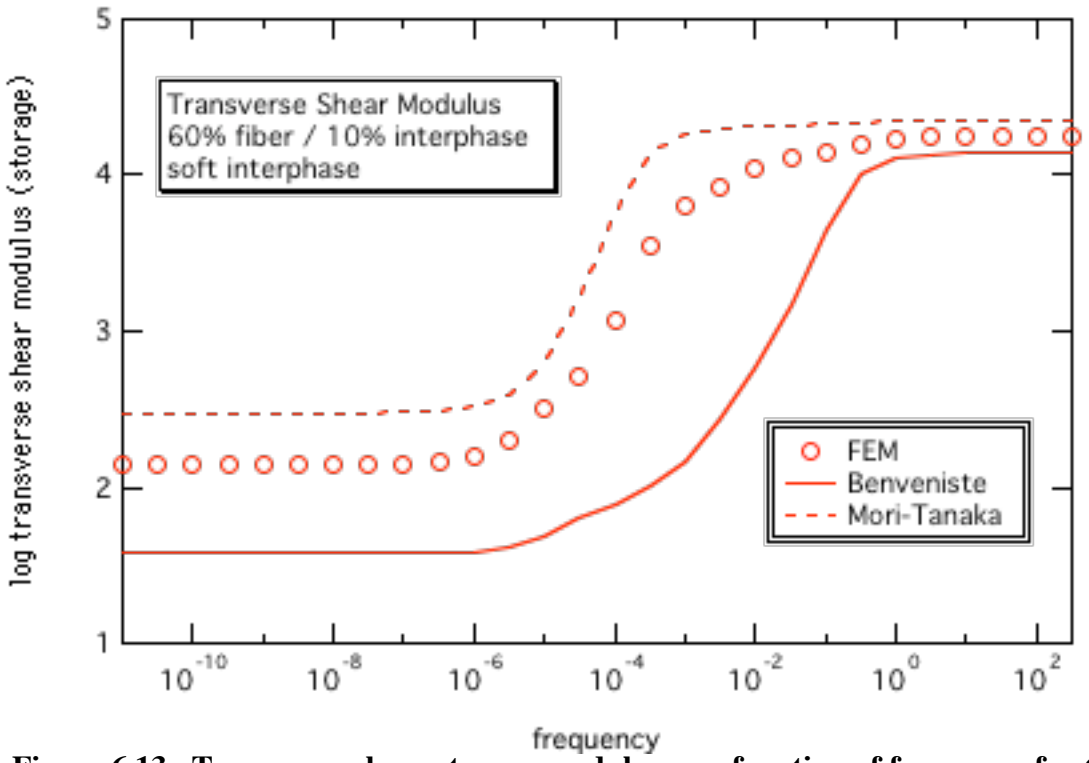

Figure 6.13. Transverse shear storage modulus as a function of frequency for 60% fiber, 10% soft interphase, 60% stiff matrix composite.

inclusions is increased one might expect that these methods may fail to accurately model the complex state of particle-particle interaction.

However, the analytical results for the transverse Young's modulus are not as accurate for those trials where the interphase is the softest of the three materials. In these instances, there is also a large discrepancy between the two analytical models (as seen in Figures 6.4, 6.5, 6.8, and 6.9), with the values calculated from the FEA falling between these two methods. It is surprising that the frequency-dependence of the Benveniste solution, for the case of a soft interphase, is dominated by the interphase material (most explicitly seen in the loss modulus), even though it is a non-continuous phase of small volume fraction within the composite. This suggests that there is a serious defect in the Benveniste when the interphase is the softest material. The Mori-Tanaka solution, even though it does not model the physical geometry of the problem, seems to better approximate the *behavior* of the moduli. Since the Benveniste method always predicts moduli lower than the corresponding FEA results, we conclude that the Benveniste method inaccurately models the influence of the interphase on the stress transfer between the fibers and matrix. This discrepancy is magnified in those cases where the interphase is the softest material. Nonetheless, the Benveniste model may be useful from a design perspective in that it always provides conservative estimates of the composite moduli.

It is interesting to note that, in the high frequency regime where the material may be expected to exhibit "pseudo-elastic" (glassy) behavior, the Benveniste model does seem to provide an adequate, if not rigorous, approximation for the transverse Young's modulus as predicted by the FEA. However, the Benveniste model does not do well in predicting the low frequency ("rubbery elastic") effective moduli. Thus although it may at first seem that the Benveniste model provides satisfactory solutions in the psuedo-elastic regime, this conclusion is probably flawed due to the limited number of composite configurations tested (see Appendix A3). While the Benveniste solution for elastic composites may be very accurate in predicting composite moduli for some cases, blanket use of the Benveniste method for a random composite (particularly one with a soft interphase) may provide poor estimates for the composite moduli.

On the other hand, the Mori-Tanaka method, even though it does not account for the physicality of the annular interphase, may do a better job in modeling the composite moduli. It at least seems to captures the "matrix-dominated" aspect of the viscoelastic properties. Because it treats the fiber and interphase as separate inclusions, the MT method overpredicts the effective moduli when the interphase is the stiff VE material and underpredicts the composite moduli when the interphase is the soft VE material. Since the interphase is physically separate from the fiber inclusion it does not effect the stress transfer to the fiber. The Benveniste model was noted to always underpredict the effective composite moduli.

To better show the relationship between the predicted transverse Young's moduli of the composite with changing volume fraction of inclusion, Figures 6.14-6.17 show results as a function of fiber volume fraction at a constant interphase fraction of 10% and fixed frequencies of 100 (high frequency / glassy behavior), 1E-3 (mid frequency / transition region), and 1E-7 (low frequency / rubbery behavior), respectively. Again, two trends are noticeable from the limited data in these figures; namely, that both micromechanical solutions provide adequate approximations in those instances where the matrix is the softest material, and that the predictions seem more accurate for lower volume fraction of inclusions. The high accuracy in the glassy domain is believed to be caused by the fortuitous selection of material properties for the constituent phases. For those composites where the interphase is the softest material, both micromechanical methods are not effective in predicting the effective transverse Young's moduli in the transition region (ω = 1E-1 ~ 1E-4) and at low (ω = 1E-7) frequencies, when compared to the FEA results.

Finally, trials were run to determine the role of the interphase volume fraction on the accuracy of the analytical models. These results are shown in Figures 6.20-6.25 as a function of interphase volume fraction for fixed fiber volume fractions of 30% and frequencies of 100 (glassy elastic behavior), 1E-3 (transition region) and 1E-7 (rubbery elastic behavior). Once again, the two trends that have been noted previously are apparent: the predictions from the analytical models are very poor in those cases where

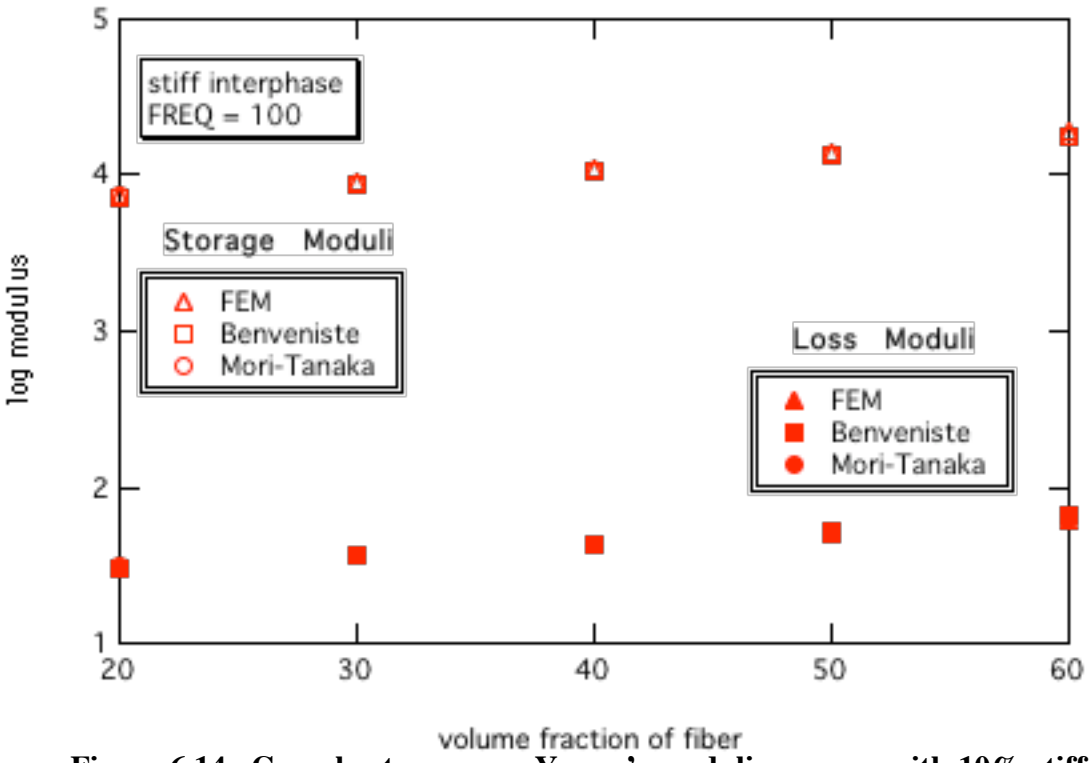

Figure 6.14. Complex transverse Young's moduli versus c_f with 10% stiff interphase and soft matrix material at a frequency of 100.

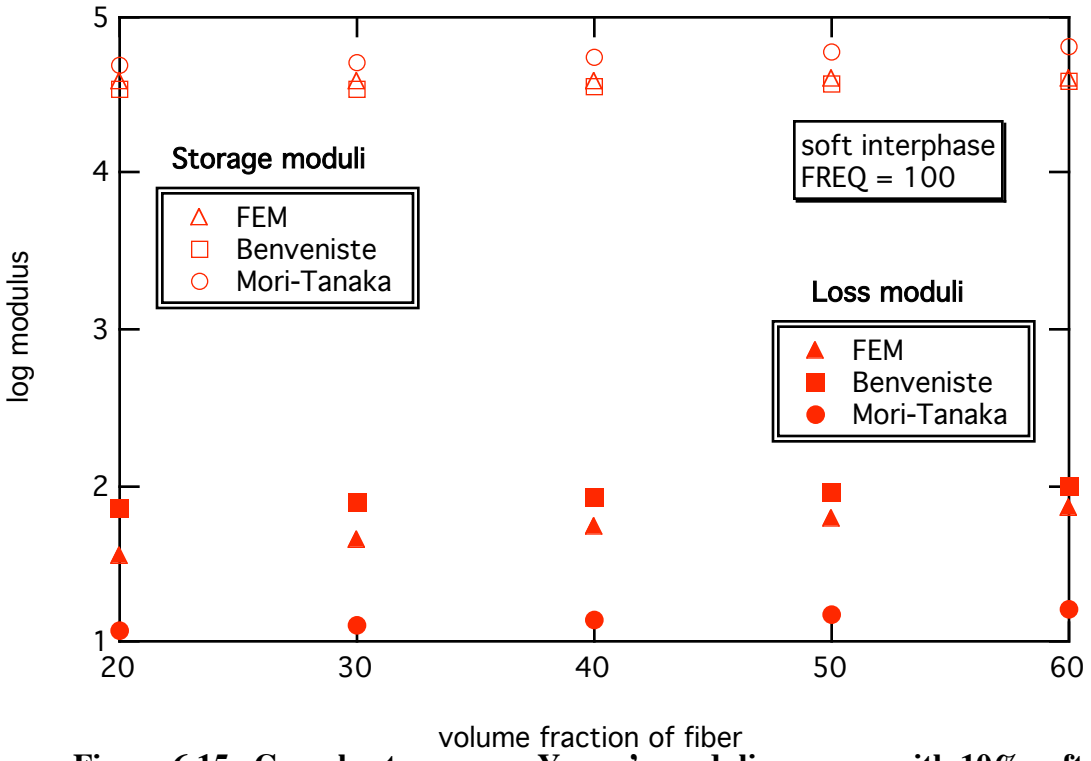

Figure 6.15. Complex transverse Young's moduli versus c_f with 10% soft interphase and stiff matrix material at a frequency of 100.

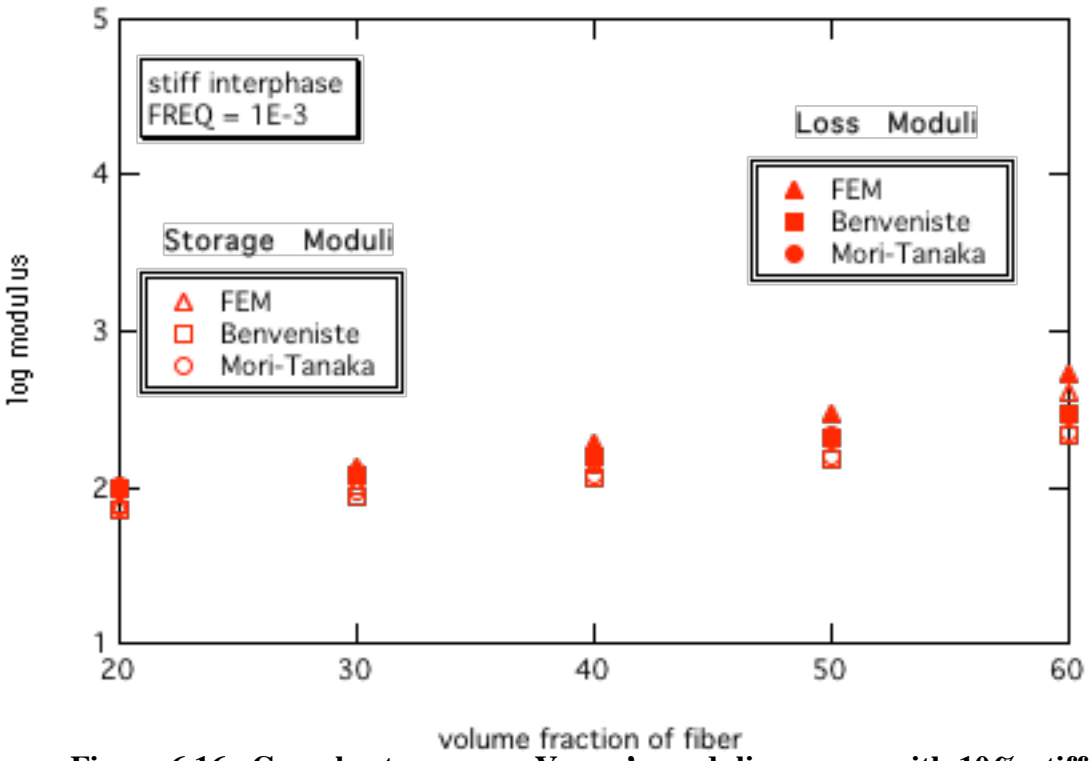

Figure 6.16. Complex transverse Young's moduli versus c_f with 10% stiff interphase and stiff matrix material at a frequency of 1E-3.

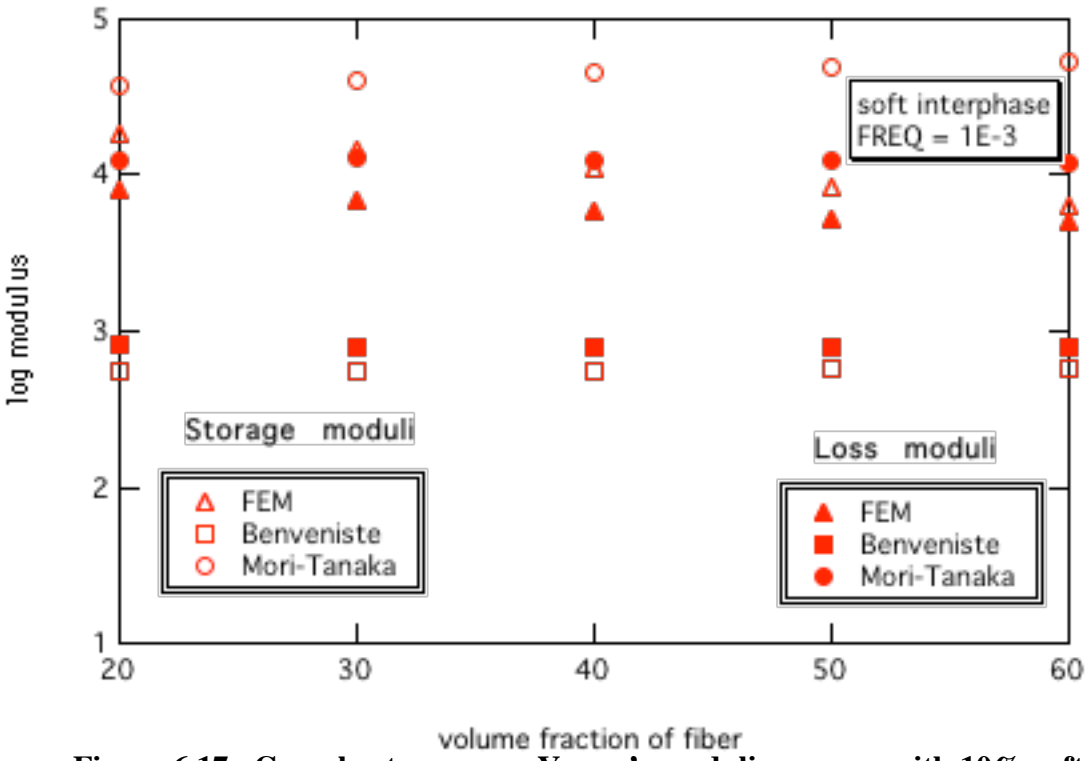

Figure 6.17. Complex transverse Young's moduli versus c_f with 10% soft interphase and stiff matrix material at a frequency of 1E-3.

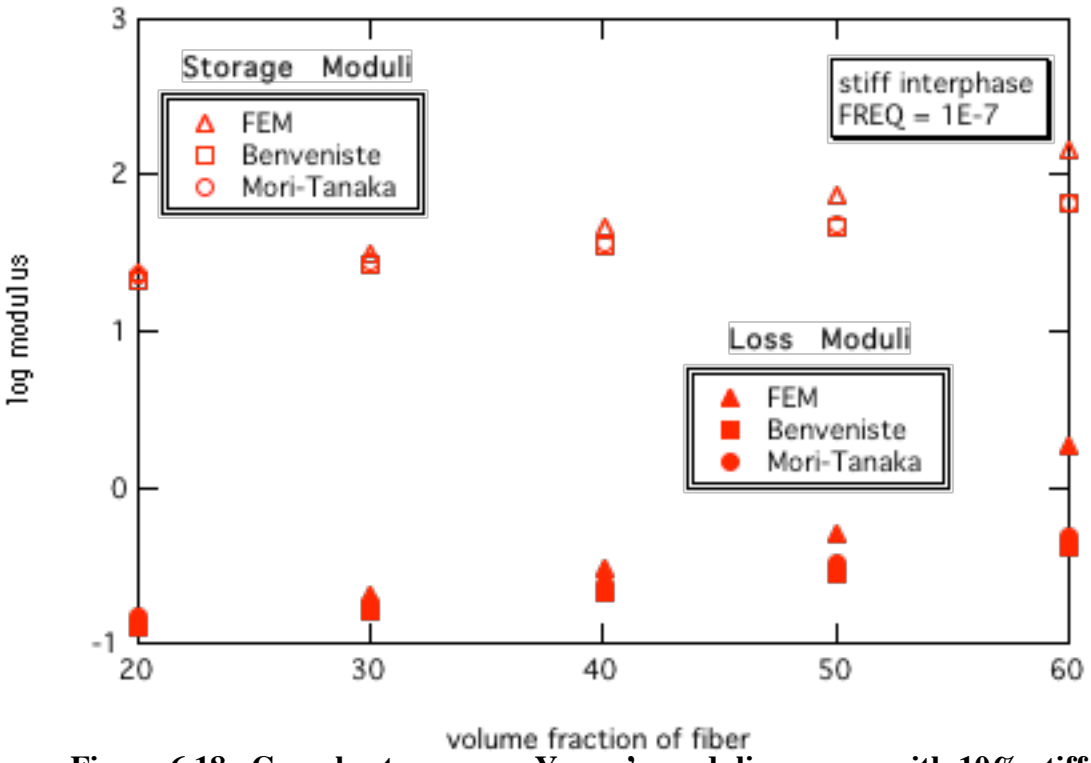

Figure 6.18. Complex transverse Young's moduli versus c_f with 10% stiff interphase and soft matrix material at a frequency of 1E-7.

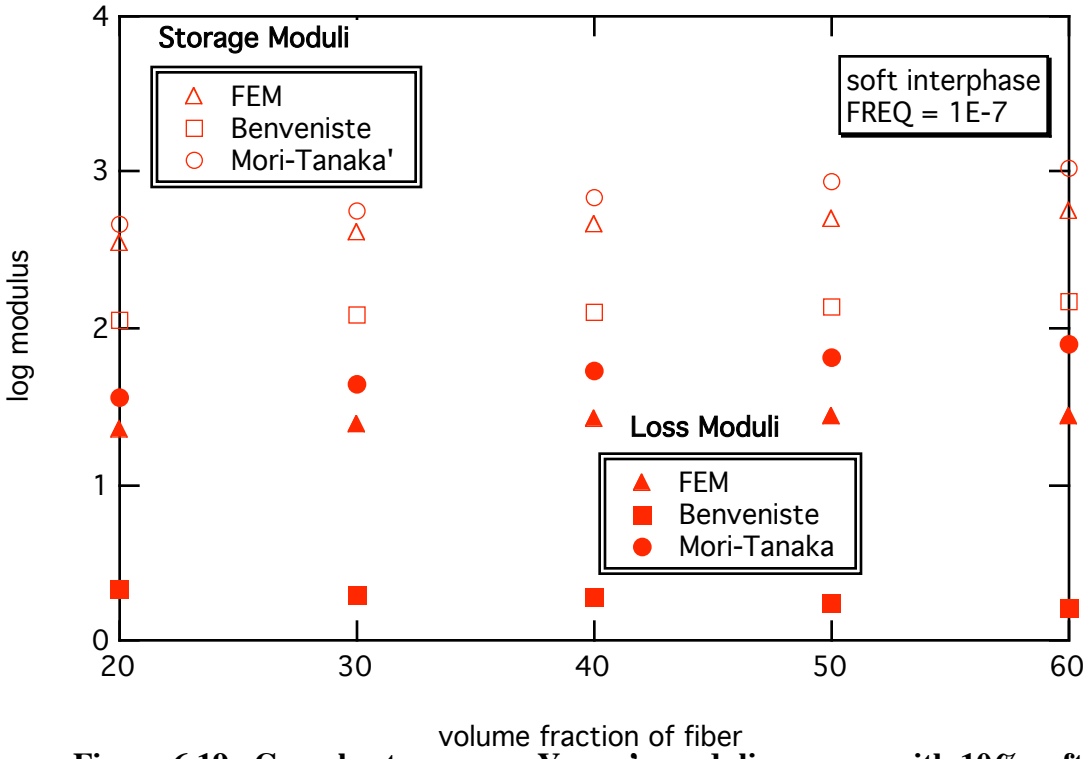

Figure 6.19. Complex transverse Young's moduli versus c_f with 10% soft interphase and stiff matrix material at a frequency of 1E-7.

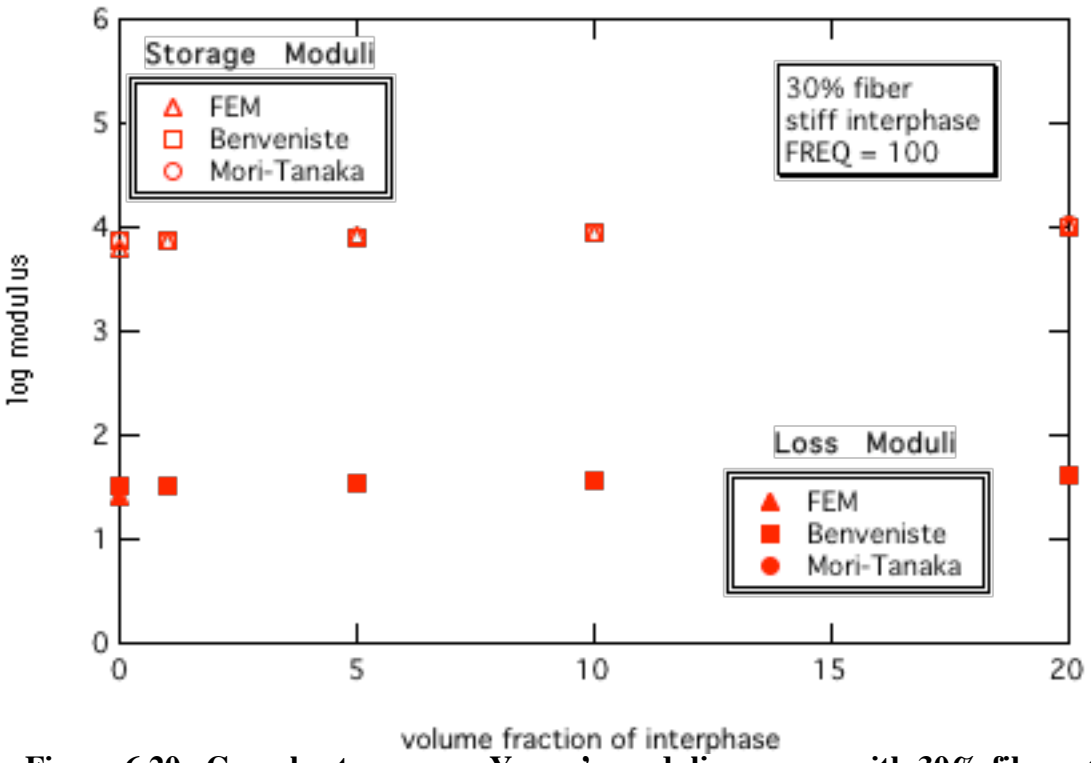

Figure 6.20. Complex transverse Young's moduli versus c_g with 30% fiber, stiff interphase, and soft matrix material at a frequency of 100.

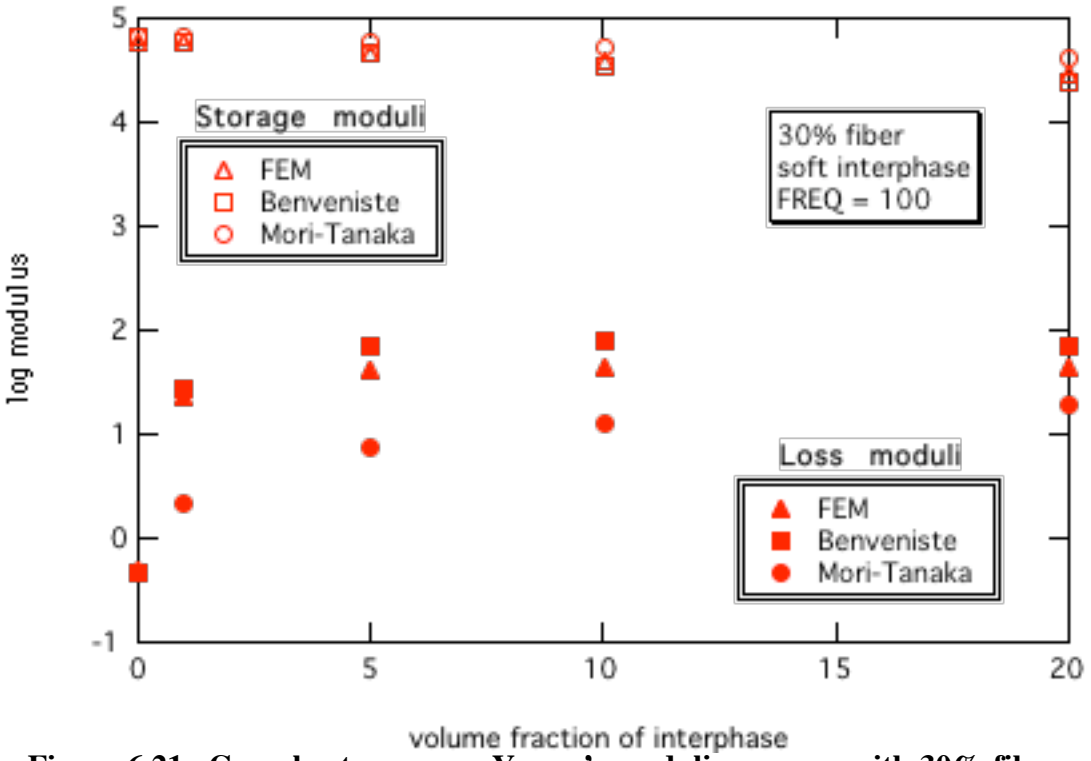

Figure 6.21. Complex transverse Young's moduli versus c_g with 30% fiber, soft interphase, and stiff matrix material at a frequency of 100.

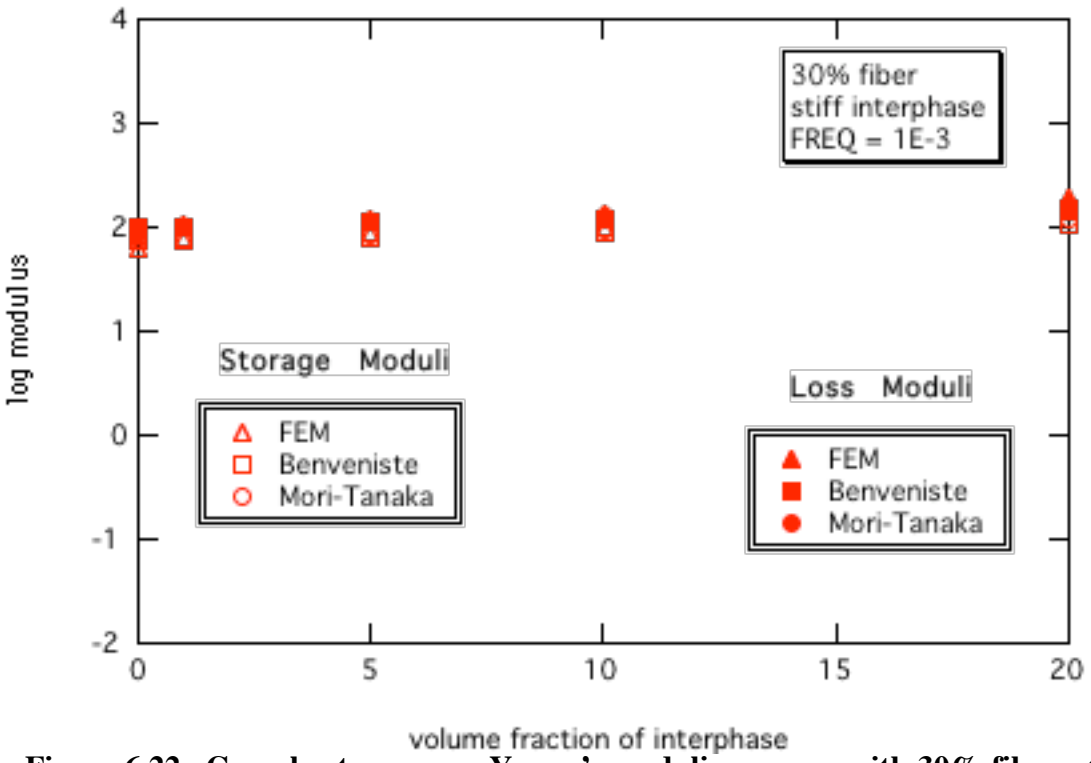

Figure 6.22. Complex transverse Young's moduli versus c_g with 30% fiber, stiff interphase, and stiff matrix material at a frequency of 1E-3.

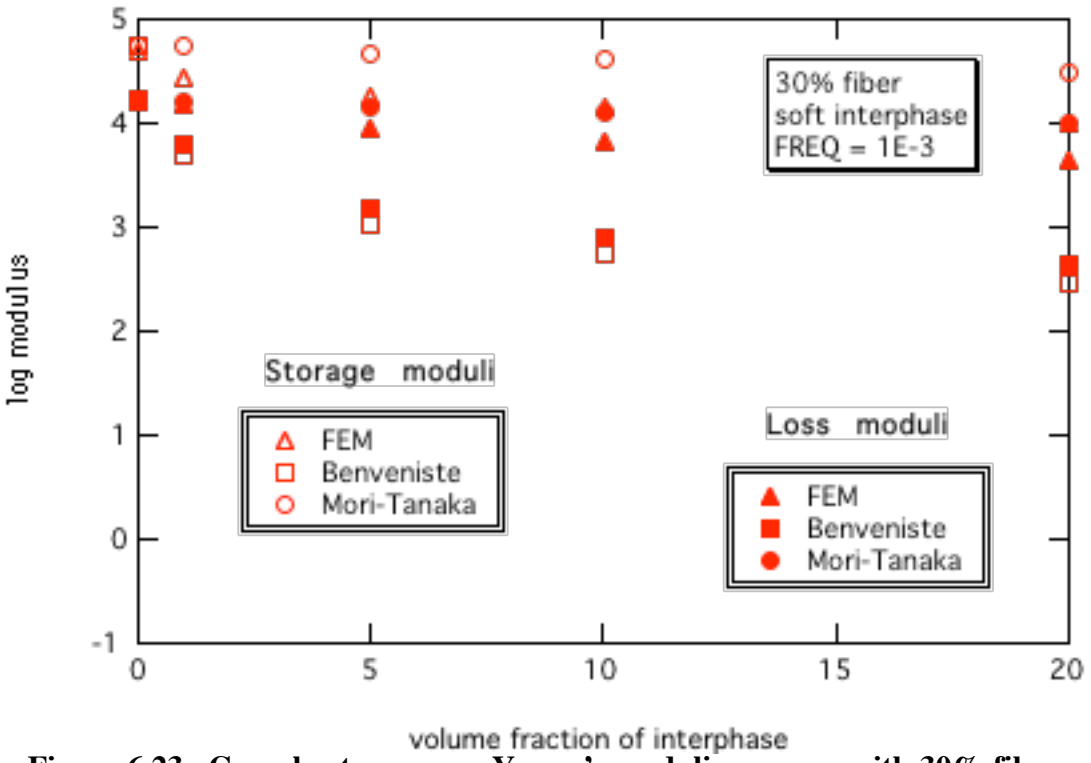

Figure 6.23. Complex transverse Young's moduli versus c_g with 30% fiber, soft interphase, and stiff matrix material at a frequency of 1E-3.

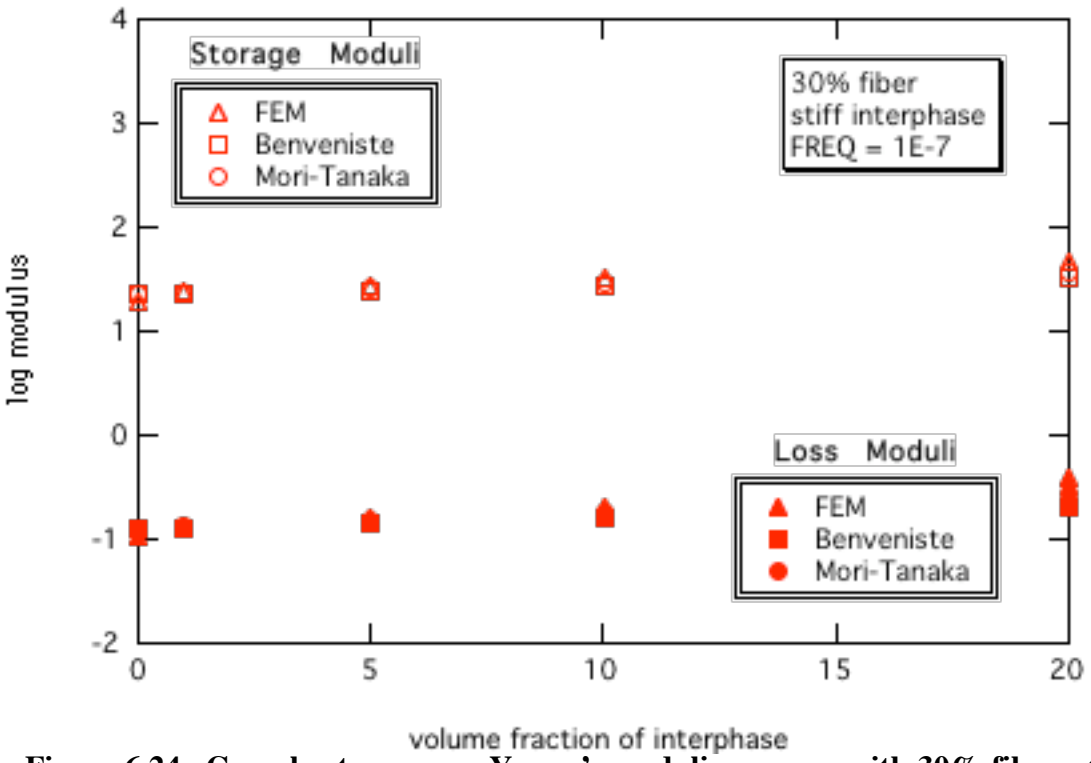

Figure 6.24. Complex transverse Young's moduli versus c_g with 30% fiber, stiff interphase, and soft matrix material at a frequency of 1E-7.

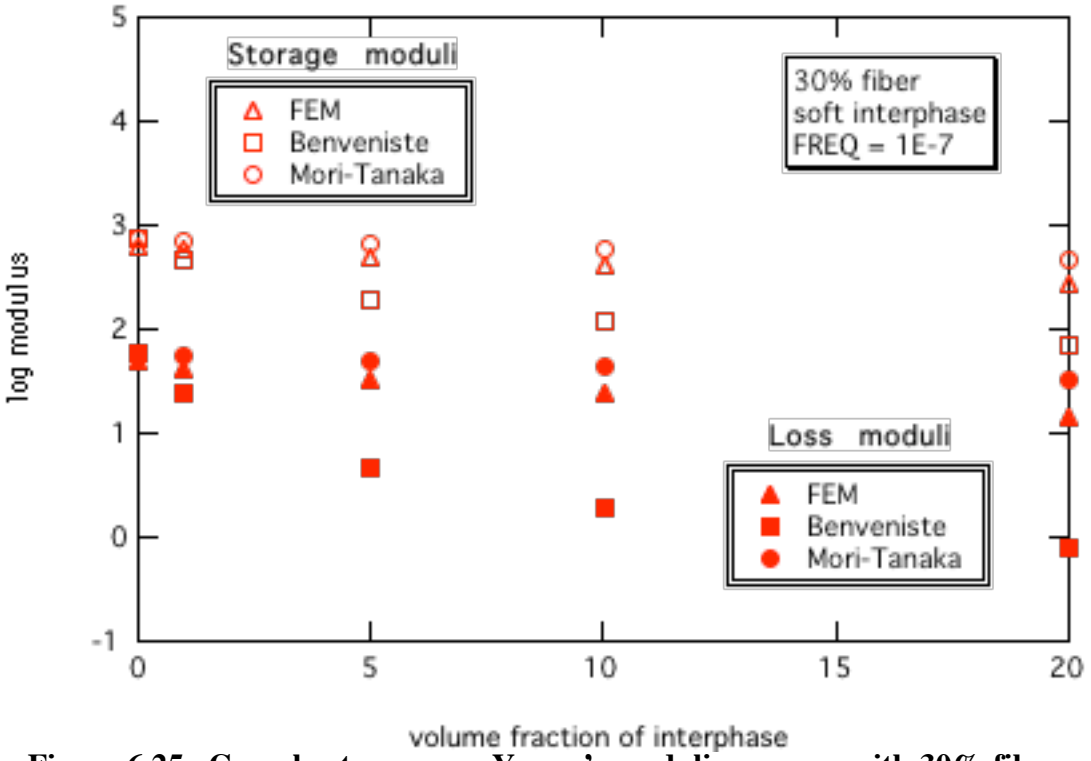

Figure 6.25. Complex transverse Young's moduli versus c_g with 30% fiber, soft interphase, and stiff matrix material at a frequency of 1E-7.

the interphase is the softest material, while the predictions are relatively close for those composites where the matrix is the softest material.

The accuracy of the analytical models slightly decreases as the interphase volume fraction is increased. However, the FEA results indicate that the effective composite moduli are largely independent of the volume fraction of the interphase (exceptions being the loss moduli in Figures 6.23 and 6.25). These results are contrary to the results obtained using a composite cylinders approach (Li and Weng 1996). This suggests that a highly accurate knowledge of the interphase volume fraction is not necessary to determine the effective composite behavior. It is worth noting that in the limiting case where the volume fraction of interphase is zero, the Mori-Tanaka and Benveniste solutions are identical. This is because both solutions use an identical "average stress in the matrix" argument to account for the interaction between inclusions.

6.4 STRESS PROFILES IN THE PHASES

We next sought to determine possible reasons why the analytical models and the FEA results drastically differ for some of the composite configurations. One manner to analyze the differences between the methods is to examine the stress fields which each method predicts. This was done by examining the stresses along a particular line of the unit cell for the FEA, and comparing those results to the average phase stresses predicted by the Benveniste solution.

For other comparisons, the phase-averaged stresses obtained through the FEA were determined. These stresses were calculated by finding the area of each element used in the FEA, and then implementing the formula

$$\hat{\sigma}_{ij}^{k} = \frac{\sum_{n} \sigma_{ij}^{k} A_{n}^{k}}{\sum_{n} A_{n}^{k}} \qquad k=\{f,g,m\} \qquad (6.1)$$

where $\bar{\sigma}_{ij}^{k}$ is the phase average of the stress component σ_{ij} for phase *k*, A_n^k is the *n*th elemental area of phase *k*, and the summations are implied over all elements of a particular phase.

For the Benveniste solution, the procedure was somewhat more complicated. Once the phase averaged stress within the matrix was determined via FEA, this value was back-substituted to determine the appropriate far-field stress σ_o of the auxiliary problem necessary to provide the same value for the phase-average matrix stress. This was done to simplify the stress-field comparisons between models. Note that the effective moduli are independent of the applied stress in the auxiliary problem.

Using this procedure, the σ_{yy} stress profiles along the unit cell at y=0 were plotted with the corresponding average stress values found via the Benveniste method. For practical purposes, the stress values at the centroid of those elements where the centroid was within a certain (small) distance from y=0 were plotted. These results are shown (for the real component of the stress only) in Figures 6.26-6.29 for different composite configurations. The fiber and interphase volume fractions were maintained at 30% and 10%, respectively.

We see that the stress profiles obtained via the FEA are far from uniform within the phases (which is contrary to the main assumption used in the Benveniste analysis). Nonetheless, in those cases where the matrix is the softest of the constituent materials, the phase averages obtained from the Benveniste solution seem to approximate the FEA solution. This, however, is obviously not the case when the interphase is the softest of the three phases, as seen in Figures 6.28 and 6.29 for frequencies of 100 and 1E-7, respectively. Here, and in Table 6.1, we see that the FEA solution suggests that the σ_{yy} stress components of the interphase experience a significant decrease in magnitude. However, this feature is not captured in the Benveniste solution, which may be one reason why the Benveniste analysis provides such a poor approximation in those cases where the interphase is the softest of the three phase materials.

To further show the difference between the calculated phase average stress values between the Benveniste solution and the FEA, Table 6.1 compares these values for several

different composite configurations. All results compiled in this table are for an interphase volume fraction of 10% and an elastic fiber. Selected data from this table are displayed in graphical form in Figures 6.30 to 6.33. The data in these figures were normalized with respect to the phase average matrix stresses. In all cases where the interphase is the stiff VE material the phase average σ_{yy} stresses in the included phases determined via the Benveniste model are less than those calculated via FEA. The opposite is true for the composite configurations where the interphase is the soft VE material.

Contour plots showing the variation of the real component of the σ_{yy} stress throughout the unit cell under a transverse normal load are shown in Figures 6.34 to 6.37 for various composite configurations at a constant frequency of 1E-7. Note that since the stress profiles were determined given identical prescribed displacements along the top face of the unit cell, the magnitudes of the stresses can vary greatly between composite configurations.

It is interesting to note how the stress profile within the unit cell is dependent on the composite configuration. For the trials where the matrix is the softest material, we see that the location of highest stress within the unit cell is in the matrix phase; this suggests that a soft interphase material fails to transfer the stress to the load-carrying fibers under transverse loading. FEA results on composites where the interphase is the softest material suggest that compressive stresses can develop in the interphase for this configuration. This could impact the material selection process for an engineered interphase. In all of these figures we see that the stress-fields in the matrix are non-uniformly distributed, which is consistent with published results for an elastic analysis of a three phase composite with an epoxy matrix (Al-Ostaz and Jasiuk 1996).

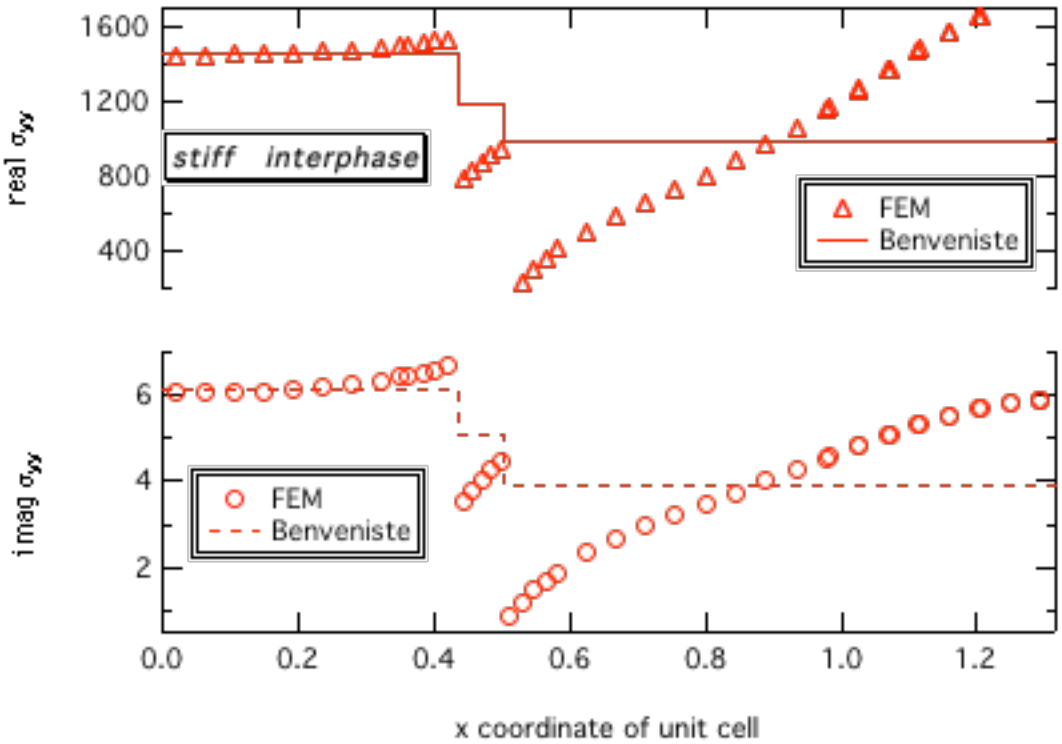

Figure 6.26. Stress profiles along y=0 of unit cell for composite with 30% fiber, 10% stiff interphase, 60% soft matrix. Frequency = 100.

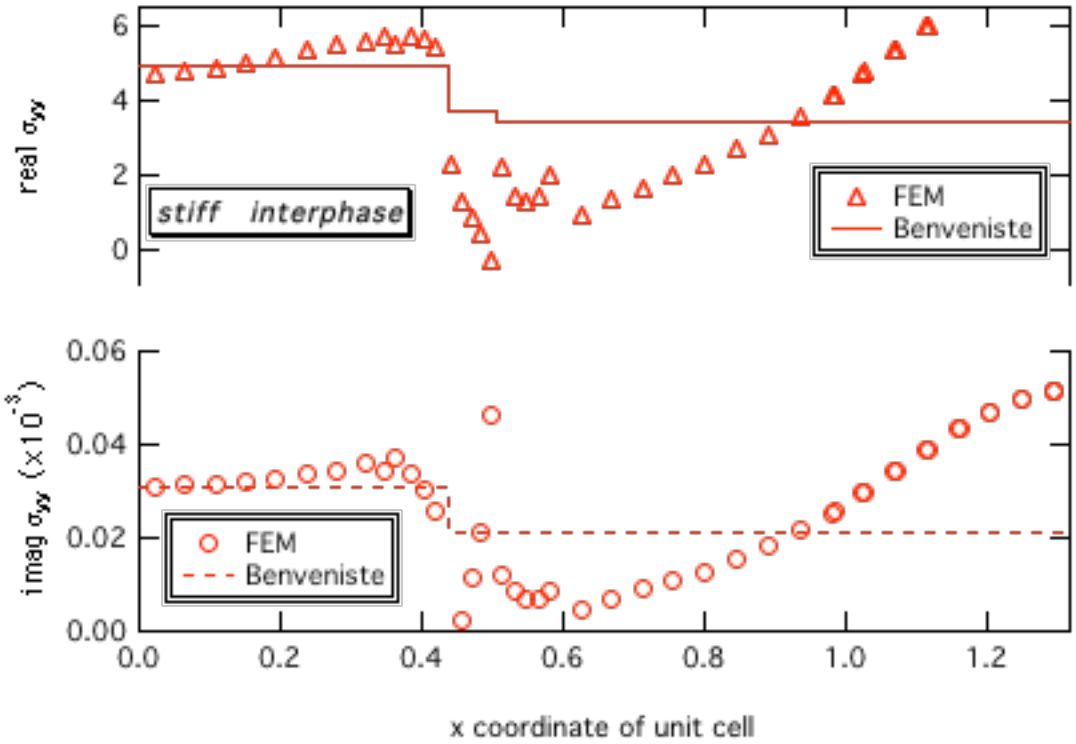

Figure 6.27. Stress profiles along y=0 of unit cell for composite with 30% fiber, 10% stiff interphase, 60% soft matrix. Frequency = 1E-7.

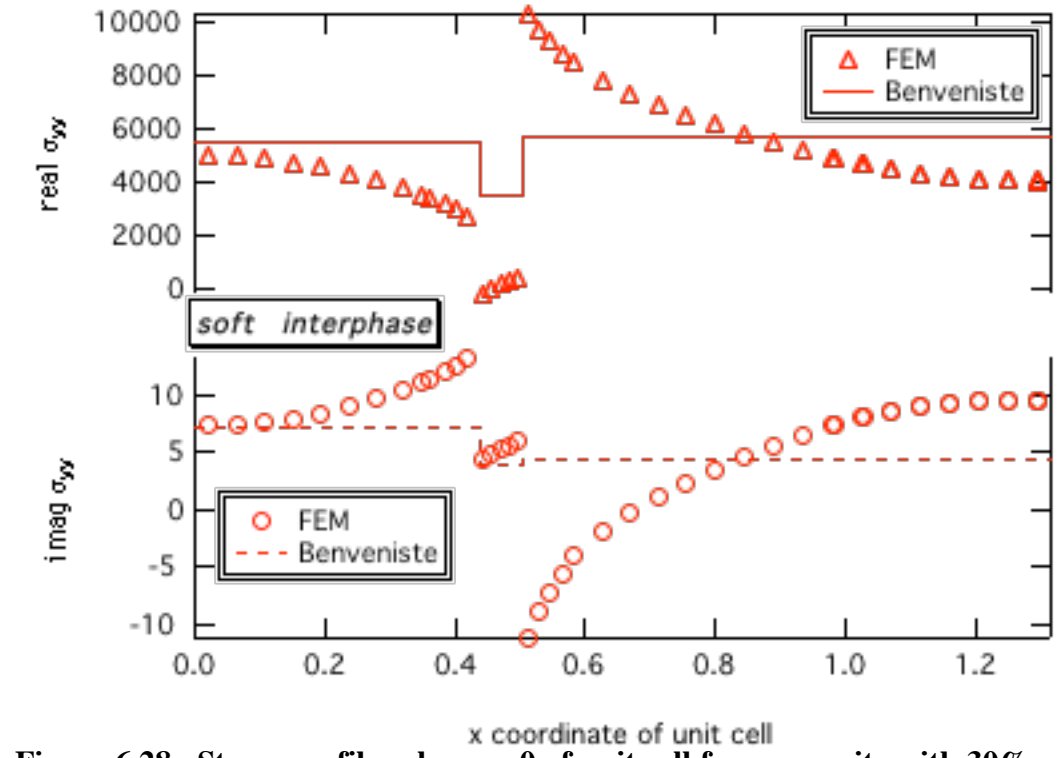

Figure 6.28. Stress profiles along y=0 of unit cell for composite with 30% fiber, 10% soft interphase, 60% stiff matrix. Frequency = 100.

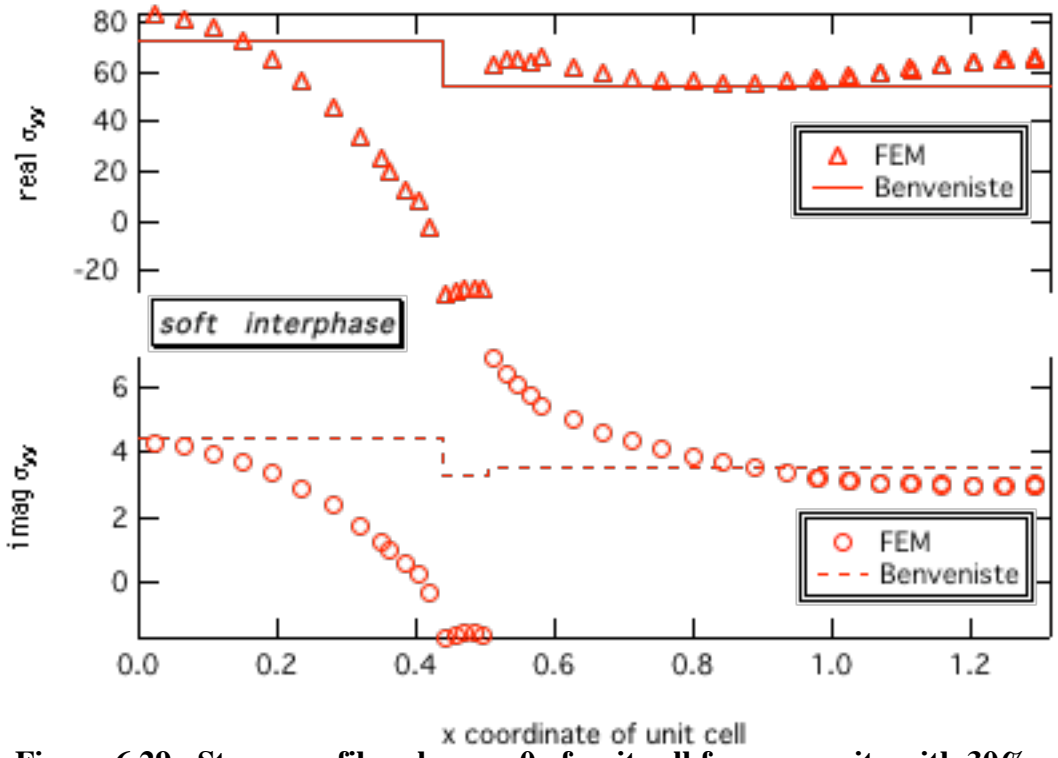

Figure 6.29. Stress profiles along y=0 of unit cell for composite with 30% fiber, 10% soft interphase, 60% stiff matrix. Frequency = 1E-7.

freq	Fiber	Interph.	Matrix		Fiber avg.	Interph. avg.	Matrix avg.
100	30% elastic	10% stiff	60% soft	FE	1503.2+6.21i	1298.5+5.33i	985.0+3.91i
				BM	1456.5+6.14i	1190.2+5.07i	985.0+3.91i
1.E-04	"	"	"	FE	10.35+4.76i	8.10+4.05i	6.41+3.05i
				BM	9.24+4.41i	6.64+3.32i	6.41+3.05i
1.E-07	"	"	"	FE	5.60+.0336i	4.32+.0349i	3.42+.0213i
				BM	4.90+.0309i	3.69+.0210i	3.42+.0213i
100	30% elastic	10% soft	60% stiff	FE	4437.5+8.80i	2733.7+6.44i	5744.2+4.40i
				BM	5513.7+7.046i	3580.1+4.01i	5744.2+4.40i
1.E-04	"	"	"	FE	213.45+59.60i	109.50+31.88i	530.44+956.97i
				BM	538.36+576.17i	371.57+352.02i	530.44+956.97i
1.E-07	"	"	"	FE	60.78+3.06i	27.63+1.39i	53.76+3.53i
				BM	72.87+4.47i	54.25+3.30i	53.76+3.53i
100	60% elastic	10% stiff	30% soft	FE	2965.05+9.19i	2380.63+7.92i	1805.42+5.81i
				BM	2651.8+9.26i	2180.6+7.65i	1805.42+5.81i
1.E-04	"	"	"	FE	40.69+16.28i	26.83+11.80i	21.22+8.83i
				BM	29.57+12.39i	22.29+9.53i	21.22+8.83i
1.E-07	"	"	"	FE	23.56+0.170i	15.42+0.122i	12.07+0.0861i
				BM	16.72+0.121i	13.30+0.086i	12.07+0.0861i
100	60% elastic	10% soft	30% stiff	FE	5415.07+10.88i	3418.69+7.75i	6067.35+6.70i
				BM	6246.9+9.48i	4135.9+4.71i	6067.35+6.70i
1.E-04	"	"	"	FE	306.28+83.86i	145.39+27.27i	551.77+589.67i
				BM	497.48+218.56i	379.02+145.33i	551.77+589.67i
1.E-07	"	"	"	FE	82.57+3.57i	40.87+1.70i	70.01+4.17i
				BM	93.13+5.27i	73.66+4.15i	70.01+4.17i

Table 6.1. Phase average stresses as a function of composite configuration at different frequencies. (FE = finite element results; BE = Benveniste results)

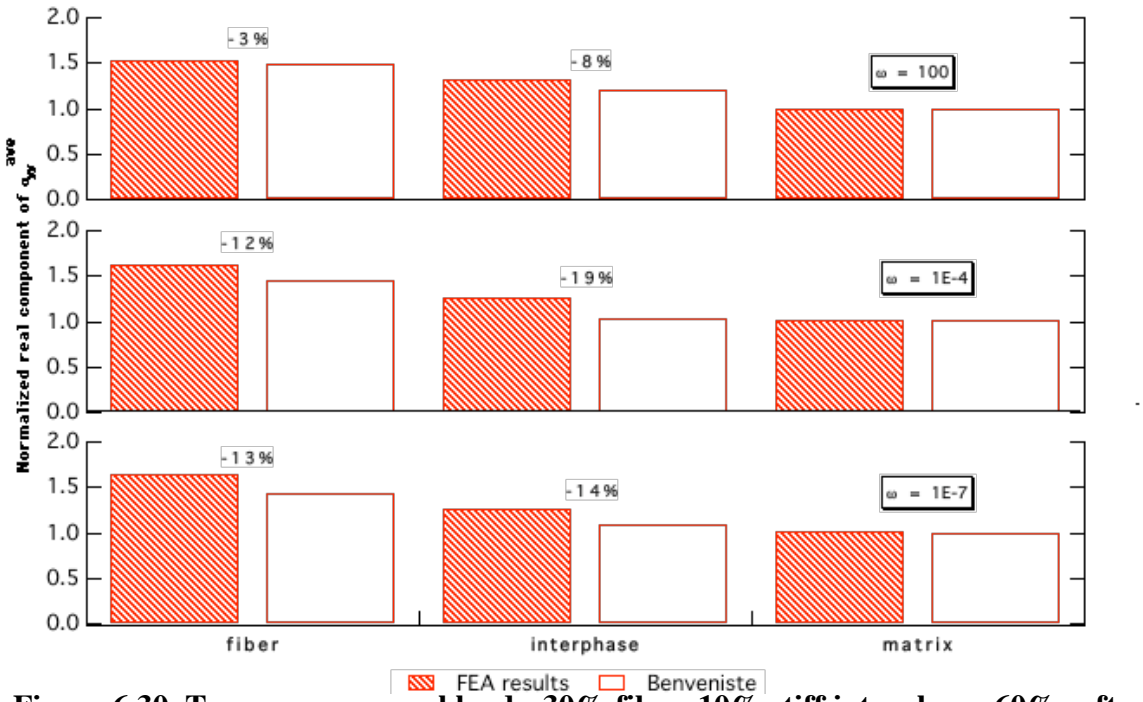

Figure 6.30. Transverse normal load: 30% fiber, 10% stiff interphase, 60% soft matrix

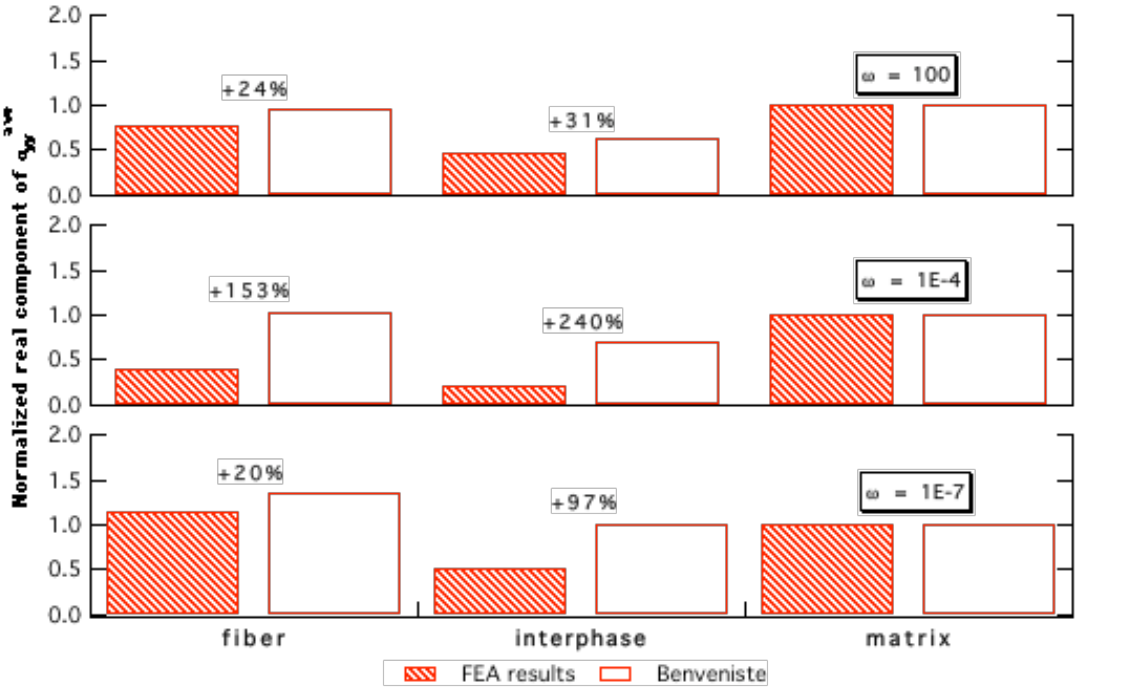

Figure 6.31. Transverse normal load: 30% fiber, 10% soft interphase, 60% stiff matrix

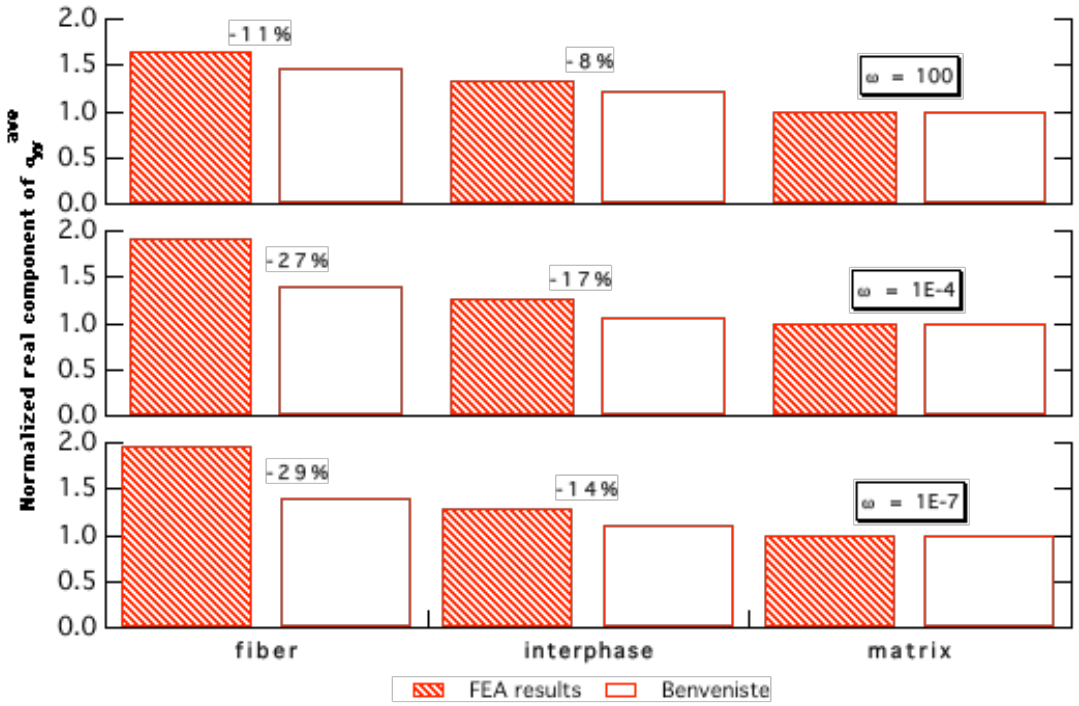

Figure 6.32. Transverse normal load: 60% fiber, 10% stiff interphase, 30% soft matrix

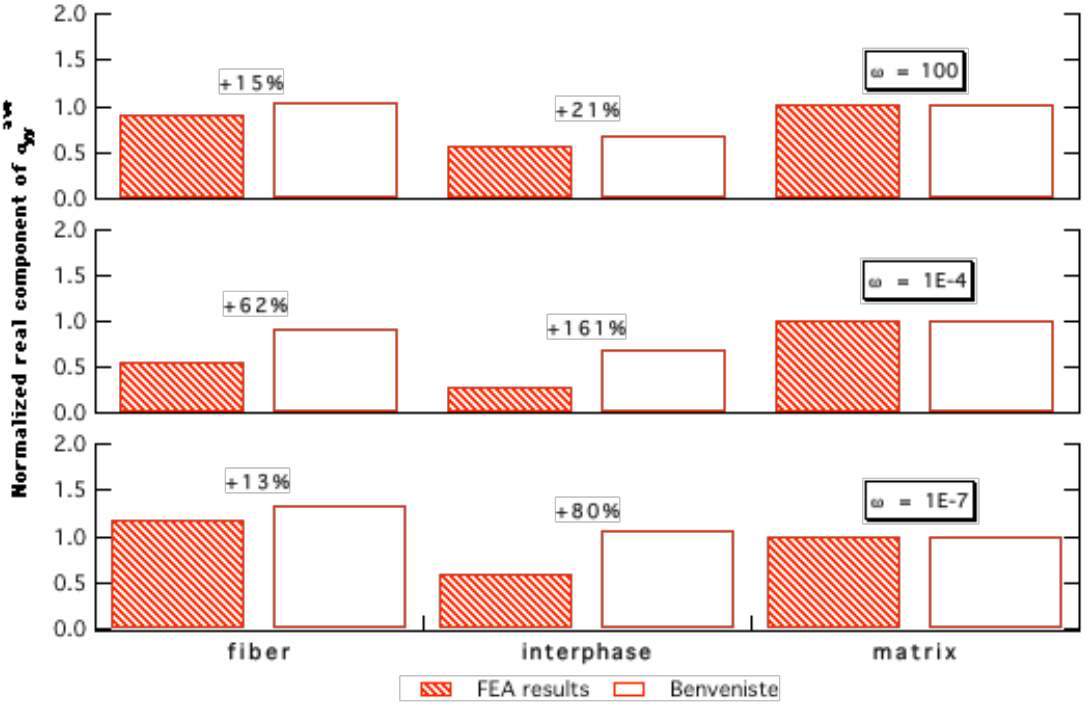

Figure 6.33. Transverse normal load: 60% fiber, 10% soft interphase, 30% stiff matrix

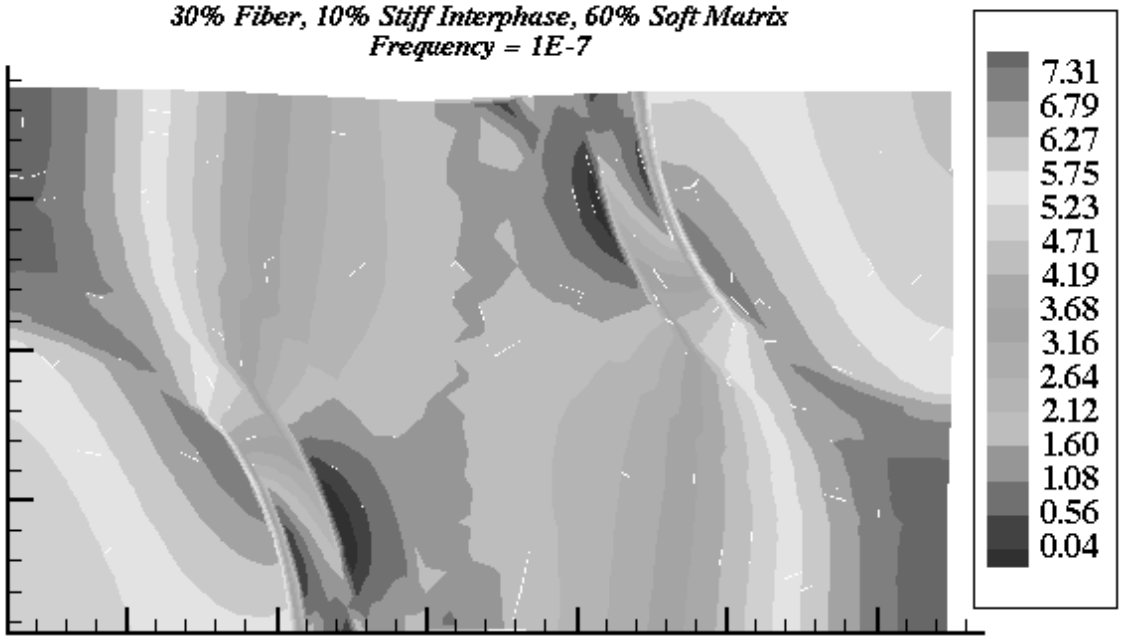

Figure 6.34. Real component of σ_{yy}^{Re} stress distribution. Phase average stresses:
FEAP (psi): fiber = 5.60, coating = 4.32, matrix = 3.42
Benveniste (psi): fiber = 4.90, coating = 3.69, matrix = 3.42

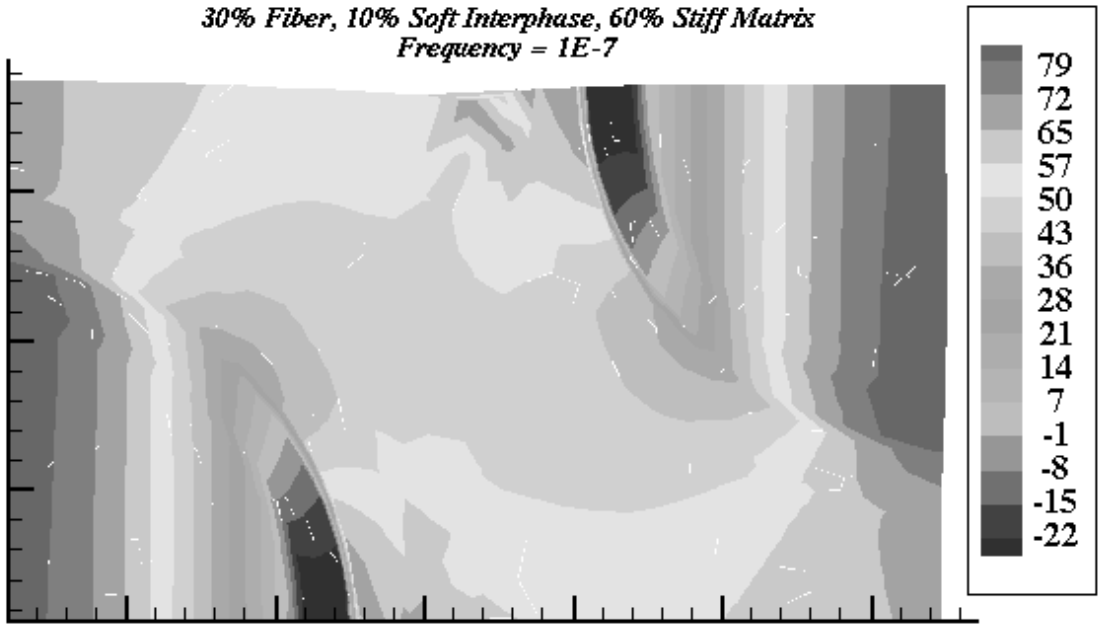

Figure 6.35. Real component of σ_{yy}^{Re} stress distribution. Phase average stresses:
FEAP (psi): fiber = 60.78, coating = 27.63, matrix = 53.76
Benveniste (psi): fiber = 72.87, coating = 54.25, matrix = 53.76

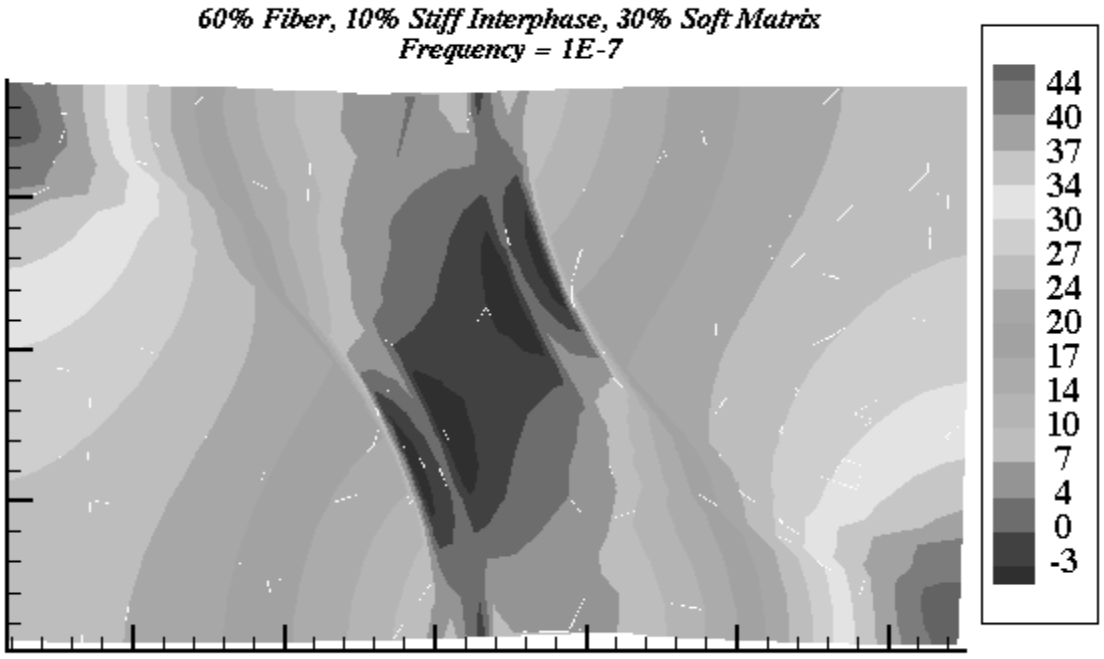

Figure 6.36. Real component of σ_{yy}^{Re} stress distribution. Phase average stresses:
FEAP (psi): fiber = 23.59, coating = 15.42, matrix = 12.07
Benveniste (psi): fiber = 16.72, coating = 13.30, matrix = 12.07

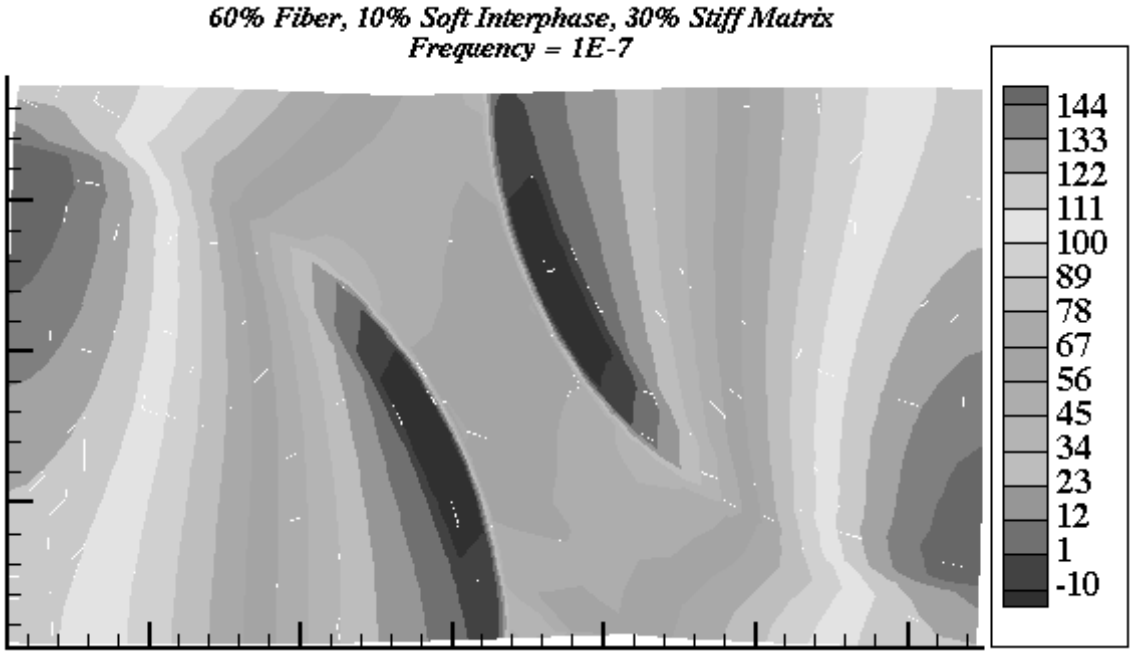

Figure 6.37. Real component of σ_{yy}^{Re} stress distribution. Phase average stresses:
FEAP (psi): fiber = 82.57, coating = 40.87, matrix = 70.01
Benveniste (psi): fiber = 93.13, coating = 73.66, matrix = 70.01

6.5 SHIFT RATES FOR MATRIX-DOMINATED PROPERTIES

For PMCs, it has been shown experimentally that different aging shift rates, μ_{22} and μ_{66}, exist for the transverse Young's and axial (longitudinal) shear moduli, respectively (Gates and Feldman 1993; Hastie and Morris 1993; Brinson and Gates 1995). This is somewhat surprising since both are typically considered matrix-dominated properties, and Struik (1978) has demonstrated that the shift rates describing all properties of a single polymer are identical. To the author's knowledge, the origin of the different shift rates for composite materials has yet to be explained. Here we will investigate whether the presence of an interphase with a shift rate different from that of the bulk matrix could account for the different shift rates under transverse shear and transverse normal loading measured experimentally.

We will use the finite element methods of this thesis, along with the results obtained via the analytical solutions, to investigate whether the difference μ_{22} and μ_{66} can be modeled. It should be stressed that this investigation is cursory in nature; the 2D finite element code used here cannot be used to determine the axial shear modulus. However, the shift rate describing the *transverse* shear modulus *can* be determined numerically using the 2D finite element code. Such results will provide an indication of whether interphase effects can account for the different composite shift rates depending on the loading mode.

Physical aging causes the free volume of the polymeric material to decrease over time; thus the behavior of the material is a function of initial aging time. This is typically manifest as an increase in the stiffness of the material, with a corresponding reduction in properties such as ductility, as the material undergoes aging. Figures 6.38-6.41 demonstrate how physical aging affects the calculated transverse Young's modulus and the transverse shear modulus of a composite as calculated via the finite element solution. Unless otherwise indicated, all individual phase shift rates were 0.85 for the interphase and 0.70 for the matrix materials.

As Figures 6.38-6.41 show, the shape of the curves are not exactly identical for all aging times shown. This trend is more noticeable in the loss moduli components at long aging times, as the curves, when shifted by a suitable amount, do not completely overlap due to a breakdown in shape. In order to better demonstrate this effect, the transverse shear loss moduli curves in Figures 6.42 and 6.43 for an initial aging time $t_{age} = 1$ have been shifted so as to best coincide with the moduli curves at other aging times. Note that when the interphase is the stiff VE material, the curves superpose very well (Figure 6.42). The shifting of the curves is not nearly as straightforward for composite configurations where the interphase is the soft VE material (Figure 6.43).

In particular, note that while the reference curve in Figure 6.43 has been shifted in order to superimpose low frequency data, the high frequency ends do not match. In effect, this difficulty prevents a unique shift factor from being determined. The fact that these curves are not superposable by means of a horizontal shift is indicative of thermo-rheologically (TRC) complex behavior. Such behavior is also characterized by the differences in curvature amongst the curves at intermediate frequencies. This behavior violates the assumptions necessary to use the standard definitions of shift factor and shift rate to characterize the aging behavior of the material.

In the first case (Figure 6.42), the aging behavior of the curves is dominated by the matrix because it is the softest VE material. In the latter case (Figure 6.43), however, where the matrix is the stiff VE material, the aging behavior seems to be controlled by two factors: the aging of the matrix material and the aging of the softest VE material in the composite (i.e. the interphase). As a result, one sees the influence of dual factors affecting the physical aging of the composite. This is characterized by the spreading of the loss moduli peak, which is responsible for the inability to simultaneously superpose low and high frequency portions of the curves. This type of behavior has been seen in other work on viscoelastic composites (Brinson and Knauss 1992; Lin 1996). The present work now indicates that a relatively small volume fraction of interphase can have a large role in determining the overall TRC behavior of the composite.

To circumvent the difficulty of shifting frequency domain moduli, the data were transformed into the time domain using a linear least squares solver (Bradshaw and Brinson 1997). The solver found a 20-term Prony series able to reproduce the original complex moduli with less than 2% total rms error. Though the behavior of the material in the time domain is clearly TRC, the errors in shifting these curves are not unlike those which would be realized in shifting experimental data, where the TRC behavior may be attributed to experimental error. Thus these numerical tests are a reasonable model to ascertain if the interphase is responsible for the different shift rates seen experimentally.

This interconversion minimizes the difficulty in properly shifting the reference curve to corresponding aged curves which may exhibit TRC behavior. Figure 6.44 shows the transverse shear modulus curves of Figure 6.38-6.39 converted to the time domain (again note that the moduli are real numbers only in the time domain). A procedure was then developed to determine the best shift factor for curve superposition. One difficulty is the definition of the "best" superposition of curves that are not identically the same

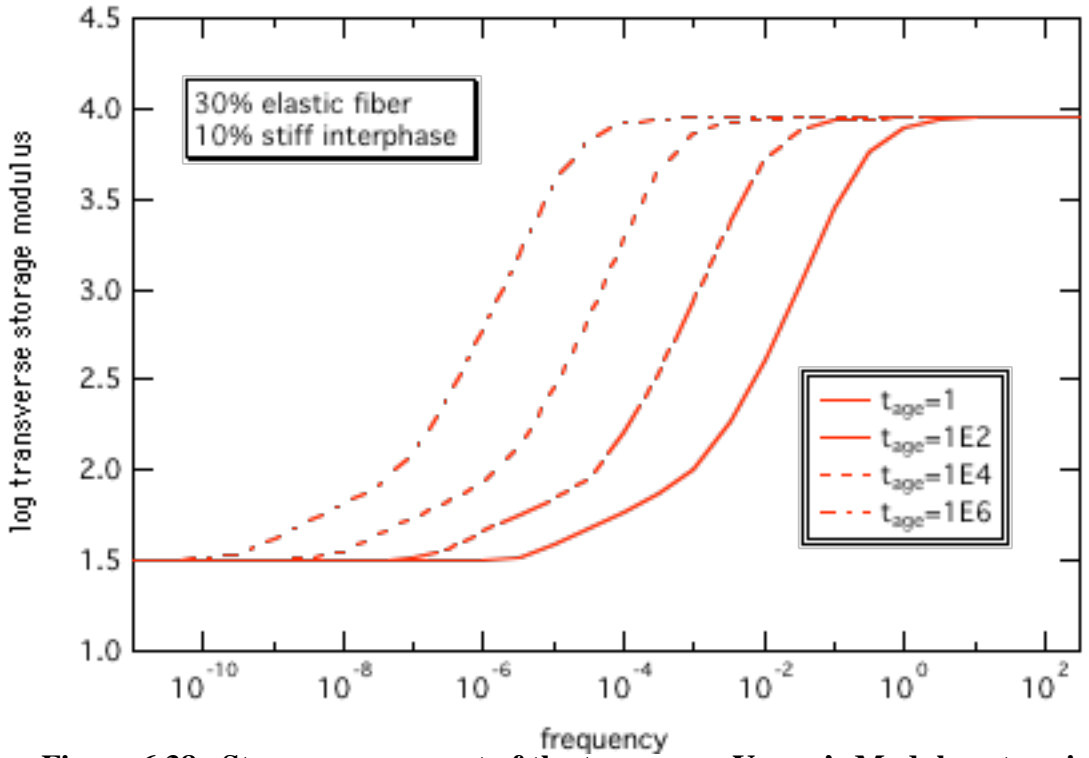

Figure 6.38. Storage component of the transverse Young's Modulus at various initial aging times. (FEA: 30% elastic fiber, 10% stiff interphase, 60% soft matrix)

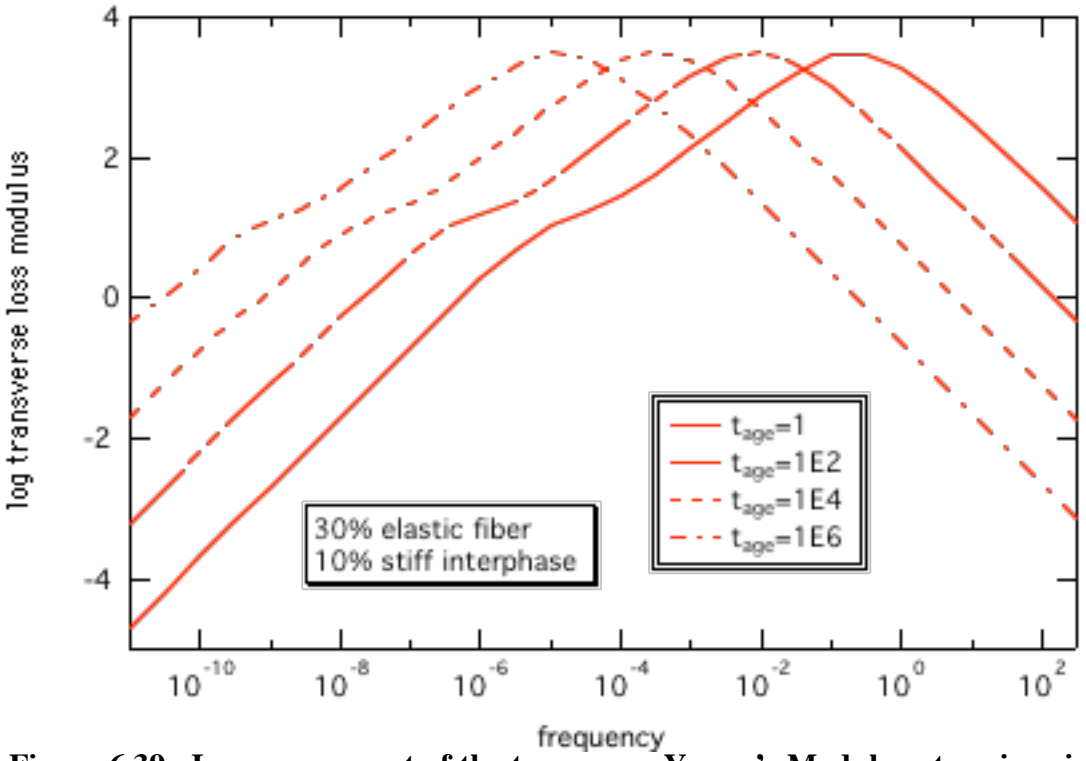

Figure 6.39. Loss component of the transverse Young's Modulus at various initial aging times. (FEA: 30% elastic fiber, 10% stiff interphase, 60% soft matrix)

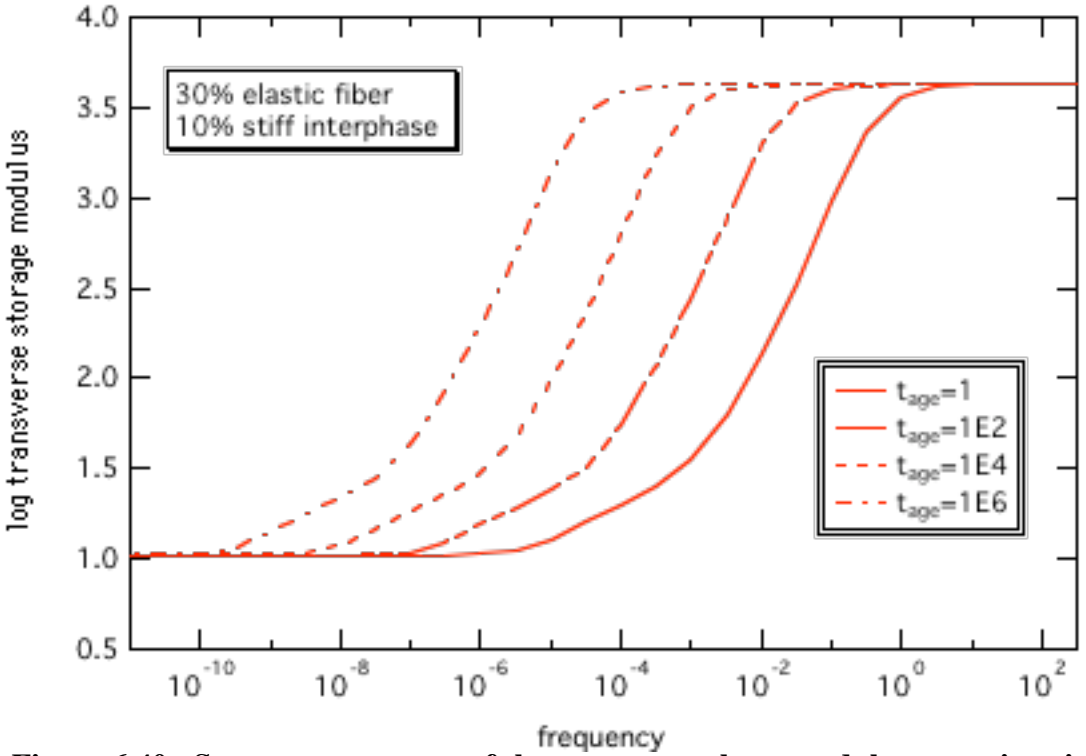

Figure 6.40. Storage component of the transverse shear modulus at various initial aging times. (FEA: 30% elastic fiber, 10% stiff interphase, 60% soft matrix)

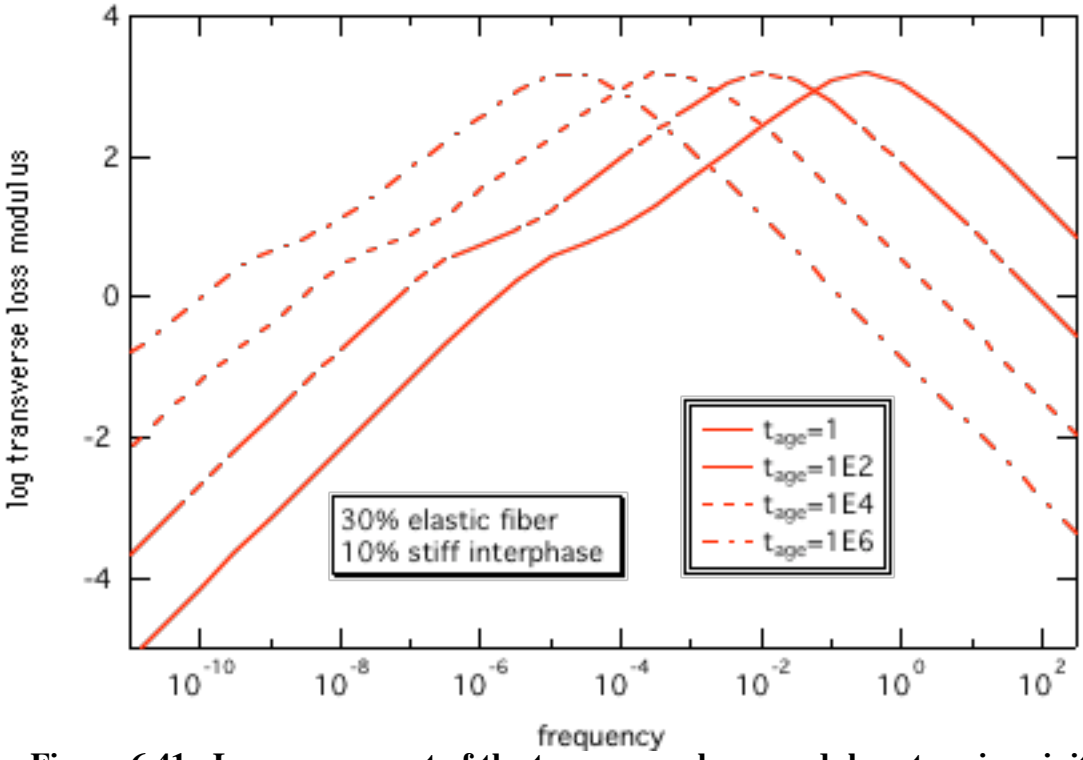

Figure 6.41. Loss component of the transverse shear modulus at various initial aging times. (FEA: 30% elastic fiber, 10% stiff interphase, 60% soft matrix)

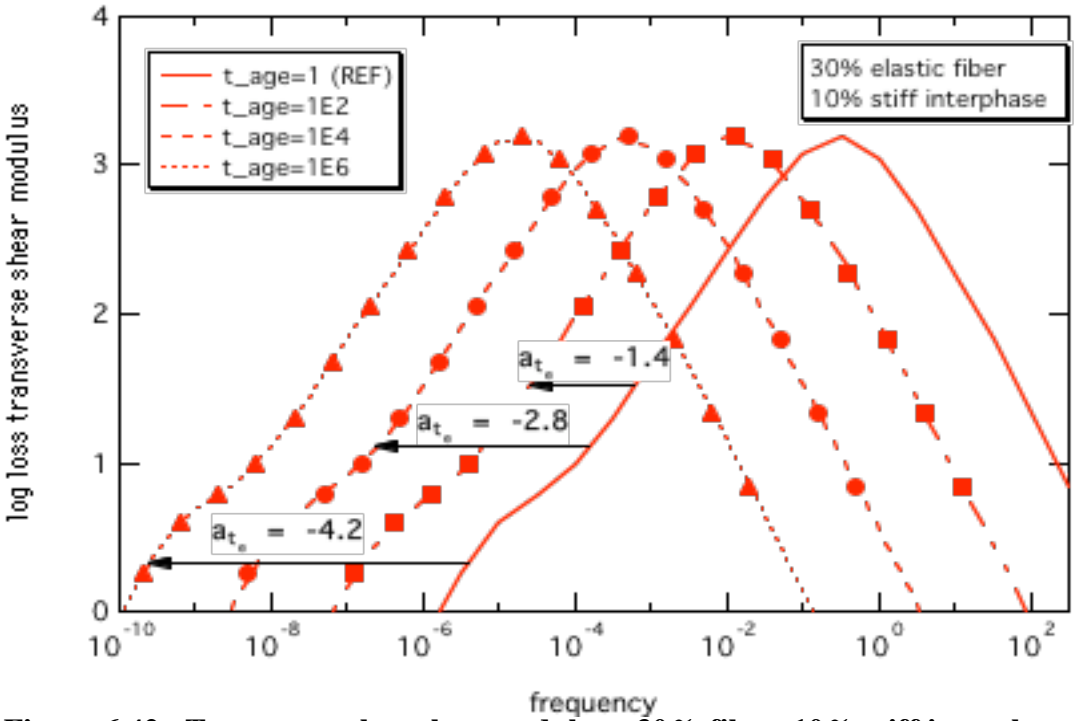

Figure 6.42. Transverse shear loss modulus: 30% fiber, 10% stiff interphase, 60% soft matrix via FEA. (solid shapes represent the shifted reference curve)

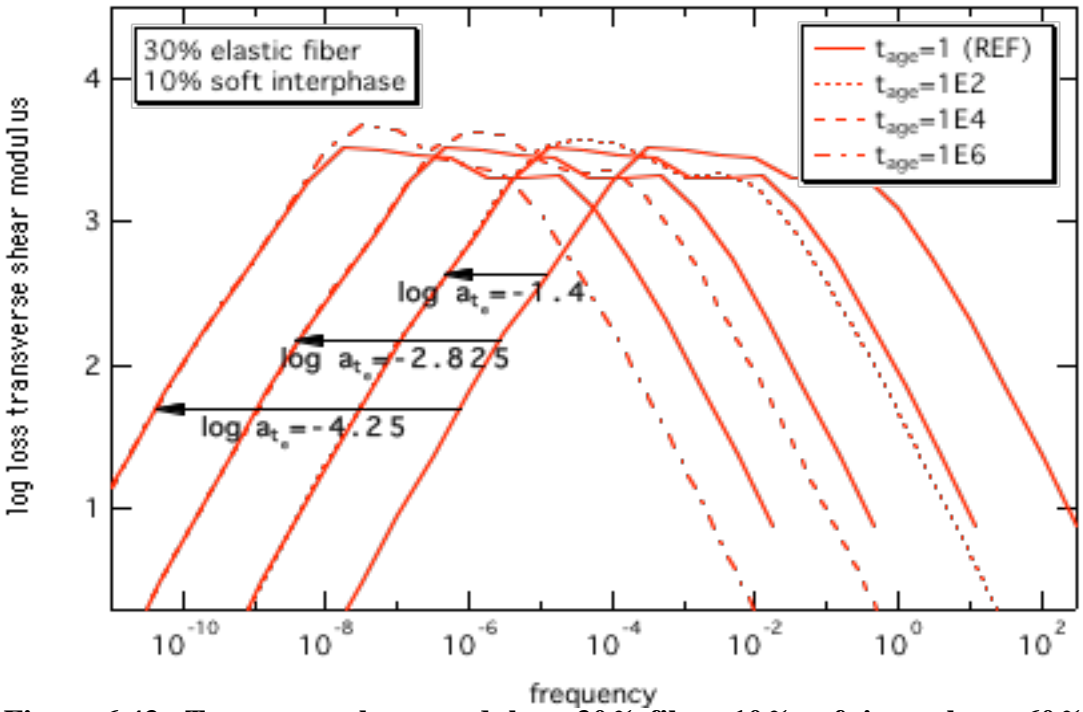

Figure 6.43. Transverse shear modulus: 30% fiber, 10% soft interphase, 60% stiff matrix via FEA. (shift factors chosen such that low frequency data was matched.)

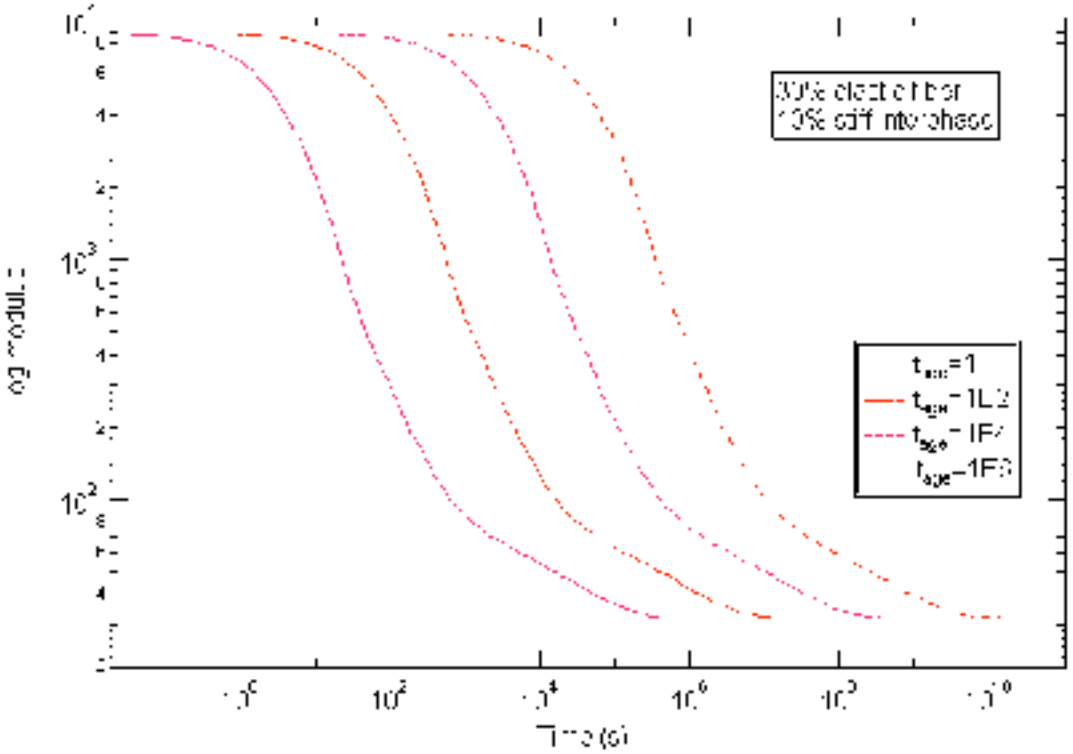

Figure 6.44. Time domain plot of transverse Young's modulus via FEA: 30% elastic fiber, 10% stiff interphase, 60% soft matrix.

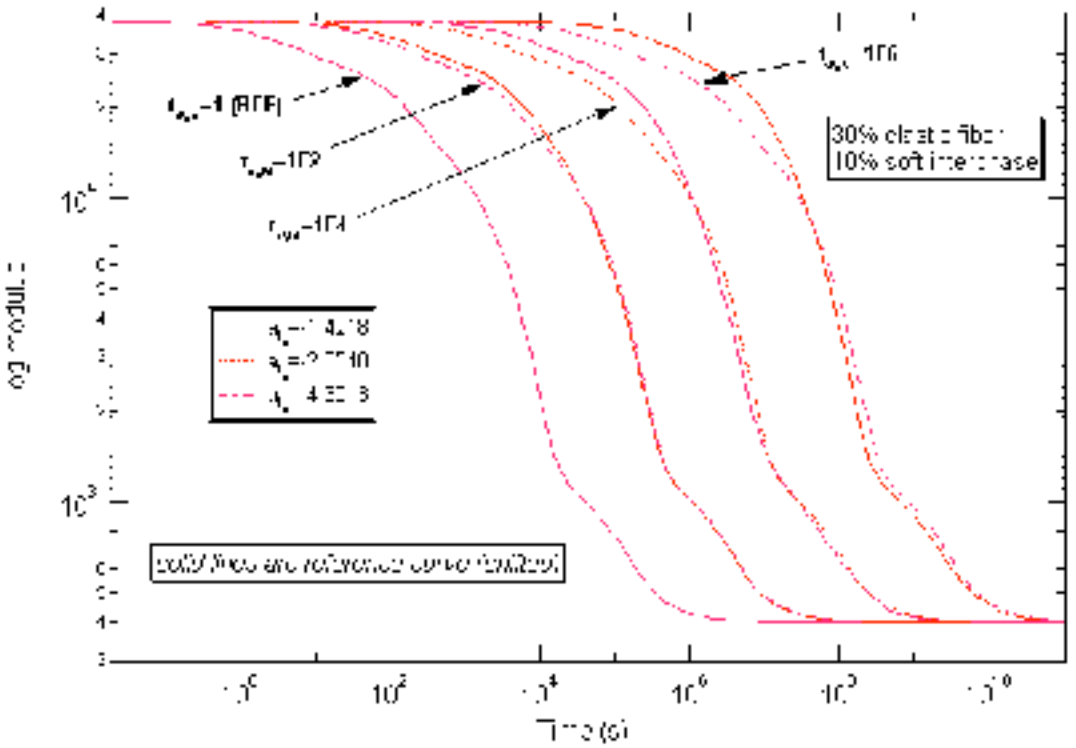

Figure 6.45. Shifting of time domain plots for transverse Young's modulus (FEA analysis). NOTE: for clarity, the reference curve was shifted to the aged curves.

shape. This was particularly troublesome for composites with interphases of the soft VE material, as shown in Figure 6.45. (Curves where the interphase material was the stiff VE material, as shown in Figure 6.42, demonstrated much less breakdown in shape for various aging times.) The best shift factor for a given initial aging time was defined as the shift factor which minimized the following expression,

$$q(a_t) = \sum_n \frac{\left(G_{shift}(a_t) - G_{ref}\right)^2}{G_{ref}} \qquad (6.2)$$

where $q(a_t)$ is defined as the error produced by a given shift factor, $G_{shift}(a_t)$ and G_{ref} are the moduli curves of the aged composite shifted by a_t and the reference moduli curves, respectively, and n is the number of discrete points in the time domain at which the moduli values were evaluated. An example of shift factors calculated in this manner can be found in Figure 6.45.

The final step of the procedure was to determine the shift rate given the shift factors and initial aging times of the composite. Given the definition presented earlier in this thesis (see Chapter 2), the shift rates were determined via a linear best fit through the data points as shown in Figure 6.46. Table 6.2 shows shift rates calculated for different mechanical properties via the FEA and micromechanical solutions.

Upon analysis of the data presented in Table 6.2, we see that the shift rates determined via FEA are largely dependent on the composite configuration. For composites where the matrix is the softest of the constituent phases, the overall shift rates provided via FEA are strongly dependent on the shift rate of the matrix material. On the other hand, for those composites where the interphase is the softest of the VE materials,

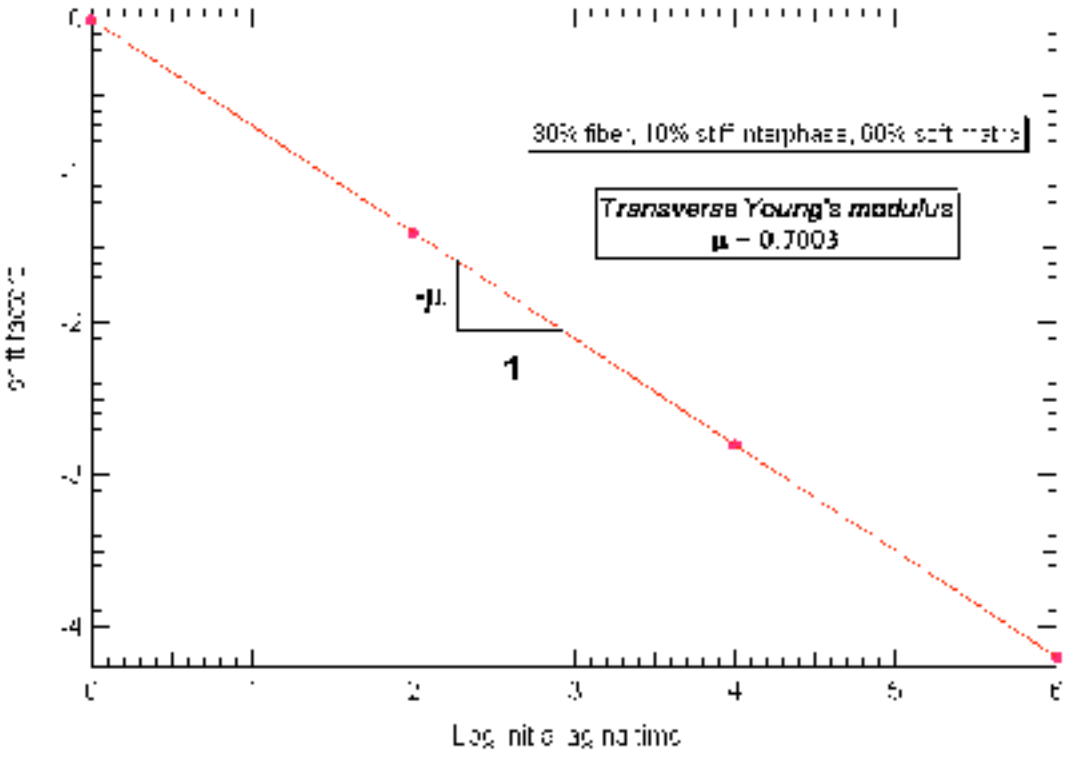

Figure 6.46. Determination of the shifts rate calculated for the FEA solution of transverse Young's modulus (30% fiber, 10% stiff interphase, 60% soft matrix).

Method	Property	Geometry†			
		30f/10stiff	30f/10soft	60f/10stiff	60f/10soft
FEAP	E_T	0.7003	0.7168	0.7003	0.7904
FEAP	α_T	0.6989	0.7144	0.6988	0.7847
BENV	E_T	0.7007	0.8395	0.7006	0.8447
BENV	α_T	0.7016	0.8421	0.7007	0.8461
BENV	α_A	0.7011	0.7080	0.7008	0.7761
MT	E_T	0.6989	0.7012	0.7011	0.7014
MT	α_T	0.6997	0.7010	0.7000	0.7103
MT	α_A	0.6987	0.7009	0.6988	0.6933

Table 6.2. Shift rates calculated for 3 phase composites. († - geometry given as fiber volume fraction, interphase volume fraction, interphase VE material) $\alpha_{int} = 0.85$; $\alpha_{mat} = 0.70$

the shift rates are intermediate of the constituent shift rates; this effect is magnified for larger fiber volume fractions as the ratio of volume fractions of the VE phases approaches unity. This type of behavior was noted earlier when discussing the role of the interphase on the TRC behavior of composites.

To look at two specific examples, consider the FEA results for composites with 60% elastic fiber. The first such composite, consisting of a 10% stiff interphase and 30% soft matrix, has shift rates dominated by the matrix material. On the other hand, the composite with 10% soft interphase and 30% stiff matrix has shift rates intermediate of the individual phase shift rates. Such a result indicates that the shift rate of the interphase can have a large impact on the overall effective shift rates of the composite.

On the other hand, the FEA results do *not* indicate that the interphase causes a difference in the shift rates describing the aging behavior of E_T and α_T. Although this is

circumstantial evidence (since the shift rate β_{66} was not determined numerically in this work), these results suggest that *the interphase is not responsible for the difference in shift rates that is measured experimentally*. Although this should be verified by a 3D finite element analysis which determines the aging behavior of the effective axial shear modulus, there may be another cause of the difference in shift rates β_{22} and β_{66} measured experimentally. One possible explanation is that the assumption of perfect bonding between the phases, used in this work, is invalid. This bonding imperfection may be characterized by different responses to applied loadings, accounting for the different shift rates which are measured experimentally. This, and other possible models, may need to be investigated in order to account for the difference in shift rates seen experimentally.

Analysis of the shift rates determined via the micromechanical methods show that they do not reproduce the general results produced by the FEA. This is not surprising considering that these methods did not accurately predict the overall composite moduli for many composite configurations. It is interesting, however, that the Benveniste solution predicts a large difference in the shift rates for the transverse and axial shear behavior. Although this observation is seriously compromised due to the questions of the legitimacy of the solution, it does suggest that a full 3D finite element analysis to determine the shift rate β_{66} may be warranted.

6.6 CONCLUSIONS AND FUTURE WORK

This thesis investigated whether two micromechanical methods, the Mori-Tanaka method and a model developed by Benveniste, could accurately determine the effective moduli of a three phase viscoelastic composite. The Mori-Tanaka method was chosen because it is a popular micromechanical tool which has been used in a wide variety of applications and is simple to apply. The Benveniste solution was chosen because it allows the physicality of the annular interphase surrounding the fiber inclusion to be maintained. The main conclusions of this work are outlined below:

2 The micromechanical methods provide good approximations for the effective composite moduli in those cases where the matrix is the softest of the three materials. However, the difference between the MT and Benveniste solutions is very small in these cases, such that either model will give roughly the same prediction.

3 When the interphase is the softest material, the accuracy of the micromechanical methods is greatly diminished. In these cases the MT method is more effective in modeling the viscoelastic behavior of the composite because it predicts matrix-dominated effective properties for the composite. The Benveniste model suggests that the effective behavior of the composite is dominated by the interphase, which seems unlikely in that it is a small volume fraction, discontinuous phase within the composite.

4 However, from a design perspective, the Benveniste model may be more useful because it provides conservative estimates of the effective composite moduli for all composite configurations. For composites where the interphase is the softest material, the MT method overestimates the composite moduli. As noted in Appendix A3, this behavior holds for an elastic analysis of composites as well.

5 According to the FEA results, the effective properties of the composite seem to be fairly independent of the volume fraction of the interphase (at least once a critical interphase volume fraction is exceeded). This suggests that a precise measurement of the interphase may not be necessary to predict effective properties.

- The micromechanical methods are not successful in modeling the physical aging of the composite when compared to the FEA results. The use of these micromechanical models to study complex composite behavior beyond effective properties is limited.

- TRC composite behavior which is evident in the Fourier domain may be masked in the time domain. Thus experimental time domain data may hide crucial information concerning possible TRC behavior. The loss modulus exhibits the greatest sensitivity to TRC behavior.

- The FEA results suggest that the interphase can play a large role in determining the overall shift rates describing the physical aging of the composite. However, the interphase did *not* cause a difference in shift rates describing the physical aging of E_T and $\Box_T$. Whether the interphase is responsible for the difference in $\Box_{22}$ and $\Box_{66}$ shift rates should be verified with a 3D FEA.

Thus the use of one of these micromechanical solutions as opposed to the other should be determined based on the composite effect to be studied. While the MT method better approximates the viscoelastic nature of the composite, the Benveniste solution may be useful for design purposes since it always provides conservative predictions for the overall effective moduli. It should be noted that from a computational perspective the MT method is easier to implement.

Although both of these methods are useful in providing rough estimates of the effective composite properties, it will undoubtedly be useful to develop an analytical model which can provide more accurate predictions. It would seem necessary that such a model would need to treat the interphase as a annular inclusion in order to ultimately provide a suitable micromechanical model with which to study interphase effects. Perhaps another analytical model, for which the "phase-averaging" of the stresses does not play such a crucial role, may be better suited for such work. On the other hand, it may be worthwhile to extend the Benveniste model following the procedure of the generalized self-consistent model. Such a model, where a fiber-interphase-matrix particle is embedded in an infinite medium of unknown composite properties, has proven useful for the study of elastic composites. Other analytical models, which allow the interphase properties to vary with location, may be useful in developing analytical models which accurately model experimental results.

It seems that it would also be beneficial to extend the FEA analysis described here so that a 3D analysis could be conducted. Such work would allow for the shift rate $\Box_{66}$ to be determined via FEA, a result which could not be obtained here. This would provide

substantial proof, as opposed to the circumstantial evidence offered here, that a viscoelastic interphase, with an effective shift rate different from that of the matrix, is not responsible for the different shift rates measured experimentally. Another extension of this work could incorporate effective time theory into the physical aging model to account for an on-going accumulation of actual aging time (Brinson and Gates 1995).

BIBLIOGRAPHY

Aboudi, J. (1991). Mechanics of Composite Materials - A Unified Micromechanics Approach. Amsterdam, Elsevier.

Al-Ostaz, A. and I. Jasiuk (1996). "The Influence of Interface and Arrangement of Inclusions on Local Stresses in Composite Materials." *Acta. Mater.* **45**(10): 4131-4143.

Avery, W. and C. Herakovich (1986). "Effect of Fiber Anisotrophy on Thermal Stresses in Fibrous Composites." *Journal of Applied Mechanics* **53**: 751-756.

Bank, L. C. and T. R. Gentry (1995). "Accelerated Test Methods to Determine the Long-Term Behavior of FRP Composite Structures: Enviromental Effects." *Journal of Reinforced Plastics and Composites* **14**: 559-587.

Benveniste, Y. (1987). "A New Approach to the Application of Mori-Tanaka's Theory in Composite Materials." *Mechanics of Materials* **6**: 147.

Benveniste, Y., G. J. Dvorak, et al. (1989). "Stress Fields in Composites with Coated Inclusions." *Mechanics of Materials* **7**: 305-317.

Bradshaw, R. and L. Brinson (1997). "A Sign Control Method for Fitting and Interconverting Material Functions for Linearly Viscoelastic Materials." *Mechanics of Time-Dependent Materials* **1**: 85-108.

Brinson, L. C. (1990). Time-Temperature Response of Multi-Phase Viscoelastic Solids Through Numerical Analysis. California Institute of Technology.

Brinson, L. and W. Knauss (1992). "Finite Element Analysis of Multiphase Viscoelastic Solids." *Transactions of the ASME* **59**: 730-737.

Brinson, L. and W. Lin (1998). "Comparison of Micromechanics Methods for Effective Properties of Multiphase Viscoelastic Composites." *Composite Structures* : *accepted*.

Broutman, L. and B. Agarwal (1974). "A Theoretical Study of the Effect of an Interfacial Layer on the Properties of Composites." *Polymer Engineering and Science* **14**(8): 581-588.

Chen, T. G. D., and Y. Benveniste (1992). "Mori-Tanaka Estimates of the Overall Elastic Moduli of Certain Composite Materials." *Transactions of the ASME, Journal of Applied Mechanics* **59**: 539-546.

Christensen, R. M. and K. H. Lo (1979). "Solutions for Effective Shear Properties in Three Phase Sphere and Cylinder Models." *Journal of Mechanics of Physical Solids* **27**: 315.

Christensen, R. (1990). "A Critical Evaluation for a Class of Micromechanics Models." *Journal of Mechanics of Physical Solids* **38**(3): 379-404.

Eshelby, J. D. (1957). "The Determination of the Elastic Field of an Ellipsoidal Inclusion, and Related Problems." *Proceedings of the Royal Society of London* **A241**: 376-396.

Ferry, J. D. (1980). Viscoelastic Properties of Polymers. New York, John Wiley & Sons, Inc.

Gardner, S., C. Pittman, Jr., et al. (1993). "Residual Thermal Stresses in Filamentary Polymer-Matrix Composites Containing an Elastomeric Interphase." *Journal of Composite Materials* **27**(8): 830-860.

Gates, T. and M. Feldman (1993). Time Dependent Behavior of a Graphite/Thermoplastic Composite and the Effects of Stress and Physical Aging. NASA Technical Memorandum 109047.

Gibiansky, L. and R. Lakes (1993). "Bounds on the Complex Bulk Modulus of a Two-Phase Viscoelastic Composite with Arbitrary Volume Fractions of the Components." *Mechanics of Materials* **16**: 317-331.

Gibiansky, L. and G. Milton (1993). "On the Effective Viscoelastic Moduli of Two-phase media. I. Rigorous bounds on the complex-bulk modulus." *Proc. R. Soc. London A* **440**: 163-188.

Gosz, M., B. Moran, et al. (1991). "Effect of a Viscoelastic Interface on the Transverse Behavior of Fiber-Reinforced Composites." *Int. J. Solids Structures* **27**(14): 1757-1771.

Haoran, C., S. Feng, et al. (1995). "The Effect of Interphase on Overall Average Mechanical Properties and Local Stress Fields of Multi-phase Medium Materials." *Computational Materials Science* **4**: 117-124.

Hashin, Z. and S. Shtrikman (1962). "A Variational Approach to the Theory of the Elastic Behaviour of Multiphase Materials." *Journal of Mechanics of Physical Solids* **11**: 127-140.

Hashin, Z. (1965). "Viscoelastic Behavior of Heterogeneous Media." *Journal of Applied Mechanics* : 630-636.

Hashin, Z. (1966). "Viscoelastic Fiber Reinforced Materials." *AIAA Journal* **4**: 1411-1417.

Hashin, Z. (1970a). "Complex Moduli of Viscoelastic Composites-II. Fiber Reinforced Materials." *Int. J. Solids and Structures* **6**: 797-807.

Hashin, Z. (1970b). "Complex Moduli of Viscoelastic Composites: I. General Theory and Application to Particulate Composites." *International Journal of Solids and Structures* **6**: 539.

Hashin, Z. (1983). "Analysis of Composite Materials- A Survey." *Journal of Applied Mechanics* **50**: 481-505.

Hastie, R. and D. Morris (1993). The Effects of Physical Aging on the Creep Response of a Thermoplastic Composite. High Temperature and Environmental Effects in Polymer Matrix Composites. Ed. C Harris and T Gates. Philadelphia, ASTM STP 1174. 163-185.

Henderson, C. and M. Williams (1985). "Asymmetric Composition Profiles in Block Copolymer Interphases: 1. Experimental Evidence." *Polymer* **26**: 2021-2025.

Ho, H. and L. Drzal (1996). "Evaluation of Interfacial Mechanical Properties of Fiber Reinforced Composites Using the Microindentation Method." *Composites Part A* **27A**: 961-971.

Jacobs, E. and I. Verpoest (1998). "Finite Element Modelling of Damage Development During Longitudinal Tensile Loading of Coated Fibre Composites." *Composites Part A* **29A**: 1007-1012.

Jayaraman, K., K. Reifsnider, et al. (1993). "Elastic and Thermal Effects in the Interphase: Part 1. Comments on Characterization Methods." *Journal of Composites Technology and Research* **15**(1): 3.

Li, J. and G. J. Weng (1994). "Anisotropic Creep Behavior and Complex Moduli of Fiber- and Ribbon-Reinforced Polymer-Matrix Composites." *Composites Science and Technology* **52**:

Li, J. and G. Weng (1996). "Effect of a Viscoelastic Interphase on the Creep and Stress/Strain Behavior of Fiber-Reinforced Polymer Matrix Composites." *Composites Part B* **27B**: 589-598.

Lin, W. (1996). A Comparison of Finite Element Analysis and Mori-Tanaka Theorem for the Transverse Behavior of Two Phase Viscoelastic Composites. Northwestern University.

Luo, H. and G. Weng (1987). "On Eshelby's Inclusion Problem in a Three-Phase Spherically Concentric Solid, and a Modification of Mori-Tanaka's Method." *Mechanics of Materials* **8**: 347-361.

Luo, H. and G. Weng (1989). "On Eshelby's S-Tensor in a Three-Phase Cylindrically Concentric Solid, and the Elastic Moduli of Fiber-Reinforced Composites." *Mechanics of Materials* **8**: 77-88.

Mahiou, H. and A. Beakou (1998). "Modelling of interfacial effects on the mechanical properties of fibre-reinforced composites." *Composites Part A* **29A**: 1035-1048.

Mai, K., E. Mader, et al. (1998). "Interphase Characterization in Composites with New Non-destructive Methods." *Composites Part A* **29A**: 1111-1119.

Mikata, Y. (1994). "Stress Fields in a Continuous Fiber Composite with a Variable Interphase Under Thermo-mechanical Loadings." *Journal of Engineering Materials and Technology* **116**: 367-377.

Mori, T. and K. Tanaka (1973). "Average Stress in Matrix and Average Elastic Energy of Materials with Misfitting Inclusions." *Acta Mettallurgica* **21**: 571-574.

Munz, M., H. Sturm, et al. (1998). "The Scanning Force Microscope as a Tool for the Detection of Local Mechanical Properties Within the Interphase of Fibre Reinforced Polymers." *Composites Part A* **29A**: 1251-1259.

Mura, T. (1982). Micromechanics of Defects in Solids. Dordrecht, Kluwer Academic Publishers.

Nelliappan, V., M. El-Aasser, et al. (1997). "Effect of the Core/Shell Latex Particle Interphase on the Mechanical Behavior of Rubber-Toughened Poly(methyl methacrylate)." *Journal of Applied Polymer Science* **65**(3): 581-593.

Norris, A. (1990). "The Mechanical Properties of Platelet Reinforced Composites." *International Journal of Solids and Structures* **26**(5/6): 663-674.

Ostoja-Starzewski, M., K. Alzebdeh, et al. (1995). "Linear Elasticity of Planar Delaunay Networks. III: Self-consistent Approximations." *Acta Mechanica* **110**: 57-72.

Papanicolaou, G., G. Messinis, et al. (1989). "The Effect of Interfacial Conditions on the Elastic-Longitudinal Modulus of Fibre Reinforced Composites." *Journal of Materials Science* **24**: 395-401.

Qui, Y. and G. Weng (1990). "On the Application of Mori-Tanaka's Theory Involving Transversely Isotropic Spheroidal Inclusions." *International Journal of Engineering Science* **28**(11): 1121-1137.

Qui, Y., and G.J. Weng (1991a). "Elastic Moduli of Thickly Coated Particle and Fiber-Reinforced Composites." *Journal of Applied Mechanics* **58**: 388-398.

Qui, Y. and G. Weng (1991b). "The Influence of Inclusion Shape on the Overall Elastoplastic Behavior of a Two-phase Isotropic Composite." *Int. J. Solids Structures* **27**(12): 1537-1550.

Shapery, R. (1967). "Stress Analysis of Composite Materials." *Journal of Composite Materials* **1**: 228-267.

Schapery, R. (1969). "On the Characterization of Nonlinear Viscoelastic Materials." *Polymer Engineering and Science* **9**(4): 295-310.

Spontak, R., M. Williams, et al. (1988). "Interphase Composition Profile in SB/SBS Block Copolymers, Measured with Electron Microscopy, and Microstructural Implications." *Macromolecules* **21**: 1377-1387.

Struik, L. C. E. (1978). Physical Aging in Amorphous Polymers and Other Materials. New York, Elsevier.

Taylor, R., K.S. Pister, and G.L. Goudreau (1970). "Thermomechanical Analysis of Viscoelastic Solids." *International Journal for Numerical Methods in Engineering* **2**: 45-59.

Taylor (1982). FEAP - Finite Element Analysis Package. Berkeley, CA, University of California.

Termonia, Y. (1990). "Fibre Coating as a Means to Compensate for Poor Adhesion in Fibre-Reinforced Materials." *Journal of Materials Science* **25**: 103-106.

Theocaris, P. (1985). "The Unfolding Model for the representation of the Mesophase Layer in Composites." *Journal of Applied Polymer Science* **30**: 621-645.

Thomason, J. (1995). "The Interface Region in Glass Fibre-Reinforced Epoxy Resin Composites: 3. Characterization of Fibre Surface Coatings and the Interphase." *Composites* **26**: 487-498.

Tschogel, N. (1989). The Phenomenological Theory Of Linear Viscoelastic Behavior. Berlin, Springer-Verlag

Wacker, G., A. Bledzki, et al. (1998). "Effect of Interphase on the Transverse Young's Modulus of Glass/Epoxy Composites." *Composites Part A* **29A**: 619-626.

Walpole, L. (1969). "On the Overall Elastic Moduli of Composite Materials." *Journal of the Mechanics of Physical Solids* **17**: 235-251.

Wang, Y. and G. Weng (1992). "The Influence of Inclusion Shape on the Overall Viscoelastic Behavior of Composites." *Journal of Applied Mechanics* **59**: 510-518.

Weng, G. J. (1984). "Some Elastic Properties of Reinforced Solids, with Special Reference to Isotropic Ones Containing Spherical Inclusions." *International Journal of Engineering Science* **22**(7): 845.

Weng, G. (1990). "The Theoretical Connection Between Mori-Tanaka's Theory and the Hashin-Shtrikman-Wadpole Bounds." *International Journal of Engineering Science* **28**(11): 1111-1120.

Yi, S., G. Pollack, et al. (1995). "Effective Transverse Modulus of Composites with Viscoelastic Interphase." *AIAA Journal* **33**(8): 1548-1550.

Zhao, Y. H. and G. J. Weng (1990). "Effective Elastic Moduli of Ribbon-Reinforced Composites." *Transactions of the ASME* **57**: 158.

APPENDIX A.1. SAMPLE MESH USED FOR FINITE ELEMENT ANALYSIS

A sample mesh used for the finite element analysis is given below. This mesh represents the geometry of a 30% fiber, 10% interphase, 60% matrix composite. All meshes were continually refined until a convergence criterion based on the relative differences in solution were met. At least 5 elements were used across the thickness of the interphase, independent of its thickness. A thin zone of matrix material around the interphase was also meshed in a fine manner to capture possible stress concentrations which may arise in these locations. All meshes used for the finite element work in this thesis were created using the FASTQ mesh generation program.

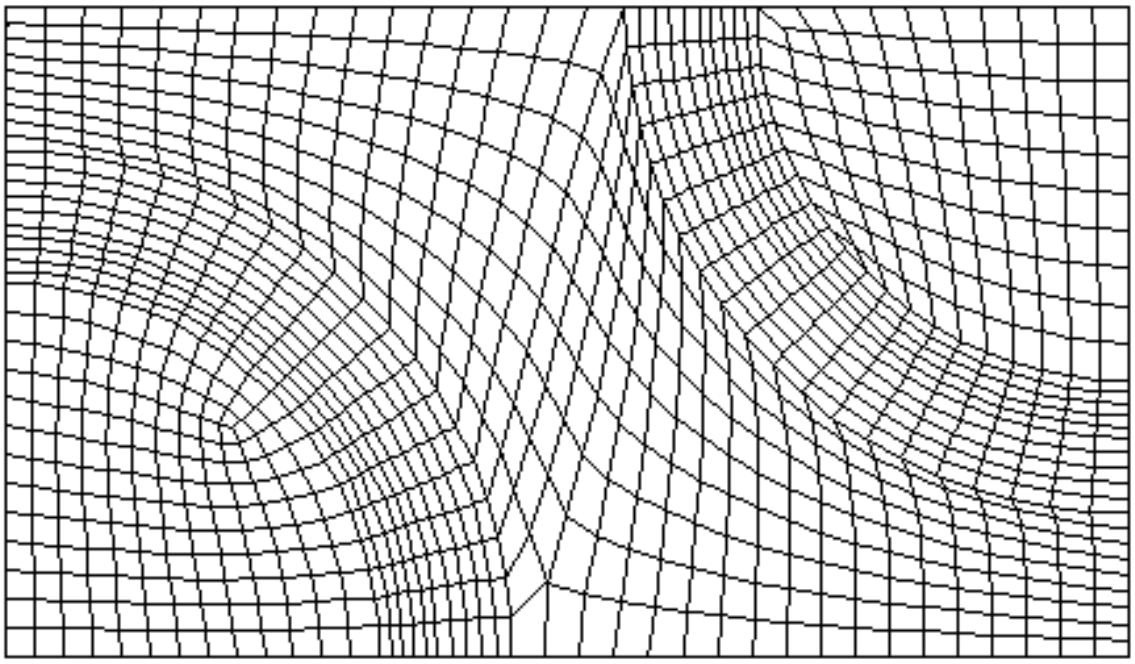

Figure A.1. Example mesh for c_f=0.30, c_g=0.10, c_m=0.60.

Appendix A.2. Eshelby Tensor for Circular, Cylindrical Inclusions

Below are the components of the Eshelby tensor for a composite material with circular, cylindrical fibers. Note that the distinction of an annular interphase region *cannot* be captured using the Mori-Tanaka method with the Eshelby tensor given below. It is assumed that the fibers are aligned parallel to the 1-axis. Below ν^m is the poisson ratio of the matrix, and all other components of the Eshelby tensor are identically zero.

$$s_{1111} = s_{2222} = \frac{5 - 4\nu^m}{8\left(1 - \nu^m\right)}$$

$$s_{1122} = s_{2211} = \frac{4\nu^m - 1}{8\left(1 - \nu^m\right)}$$

$$s_{3333} = s_{3311} = s_{3322} = 0$$

$$s_{2233} = s_{1133} = \frac{\nu^m}{2\left(1 - \nu^m\right)}$$

$$s_{1212} = \frac{3 - 4\nu^m}{8\left(1 - \nu^m\right)}$$

$$s_{2323} = s_{3131} = \frac{1}{4}$$

For the general form of the Eshelby tensor valid for ellipsoidal inclusions of random dimensions, see Mura (1982).

APPENDIX A.3. ELASTIC ANALYSIS OF THE MICROMECHANICAL METHODS

Although the Benveniste solution seems to provide more accurate results for the viscoelastic composite in the glassy elastic (high frequency) range, it was noted this same accuracy was not seen in the rubbery elastic (low frequency) range. In order to provide a better understanding of the micromechanical solutions for elastic composites, trials with elastic phase properties were completed. This appendix details the results of this analysis.

The pseudo-elastic properties of the same phase materials used in the viscoelastic analysis were estimated. The values used for the elastic analysis can be found in Table A1. Using these values, a purely elastic analysis of the effective composite behavior was completed for a limited number of the composite configurations presented in this thesis. The results for the transverse Young's modulus E_T and the transverse shear modulus $\square_T$ are presented in Table A2.

phase	property	Glassy elastic	Rubbery elastic
Fiber	K	100,000	100,000
	G	40,000	40,000
Stiff inclusion phase	K	48,000	8,000
	G	8,000	100
Soft inclusion phase	K	3,162	200
	G	1,600	3.162

Table A1. Elastic phase materials.

Property	Method	Geometry†			
		30f/10stiff	30f/10soft	60f/10stiff	60f10soft
E_T - glassy	MT	3.9168	4.5035	4.2207	4.6558
	BENV	3.9102	4.4014	4.2186	4.5154
	FEA	3.9223	4.4087	4.2607	4.5154
$\square_T$ - glassy	MT	3.4695	4.0005	3.7706	4.1772
	BENV	3.4600	3.9012	3.7674	4.0396
	FEA	3.5971	4.0297	3.9457	4.1601
E_T – rubbery	MT	1.4507	2.7516	1.8285	3.0290
	BENV	1.4291	2.0776	1.8144	2.1700
	FEA	1.4999	2.6030	2.1658	2.7501
$\square_T$ – rubbery	MT	0.8579	2.1765	1.2375	2.4746
	BENV	0.8358	1.4826	1.2231	1.5764
	FEA	1.0228	2.1436	1.7342	2.3002

Table A2. Log 10 values of the effective composite properties for an elastic analysis.
(† - geometry given as fiber volume fraction, interphase volume fraction, interphase material)

The elastic analysis verifies some of the conclusions that were based on the viscoelastic behavior of the composite. First, the micromechanical solutions are closer to the FEA when the matrix is the softest material. Secondly, although the Benveniste method does not model the viscoelastic behavior of the composite as well as the MT method does, it may be more useful from a design perspective since for all configurations it underestimates the overall effective composite moduli.